ROLES OF SETD4 IN RADIATION SENSITIVITY AND TUMORIGENESIS

By

XING FENG

A dissertation submitted to the School of Graduate Studies

Rutgers, The State University of New Jersey

In partial fulfillment of the requirements for the degree of

Doctor of Philosophy

Graduate Program in Cellular and Molecular Pharmacology

Written under the direction of

Professor Zhiyuan Shen, MD., Ph.D. And approved by

_____

_____

_____

_____

New Brunswick, New Jersey

October, 2018

ABSTRACT OF THE DISSERTATION

ROLES OF SETD4 IN RADIATION SENSITIVITY AND TUMORIGENESIS

By XING FENG

Dissertation Director:

Professor Zhiyuan Shen, MD., Ph.D.

The SET domain protein methyltransferases play a critical role in histone modifications and global epigenetic regulations. Recent evidence suggests that some SET domain proteins may have the ability to modify non-histone proteins. The SET domain containing protein 4 (SETD4) was believed to be a non-histone methyltransferase, but no physiological substrate or biological functions of SETD4 has been identified. In this study, we constructed an inducible Setd4 knockout model and investigated the role of Setd4 in radiation sensitivity and tumorigenesis. We found that *Setd4* deficient mice were significantly more resistant to radiation-induced hematopoietic syndrome than littermate wild type mice. Using several long-term bone marrow transplantation assays, we found that Setd4 deficient hematopoietic stem cells (HSCs) and progenitor cells (HPCs) have a slight *in vivo* growth advantage than the wild type cells, but are more sensitive to radiation. We also found that the Setd4 deficient recipient mice have an enhanced ability to engraft

transplanted HSCs, suggesting an improved bone marrow niche for the Setd4 deficient animals. Using a radiation-induced thymic lymphoma model, we also found that Setd4 deletion delayed radiation-induced tumorigenesis. Collectively, our study suggests that Setd4 defect can enhance the recovery of radiation-induced bone marrow damage and suppress radiation-induced thymic lymphoma, and that Setd4 is a new gene involved in regulating bone marrow and hematopoietic functions in mice.

Acknowledgements

Life as a PhD candidate in United States is a stage full of challenges, self-doubt, and achievement. I am very fortunate that I have experienced such precious growth, though there has been really tough time that you probably felt desperate. Over the course of my PhD training, I learned what research is and how to become a scientist. That is why I would like to express my sincere gratitude to my advisor Dr. Zhiyuan Shen for the continuous support of my PhD study and related research, for his patience and immense knowledge. His guidance helped me all through my research and writing of this dissertation. I could not have imagined having a better advisor and mentor for my PhD study.

Besides my advisor, I would like to thank my committee: Dr. Samuel Bunting, Dr. Lisa Denzin and Dr. Ping Xie, not only for their insightful comments and encouragement, but also for the challenging questions which incented me to widen my research from various perspectives.

My sincere thanks goes to Dr. Lisa Denzin, who gave me access to her laboratory and research facilities especially flow cytometer and autoMACS separator. She is so supportive and kind to me. And I would like also to thank people from Dr. Denzin's lab, Dr. Megha Shettigar, who had graduated from Dr. Denzin lab and helped me to set up the multi-color flow cytometric analysis of bone marrow cell populations; and the gentleman Louis Osorio, who helped me to inject bone marrow transplantation cells to recipients. Without their precious and generous support, it would not be easy for me to conduct my project. Also I

would like to thank Dr. Sharon Pine lab, where I learned qRT-PCR technique.

I thank my fellow lab members, Jingmei Liu, for her stimulating discussions, and Dr. Huimei Lu, for her generous advice about mouse model studies. And also it is a great honor to work with my lab mates, Caiyong Ye, Ning-ang Liu, Bochao Liu, and Yuan Wang. My sincere thank also goes to my former lab members, Dr. Jingyin Yue, Dr. Yiyuan Huang and Dr. Roberto Droz, who taught me animal studies in the beginning my study in Dr. Shen's lab. I appreciate the assistance with some of the mouse works provided by Neta Schneider, an undergraduate intern in the lab during the last two years of my study.

Last but not the least, I would like to thank my family: my parents, my sister and brother for supporting me spiritually throughout my oversea study and my life. Although they cannot visit me and be my side all the time, they are always there whenever I need them.

Tables of contents

Abstract ……..… ii

Acknowledgment ……..…… iv

Tables of contents …….…..…….….. vi

List of tables …….…..…….…...… x

List of figures …….…..……. xii

Chapter 1. Introduction ……..……. 1

1.1 Protein Methylation and SET Domain Protein Family ……..…… 1

1.2 Human SETD4, a Putative Lysine Methyltransferase …….……..…… 9

1.3 Hematopoietic Stem Cell Injury by Ionizing Radiation …….…..… 11

1.4 Major Mechanisms of IR-induced HSC Damage and Bone Marrow (BM) Injury ……...… 13

1.5 Radiation Induced Tumorigenesis ...…….…... 23

1.6 Gene Targeting in Mice ……..…. 24

1.7 Mouse Setd4 Gene ……...…….…..… 26

Chapter 2. Rationales and Hypotheses ……...……. 29

Chapter 3. Materials and Methods ……..…….. 31

3.1 Mouse Strains ……..……..…….. 31

3.2 Breeding of Setd4 conditional knockout mice with EIIa-Cre transgenic mice ……..…. 31

3.3 Breeding of Setd4 conditional knockout mice with Rosa26 transgenic mice …… 32

3.4 Breeding of Tp53 mice with Setd4 knockout mice …… 32

3.5 PCR genotyping …… 33

3.6 RNA extraction and qRT-PCR …… 33

3.7 Western blot …… 34

3.8 Tamoxifen treatment …… 34

3.9 Whole body irradiation of mice …… 34

3.10 Histological and immunohistochemically (IHC) analysis …… 35

3.11 Flow cytometric analysis and antibodies …… 36

3.12 Isolation of lymphocytes from mouse peripheral blood …… 38

3.13 Competitive repopulation assay …… 38

3.14 Serial competitive bone marrow transplantation …… 39

3.15 Non-competitive bone marrow reconstituted survival assay …… 39

3.16 Non-competitive HSC dilution survival assay …… 39

3.17 Mouse cytokine protein assay analyses …… 40

3.18 Necropsy analysis …… 40

3.19 RNA-seq …… 40

3.20 RNA-Seq data analysis …… 41

Chapter 4. Establishment of Setd4 Deficient Mouse Models …… 42

4.1 Isolation of conditional Setd4 knockout ES clones by in vitro FLP-

recombination ……...…….……...…..... 42

4.2 Generation of a conditional founder mouse lines with floxed Setd4 exon-6 ……. 47

4.3 Verification of the conditional *Setd4*$^{flox/wt}$ and *Setd4*$^{flox/flox}$ mouse line ……... 49

4.4 EIIa-Cre mediated whole body conditional *Setd4* knockout in mice …...…..... 51

4.5. Generation of Rosa26-CreERT2 Mediated Inducible *Setd4* Knockout Model ……..... 54

4.6 Induced whole body *Setd4* knockout mice were viable and not susceptible to spontaneous tumorigenesis ……...…….....….. 61

Chapter 5. Roles of Setd4 in Radiation Sensitivity and Bone Marrow Regeneration ……... 64

5.1 Deletion of Setd4 protects mice from IR induced bone marrow failure ……. 64

5.2 Setd4 deletion promotes bone marrow recovery from radiation damage ……... 69

5.3 Enhanced erythropoiesis in Setd4 deficient mice spleen post high-dose ionizing radiation …….…….... 74

5.4 Setd4 loss further enhances the survival of p53 deficient mice post IR …...….. 75

5.5 Contribution of the HSC hierarchy in radiation sensitivity ……...…. 78

5.6 *Setd4* deletion confers an improved bone marrow microenvironment to support HSC transplantation …….…….... 91

Chapter 6. Roles of Setd4 in Radiation Induced Tumorigenesis ……..……...…….. 95

6.1 Loss of *Setd4* extends the survival of radiation-induced thymic lymphoma ….. 95

6.2 Setd4-deficient thymic lymphomas were more disseminative in peripheral organs 99

6.3 Distinct subtypes of thymic lymphoma in *Setd4*$^{\Delta/\Delta}$ mice 102

6.4 Insignificant change of the suppressive immunological environment in Setd4 deficient lymphoma 103

6.5 Generation of Setd4 and Tp53 double deficient mice 105

6.6. Setd4 deletion does not affect spontaneous tumorigenesis in p53 deficient mice 106

6.7 Setd4 deletion does not delay radiation-induced tumorigenesis in p53 knockout mice 111

Chapter 7. Discussion and Future Directions 115

References 125

List of tables

Table 1	The major classes of SET-domain protein lysine methyltransferases and their substrates	4
Table 2	Summary of mouse lines	31
Table 3	List of antibodies used in bone marrow study	37
Table 4	Antibody cocktails and their compositions	38
Table 5	Number of chromosomes on metaphase spreads of *Setd4*-exon 6 conditional clones	45
Table 6	Primers used for SETD4 genotyping	46
Table 7	Primer pairs and anticipated PCR products for different genotypes of ES clones	47
Table 8	Number of screened newborns of chimera mice generated from trapped *Setd4* ES clone	48
Table 9	Primer pairs and anticipated PCR products with different mouse genotypes	48
Table 10	Genotype distribution of newborns (Male: $Setd4^{flox/wt}$;$EIIaCre^{+/-}$; Female: $Setd4^{flox/flox}$;$EIIaCre^{-/-}$)	52
Table 11	Genotype distribution of newborns (Male: $Setd4^{flox/flox}$;$EIIaCre^{-/-}$; Female: $Setd4^{flox/wt}$;$EIIaCre^{+/-}$)	52
Table 12	Genotype distribution of newborns (Male: $Setd4^{flox/wt}$;$EIIaCre^{+/-}$;	

Female: *Setd4*$^{flox/wt}$;*EIIaCre*$^{+/-}$) 53

Table 13 Genotype distribution of embryos (Male: *Setd4*$^{flox/wt}$;*EIIaCre*$^{+/-}$; Female: *Setd4*$^{flox/wt}$;*EIIaCre*$^{+/-}$) 53

Table 14 SETD4 antibodies tested in this study 59

Table 15 Synopsis of Aged Mice (>19 months) Necropsy Outcomes 63

Table 16 Survival of transplanted recipient mice 93

Table 17 Infiltration of thymic lymphoma in peripheral organs 99

List of figures

Figure 1: Lysine methylation modification by KMTs and its reversible process by KDMs …… 2

Figure 2. Predicted 3D structure of human SETD4 (left) by the program at the I-TASSER server …….. 9

Figure 3. Dose-dependent response to ionizing radiation in mice …….. 15

Figure 4. Mouse genomic location of Setd4 gene ……..……. 27

Figure 5. Domain structure of mouse SETD4 ……..…….. 27

Figure 6. Sequence alignment of mouse and human SETD4 protein ……...…….. 28

Figure 7. Genomic structure of the trapped *Setd4* allele in an ES clone …… 42

Figure 8. Generation of LoxP-flanked conditional *Setd4*-exon 6 (*flox*-Exon6) allele from the trapped Setd4 allele by FLP-mediated recombination in ES cells ...……. 44

Figure 9. PCR genotyping strategy and primer location for ES clone screen …….…... 45

Figure 10. Representative PCR result of germ-line transmission of *Setd4* flox-Exon6 allele ……..…… 48

Figure 11. Verification of Setd4 exon 6 deletion …….……...……. 50

Figure 12. Representative PCR genotyping of EIIa-Cre mating …….…… 51

Figure 13. Kaplan-Meier survival curves of $Setd4^{\Delta/flox};EIIaCre^{+/-}$ and $Setd4^{\Delta/wt};EIIaCre^{+/-}$ mice ……...……..……. 54

Figure 14. Strategy and verification of Cre-mediated Setd4 exon 6 deletion in mice 57

Figure 15. Confirmation of Setd4 knock out after tamoxifen treatment ……..…… 60

Figure 16. Survival of *Setd4*$^{flox/flox}$ and *Setd4*$^{\Delta/\Delta}$ mice ……..…… 62

Figure 17. Kaplan-Meier survival of conditional mice treated with tamoxifen before total-body γ-irradiation ……..……. 66

Figure 18. Kaplan-Meier survival of control mice treated with tamoxifen ……..... 67

Figure 19. Kaplan-Meier survival of conditional mice treated with tamoxifen before 13 Gy of total-body γ-irradiation ……...…. 68

Figure 20. Kaplan-Meier survival of long-term survival of the *Setd4*$^{\Delta/\Delta}$, *Setd4*$^{\Delta/wt}$, and control mice that survived 30 days after the 8Gy initial irradiation ……..... 69

Figure 21. Bone marrow cell counts of HSCs and HPCs after 8 Gy of irradiation …..… 71

Figure 22. Myeloid and lymphoid progenitor counts after 8 Gy of irradiation ……..…. 73

Figure 23 Splenic erythropoiesis post high-dose of ionizing radiation …….…….. 77

Figure 24 Comparative survival of *Setd4*$^{\Delta/\Delta}$ and *p53*$^{\Delta/\Delta}$ mice to total-body γ-irradiation ……. 78

Figure 25. *Setd4*$^{\Delta/\Delta}$ reconstituted mice are significantly more sensitive than *Setd4*$^{flox/flox}$ reconstituted mice given 8 Gy TBI ……..…… 80

Figure 26. Radiation sensitivity of engrafted *Setd4*$^{\Delta/\Delta}$ HSCs ……..……. 85

Figure 27. Radiation sensitivity of engrafted *Setd4*$^{\Delta/\Delta}$ HSCs (Part II) ……...…….. 86

Figure 28. *Setd4*$^{\Delta/\Delta}$ HSCs are functionally comparable ……..……. 88

Figure 29. *Setd4*$^{\Delta/\Delta}$ HSCs are functionally comparable (Part II) ……..…… 90

Figure 30. Survival rate of lethally-irradiated recipient mice after transplantation of Lin^{-}

bone marrow donor cells ……...…….. 93

Figure 31. Characterization of radiation-induced thymic lymphoma …….……. 96

Figure 32. Loss of *Setd4* delays radiation-induced thymic lymphoma …… 98

Figure 33. Kaplan-Meier survival of wild type mice treated with tamoxifen ……..… 98

Figure 34. Setd4 deficiency enhances dissemination of thymic lymphoma to peripheral tissues ……..……... 101

Figure 35. Different subtypes of thymic lymphoma in $Setd4^{\Delta/\Delta}$ mice ……..…..…… 103

Figure 36. Insignificant MDSC infiltration in thymic lymphoma ……..…...…… 104

Figure 37. Genomic structure of conditional Tp53 allele …….…..…... 105

Figure 38. Kaplan-Meier survival of $p53^{\Delta/\Delta}$ and $Setd4^{\Delta/\Delta}$; $p53^{\Delta/\Delta}$ mice ……. 108

Figure 39. Tumor type distribution in p53 mutant mice ……....…… 109

Figure 40. Histopathology and IHC of representative tumors from $Setd4^{\Delta/\Delta}$; $p53^{\Delta/\Delta}$ mice 109

Figure 41. Kaplan-Meier survival of $p53^{\Delta/wt}$ and $Setd4^{\Delta/\Delta}$; $p53^{\Delta/wt}$ mice ……...…… 110

Figure 42. Loss of p53 abrogates the delayed development of radiation-induced thymic lymphoma in Setd4 deficient mice …… 112

Figure 43. Loss of p53 abrogates the delayed development of radiation-induced thymic lymphoma in Setd4 deficient mice …….……...…… 113

Chapter 1, Introduction

1.1 Protein Methylation and SET Domain Protein Family

In recent years, lysine methylation of histones and non-histone proteins has emerged as a very important posttranslational modification in diverse biological processes. It is now recognized that this modification plays fundamental roles in transcriptional regulation (1-4), heterochromatin formation (5,6), X chromosome inactivation (7), DNA damage response (8,9), and in the epigenetic regulation of cell identity and fate (7,10). Distinct from other posttranslational modifications, lysine methylation occurs with three different configurations. The ε-NH_2 on lysine may be modified by one, two, or three methyl groups to form mono-, di-, or tri-methylated lysine (Kme1, Kme2, and Kme3), respectively. These incremental methylation states afford diverse regulatory functions and have the potential to lead to diverse biological outcomes through reader molecules. Lysine methylation is catalyzed by lysine-specific methyltransferases (KMTs) and reversed by lysine demethylases (KDMs) (**Figure 1**). The human genome encodes an estimated 52 KMTs and 32 KDMs (11-13), and many of which are evolutionarily conserved. In many instances, lysine methylations are mediated by a class of proteins known as lysine methyltransferases (KMTs). Most of KMTs harbor a predicted Su(var)3-9-Enhancer of zeste–Trithorax (SET) domain which transfers a methyl group from S-adenosylmethionine (AdoMet, or SAM) to the ε-amine on the side chain of the lysine residue.

Many studies have established that functional defects of KMTs can lead to cancer (14,15), neurological disorders (16), and other human pathologies. In 2000, the first KMTs, mammalian SUV39H1 and its *Schizosaccharomyces pombe* homolog, Clr4, were reported (4,17), representing a milestone in the field of lysine methylation. From then on, numerous SET domain-containing molecules have been identified and found to be novel lysine methyltransferases in various species, including viruses, bacteria, yeast, fungi, and other multicellular organisms. All of the identified KMTs are SET domain-containing molecules. However, Dot1/Dot1L is the sole exception, which dosen't have a SET domain (18), and it methylates Lys 79 of histone H3 (19). Herein I will summarize the most recent findings on these KMT proteins.

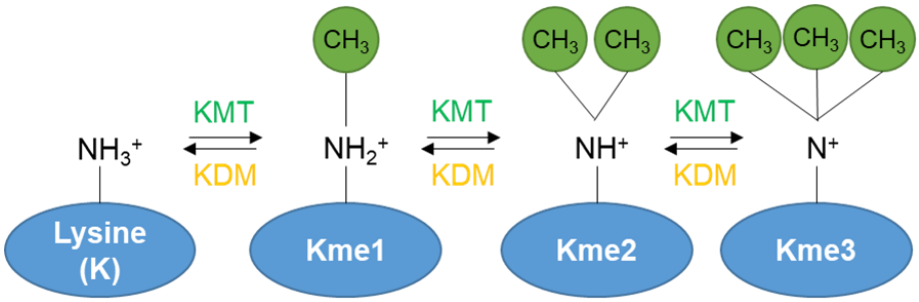

Figure 1: Lysine methylation modification by KMTs and its reversible process by KDMs.

Structure of the SET-domain protein lysine methyltransferase superfamily. KMTs exist in all eukaryotes studied to date. This protein family is characterized by an approximately 130 amino acid-long module called the SET domain, which was named after the *Drosophila* proteins **S**uppressor of variegation 3–9 (Su(var)3–9), **E**nhancer of zeste (E(z)), and **T**rithorax (Trx) (20). Most lysine methyltransferases catalyzes methyl transfer by way

of the SET domain. The SET domain structure is composed of three groups of canonical β-sheets arranged in a triangular fashion with a group of 2 β-sheets closely neighboring a conserved α-helix defining a cleft for the binding of the lysine-(histone) ligand (21,22). The cofactor S-Adenosylmethionine (AdoMet, or SAM) and substrate bind at two adjacent sites of the SET domain. The methyl donor AdoMet binds to a distinct pocket located on the one side of the SET domain. Both AdoMet and the l-lysine-[histone] are connected through a narrow tunnel where the methyl group is channeled.

It has now become increasingly clear that the SET domain does not generally exist as an independent entity, as in many proteins it co-occurs with other protein domains to exert their catalytic activities. Moreover, some SET domain-containing proteins are found in complexes or interact with proteins that regulate their target specificity and catalysis, such as SET1/MLL (23,24) and EZH2 (25), are only functional within large heteromeric complexes whose subunits have a pivotal role in defining their respective substrate and product specificities.

Classification of the SET-domain protein of lysine methyltransferase superfamily. The grouping of the KMTs based on sequence similarity of their SET domains often closely reflects an already reported specificity for certain substrates. A partial list of currently known SET-domain proteins and their substrates are exemplified in **Table 1**.

Table 1. The major classes of SET-domain protein lysine methyltransferases and their

substrates.

	Histone substrate	Non-histone substrate	Reference
SET1/MLL family			
MLL1	H3(K4)		
MLL2			
MLL3			
MLL4			
SETD1A		HSP70	(26)
SETD1B		TAT	(27)
SUV39 family			
SUV39H1	H3(K9)		
SUV39H2			
G9a		P53 RuvBL2 DNMT1 DNMT3a G9a GLP	(28) (29) (30) (10) (31) (10)
GLP		P53 DNMT3a	(28) (10)
SETDB1		P53	(32)
SETDB2			
EZ family			
EZH1	H3(K27)		
EZH2		STAT3 GATA4	(33) (34)
SET2/NSD family			
NSD1	H3(K36)	RELA/P65	(35)
NSD2			
NSD3		EGFR	(36)
SETD2			
SUV420 family			
SUV420H1	H4(K20)	CBX4/PC2	(37)
SUV420H2			
PRDM family			
PRDM3	H3(K9)		

PRDM16			
SMYD family			
SMYD2		P53 RB1 HSP90	(38) (39) (40)
SMYD3	H4(K5)	MAP3K2 VEGFR	(41,42)
Others			
SETD7	H3(K4)	P53 RB1 E2F1 RELA/p65 TAF10 YAP STAT3 FoxO3	(43,44) (45) (46) (47) (48) (49) (48) (50)
SETD3	H3(K36)		(51,52)
SETD6		RELA/p65	(53,54)
SETD4	H4(K20)		(55)

***The SET1/MLL family*.** The members of the mixed lineage leukemia (MLL) family of KMTs are the mammalian homologs of the Drosophila Trithorax proteins, which specifically methylate lysine 4 of the histone H3 protein (responsible for H3K4me1/me2/me3) (56) and regulate gene transcription during embryogenesis and development. The MLL family consists of several members. In humans, it includes MLL1 (KMT2A), MLL2 (KMT2D), MLL3 (KMT2C), MLL4 (KMT2B), MLL5 (KMT2E), SET1A (KMT2F), and SET1B (KMT2G). Although harboring a SET domain, no methyltransferase activity has been reported for MLL5 (KMT2E) so far. Like EZH2, MLL proteins function in the context of large protein complexes. Namely, six members of this SET/MLL family exhibit relatively moderate-to-weak enzymatic activity as recombinant

domains *in vitro* but are markedly and variably enhanced by association with core subunits shared by the entire family (57,58). The minimal subunit complex is comprised of WDR5, RbBP5, ASH2L, and DPY30 (WRAD), which can enhance the methyltransferase enzymatic activity of recombinant SET domains of all six family members.

The deletion or truncation of different MLL proteins in mice leads to distinct phenotypes, which indicates that the proteins are not redundant but instead they have specific cellular functions. MLL1 (KMT2A) (57) and MLL4 (KMT2B) (59) are mainly responsible for H3K4me3 at the promoters of genes and regulation of gene expression. In contrast, MLL3 (KMT2C) and MLL2 (KMT2D) (60) mainly introduce a single methyl group on lysine 4 of H3 at the enhancers and promoters of target genes. The SET1A and SET1B proteins are mammalian orthologs of yeast Set1 and they contribute to the bulk of H3K4 trimethylation in mammals (61). Due to the role of the first-found member KMT2A in this disease, the human Set/MLL family was initially named the mixed-lineage leukemia (MLL) family (62).

The SMYD family. SET and MYND domain-containing proteins (SMYD) are a special class of protein lysine methyltransferases involved in methylation of histones and non-histone targets. So far, five members of the SMYD family, SMYD1–5 were identified (63-66). In all of the available SMYD structures, SMYD proteins share a homologous bilobal structure separated by a non-conserved primary sequence of variable length. The N-terminal lobe is divided into four domains: SET, MYND, SET-I, and post-SET. The

catalytic SET domain is located in the middle of the N-terminal lobe in proximity to the C-terminal lobe. The C-terminal lobe is organized into helices that were found to be orientated in open or closed conformations. The MYND domain functions as a zinc finger motif which binds to proline-rich regions serving as a protein–protein interaction module (67). In SMYD proteins, the MYND domain is part of the N-terminal lobe that interacts with the catalytic SET domain, but it does not participate in substrate or cofactor binding. Another feature is the C-terminal domain (CTD) found in SMYD1–4 which is structurally similar to tetratricopeptide repeats (TPR). SMYD proteins are initially believed to play a role in myogenesis (68) and cardiomyocyte differentiation (69) by acting as an epigenetic regulator because they are abundantly expressed in cardiac and skeletal muscle. Current data indicate that SMYD proteins are related to carcinomas (65,70) and cardiovascular diseases (71).

SETD7 (SETD7/9). Originally isolated from HeLa nuclear extracts, Set7 (also known as Set9, or Set7/9, or KMT7) is a 41 kDa lysine-specific SET-domain methyltransferase encoded by a gene conserved in vertebrates (72). Similar to MLL1 and SET1, human SET7/9 was initially isolated as an H3K4-specific KMT (73). Despite the initial characterization of Set7 as a histone H3-specific lysine methyltransferase, the physiological validity of histone H3 as a biochemical substrate has been recently questioned. Recent experimental findings indicate that SET7 methylates recombinant full-length H2A and H2B peptides (74) and linker histone variant H1.4 (75).

In addition, recent investigation of Set7 target specificity revealed numerous non-histone substrates and additional mechanisms of transcriptional regulation by modification of specific transcription-associated proteins (43,76,77). Also, dimethylation by Set7 unexpectedly reported for the two novel substrates: signal transducer and activator of transcription 3 (STAT3) (48) and Msx2-interacting protein (MINT) (74), questioning the classification of SET7 as exclusively a monomethylase. After examining all of non-histone Set7 substrates, a consensus recognition motif: [K/R]-[S/T/A] preceding the modified lysine was proposed to account for the selective methyltransferase substrates (78). According to this motif, DNMT1 (73), TAF10, p53, and ERα were successfully identified as an in vitro substrate. Methylation of non-histone protein will likely receive increased attention. Characterization of *in vivo* substrates is an avenue of investigation that deserves further attention as such studies have revealed numerous novel SET7 and target promoter associations.

Embryonic lethality of SET7 knockout mice indicates an important role of SET7 in development. Transcriptional activation of the SETD7 promoter mediated through an islet-specific enhancer element was shown to be PDX1-dependent in β-cells (79). Similarly, SET7 expression affects skeletal muscle differentiation (80). Thus, SET7 may function in development through cellular differentiation and tissue-specific gene activation.

1.2 Human SETD4, a Putative Lysine Methyltransferase

The human SETD4 gene is located at the 21q22.13, which transcribes an mRNA of 3001 bp. The predicted human SETD4 protein consists of 440 amino acids and has a molecular weight of 44 KD. The encoded protein has a SET domain at its N-terminus (amino acids 59–273) and a Rubis-subs-bind domain at its C-terminus (amio acids 307–425). The Rubis-subs-bind domain, also referred to as the Rubisco LSMT substrate-binding domain, permits the binding of the protein to a substrate, such as the N-terminal tails of histones and other targets. Based on structural modeling, we predicted that human SETD4 shares highly similarity of conformational features as human SETD3 protein, which has been already reported (**Figure 2**).

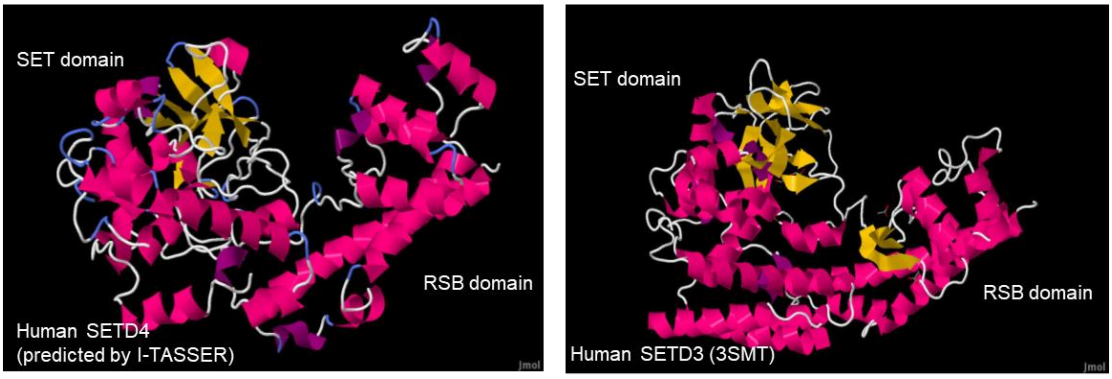

Figure 2. Predicted 3D structure of human SETD4 (left) by the program at the I-TASSER server. The SET domain and the enzymatic activity center (yellow ribbon) and the RSB domain are shown. As shown here, it has a similar structure as the recently solved structure of the SETD3 protein (right).

SETD3, SETD4 and SETD6 can be grouped into methyltransferase class VII, which represents classical non-histone SET domain methyltransferases (81); proteins of this class are most similar to the plant Rubisco methyltransferase. The comparative analysis of the 3D molecular models of SETD4 and SETD3 supports the hypothesis of SETD4 as a functional lysine methyltransferase. However, its specific substrates and modification sites remain to be identified.

***Potential roles of SETD4 in cancer*.** By virtue of its SET domains, the *Artemia* SETD4 homologue (ar-SETD4) mediates trimethylation of H4K20 (H4K20me3) (55). Ar-SETD4, was found to be overexpressed abundantly in Artemia diapause embryos, in which cells were in a quiescent state. The knockdown of Ar-SETD4 reduced the level of H4K20me3 significantly, promoted cell division and thereby and prevented the formation of the cell cycle arrested quiescent diapause embryos (55). Dai et al further showed a catalytic activity of Ar-SETD4 by an *in vitro* histone methyltransferase (HMT) assay (55). This study provides insights into the function of the human SETD4 and the mechanism of cell quiescence regulation. Although Faria et al reasoned that SETD4 might be grouped into classical non-histone SET domain methyltransferase (81), Dai et al obviously points out the effect of SETD4 on the histone protein modification.

The regulation of cell quiescence is shown to be involved in cancer development. Moreover, tumors typically show a multitude of epigenetic abnormalities, including the global loss and regional alterations in histone methylation. Faria et al showed elevated

expression levels of SETD4 in several breast cancer cell lines and in breast cancer with a lack of the estrogen receptor (ER) (81). SETD4 in breast cancer cell lines significantly stimulated their proliferation and cell cycle progression without affecting apoptosis, suggesting an involvement of SETD4 in cell cycle regulation (81). Similarly, Li et al found that SETD4 upregulated AKT phosphorylation, inhibited HCC cells death, and reduced the sorafenib sensitivity (82). Zhu et al indicated that SETD4 has an anti-apoptotic role in the androgen-independent prostate cancer (PCa) cells (83). Together, all of these data imply that SETD4 is an oncogene and could be a novel molecular target for the development of new strategies for the diagnosis and treatment of breast cancer. Other study suggests that SETD4 might be related to Down syndrome (DS) (84), caused by trisomy 21, a the most common chromosomal disorder associated with developmental cognitive deficits.

Although accumulated information about function of SETD4 *in vitro*, to our knowledge, role of SETD4 *in vivo* has rarely been reported. The aim of this project is to determine the biological functions of SETD4 through its inactivation in mouse, so that role of Setd4 in mouse development and tumorigenesis can be elucidated.

1.3 Hematopoietic Stem Cell Injury by Ionizing Radiation

Ionizing radiation (IR) is probably the one of most extensively studied environmental hazards. It has been well established that exposure to a moderate or high dose of IR leads

to hematopoietic stem cell (HSC) and hematopoietic progenitor cells (HPCs) injuries, which are the primary cause of death. Protecting HSCs from IR should be a primary goal in the development of novel medical countermeasures against radiation, as it could cause high mortality and morbidity and worsen the outcome of cancer treatment. Apoptosis and mitotic catastrophe in HSCs and HPCs are primarily responsible for IR-induced acute bone marrow (BM) failure (85). Long-term BM suppression caused by IR is mainly attributable to the induction of HSC senescence (86,87). However, the damage to the HSC niche and the promotion of HSC differentiation also contribute to both the long-term and acute effects of IR on the hematopoietic system (88). In recent years, management of acute myelosuppression has been significantly improved by the use of various hematopoietic growth factors such as IL-6 (89), IL-12 (90), and thrombopoietin (91). These factors have been demonstrated to promote the recovery of BM hematopoietic function primarily by stimulating HSC and HPC proliferation and differentiation. These findings will provide new opportunities for developing a mechanism-based strategy to prevent and mitigate IR-induced BM suppression.

After the discovery of X-rays in 1895, Warren and Whipple and Shouse et al. first reported the devastating effects of IR by exposed dogs to a high dose of X-rays. They found that IR-induced hematopoietic failure led to the death of the dog after exposure to a high dose of total body irradiation (TBI). The pioneering studies in 1940s by Jacobson and his colleagues indicated that lead shielding of the spleen or one entire hind leg or

transplantation of splenocytes protected mice from the lethal effect of IR (92). Lorenz et al. soon described a similar finding in which intravenous infusions of bone marrow (BM) cell suspensions protected mice against IR injury (93). And it was further demonstrated that the radioprotective effects of the spleen and BM cell suspensions were not ascribed to a "humoral factor" but the transplanted cells. The identity of those cells that protected animals from IR-induced lethal hematopoietic damage was unknown until Till and McCulloch discovered hematopoietic stem cells (HSCs) in the early 1960s (94). They found that HSCs not only are sensitive to radiation but also can self-renew, which produces multiple lineages of progeny after transplantation into lethally irradiated animals. This landmark discovery laid the foundation for radiation biology and modern stem cell research. Since then, our understanding of the mechanisms by which IR causes hematopoietic damage has been expanded significantly. Some of the mechanisms of action of IR on HSCs are summarized as follows.

1.4 Major Mechanisms of IR-induced HSC Damage and Bone Marrow (BM) Injury

Cell and tissue injury as a result of exposure to IR occurs by the direct ionization of cellular macromolecules or by the reaction of macromolecules with free radicals. Because of the formation of various reactive oxygen species (ROS), free radical-mediated cell injury can be enhanced in the presence of oxygen. In addition, reaction with free radicals/ROS and

ionization damage the structure and function of lipids, DNA, and proteins, which lead to metabolic and functional alterations and ultimately to a cell injury or death. Among various macromolecules, DNA is considered to be the most critical molecular target for IR-induced cell injury and death (95).

As summarized in **Figure 3**, after exposure to a significant dose of TBI, a series of characteristic clinical complications termed the acute radiation injury appear. TBI doses in the range of 3–10 Gy causes the bone marrow injury occurs in mice, which is due to severe depletion of blood elements resulting from BM suppression. The radiation doses over 5.5 Gy of TBI leads to the gastrointestinal injury, while the brain injury occurs following larger doses of TBI (above 20 Gy), indicating that the hematopoietic system is the most radiosensitive tissue of the body (**Figure 3**). A moderate dose (< 4 Gy) of TBI typically causes transient myelosuppression, which primarily results from the damages of HPCs and MPPs because they are rapidly proliferating and thus highly sensitive to IR (96,97). However, exposure to a high dose makes persistent myelosuppression, or BM failure due to severe injury to HSCs.

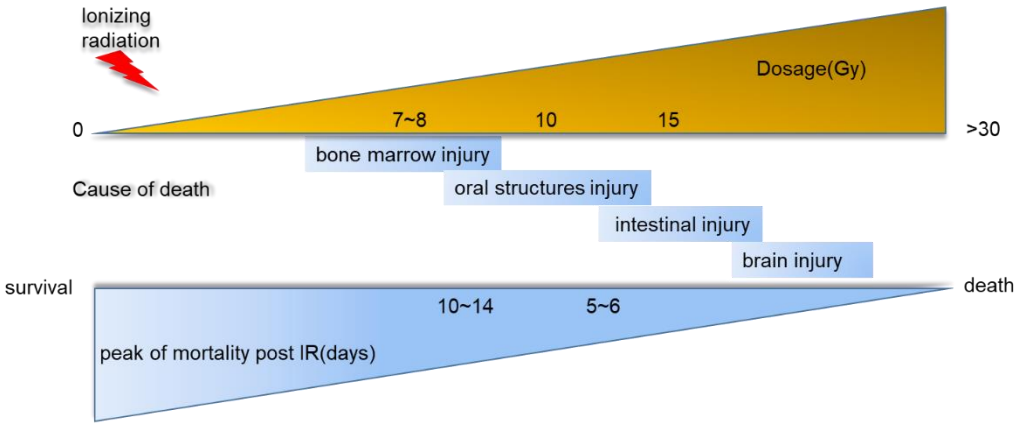

Figure 3. Dose-dependent response to ionizing radiation in mice.

The mode of radiation induced cell death is determined by the type of radiation, the dose of radiation to which the cells are exposed, and the molecular profile of the cells. Several mechanisms have been proposed to explain how IR induces HSC injury, including: 1) HSC cell death; 2) HSC differentiation; 3) HSC senescence; and 4) Damage to the HSC niche.

IR-induced cell death. Radiation-induced apoptosis is considered to be one of the main cell death mechanisms following exposure to irradiation. The significance of p53 in early apoptosis has been reported in several studies (98-101). Wild-type p53 thymocytes were found to be extremely radiosensitive, whereas thymocytes lacking functional p53 were radiation-resistant (98). Radiation-induced p53-dependent apoptosis occurs within a few hours following irradiation exposure in the interphase as a premitotic event without the requirement of cell division (102). Radiosensitive tissues generally have high basal p53

mRNA expression and are more prone to respond to radiation exposure with induction of apoptosis (103-108). Accordingly, tumors from tissues highly susceptible to apoptosis more commonly respond to radiation with the induction of p53-dependent apoptosis (109). Suppression of p53 in these tumors results in resistance to treatment and clinical data indicate that presence of a wild-type p53 in these tumors is a favorable prognostic marker (110).

The intrinsic apoptotic pathway, also called the mitochondrial pathway, involves mitochondrial outer membrane permeabilization (MOMP) that disrupts the mitochondrial function. MOMP is mainly controlled and mediated by members of the Bcl-2 family (111). This family is divided into pro-apoptotic members and anti-apoptotic members. The pro-apoptotic members comprise two subfamilies, the Bax-like family (Bax, Bak, Bok) and the BH3-only proteins (Bid, Bad, Bim, Bik, Bmf, Noxa, Puma, Hrk), which both seem to be required to promote induction of apoptosis by formation of Bax–Bak pores in the mitochondrial outer membrane. Following exposure to radiation, p53 activates transcription of proapoptotic genes, the most important being proapoptotic members of the Bcl-2 family (112,113). Bax as well as members of the BH3-only subgroup appear to play a critical initiating role in radiation-induced apoptosis and have also been shown to be rate-limiting for gamma-radiation induced apoptosis in several cell types (114-116). Puma has been shown to be essential for cell death triggered by ionizing radiation in hematopoietic cells (117,118), lymphoid cells (119). Additionally, Noxa and Bim are other BH3-only

proteins which contribute to radiation induced p53-dependent apoptosis. Also, genes encoding proteins which localize to the cytoplasm including PIDD (p53-inducible death domain) can be transcriptionally upregulated in a p53-dependent way following an apoptotic stimulus (120). Finally, expression of genes that lower the apoptotic threshold can be induced in a p53-dependent way.

The extrinsic apoptotic pathway has also been implied in radiation-induced apoptosis. This pathway is often referred to as the death receptor pathway and requires ligand-dependent activation of plasma-membrane receptors from the TNF receptor superfamily. The expression of TNF death receptor family members Fas/CD95 (121,122), DR5/TRAIL receptor 2 (123) can be upregulated by radiation and activate caspases by mitochondria-dependent and independent mechanisms. The interaction between specific ligands and the death receptors induces receptor-proximal recruitment of the death-inducing signaling complex. The resulting activation of caspase-8/10 leads to cleavage and activation of effector caspase-3, caspase-6, caspase-7, which subsequently cleave cell death substrates. Caspases-8/10 cleave and activate the pro-apoptotic Bcl-2 family member Bid, which triggers cytochrome c release from the mitochondria and subsequent activation of caspase-9 and caspase-3, strongly amplifying the initial apoptotic signal (124).

Upon DNA damage, hematopoietic stem cells (HSCs) elicit a strong activation of p53, resulting in enhanced activation of proapoptotic signals. ASPP1, an apoptosis-stimulating protein of p53, is highly expressed in HSCs, which selectively induces apoptosis to

preserve HSC pool integrity (125). Recent studies also report many novel findings about the regulation of HSCs apoptosis during IR. Exposure to γ-radiation causes damage to DNA, lipids, and protein in mammalian cells. DNA damage poses a constant threat for maintenance of HSCs. Radiation initiates an intrinsic apoptotic program by inhibiting Bcl-2 family antiapoptosis factor Mcl-1, Bcl-2, and Bcl-x, causing a conformational changes in Bax and Bak proteins, thereby leading to apoptosis. It is well-known that Bcl-2 overexpression increases HSC number and repopulation potential in lethally irradiated mice (126). MicroRNA had been shown to play a key role in radiation-induced apoptosis through directly targeting Mcl-1 or other apoptosis-related proteins in hematopoietic cells (127). In the response to IR, Xeroderma pigmentosum, complementation group G (XPG), encoded by the gene Ercc5, was significantly upregulated in mRNA and protein levels. As a component of the core machinery of nucleotide excision repair (NER), upregulated XPG significantly reduced the number of HSCs and early hematopoietic progenitors after sub-lethal doses of IR by upregulating DNA damage response effector genes such as p21 or Noxa and inducing apoptosis (128). Ppm1d, the gene encoding Wip1 phosphatase, is expressed in hematopoietic progenitors and stem cells in bone marrow and peripheral blood. Recent study indicates that Wip1 is a key negative regulator of DNA damage response and p53 signaling pathway. It is also essential for normal development and differentiation of hematopoietic cells by targeting p53, ATM, NFkB, p38MAPK kinase, and mTOR signaling (129). Additionally, TGF-β1 slowed down the cell cycle progression of HSCs and suppressed their self-renewal potential, revealing a negative role in the regulation of

the HSC number and reconstitution activity (130). Together, given that the epigenetic processes are known to regulate HSCs functional changes including apoptosis, it will be important to identify and study new epigenetic cofactors that have the ability to regulate maintenance of hematopoietic stem cells during IR.

Mitotic catastrophe is a form of cell death that occurs during or as a result of an aberrant mitosis (131). The mitotic catastrophe is highly cell-type dependent and is executed by most non-hematopoietic tumor cells in response to ionizing radiation and is frequently observed in experimental tumors following radiotherapy and radioimmunotherapy.

IR-induced cell differentiation. HSCs not only have the ability to self-renewal but also differentiate into multiple lineages of blood cells. Given that inhibition of HSC differentiation can increase HSC self-renewal whereas promotion of HSC differentiation has an opposite effect that may lead to HSC premature exhaustion and BM failure, these two functions have to be tightly regulated. Furthermore, HSC differentiation to different lineages of blood cells has to be balanced to prevent lineage skewing. Whether IR affects HSC differentiation was not known until a recent study reported by Wang et al. (132). In this study, it was found that DNA damage after exposure to IR in HSCs depleted HSCs and stimulated the differentiation to lymphoid lineage by activating the granulocyte colony-stimulating factor (G-CSF)/Stat3/BATF-dependent differentiation checkpoint in HSCs (132). G-CSF knockout, Stat3 knockdown, or BATF deletion abolished the response to IR

and improved HSC self-renewal and function. More importantly, after the activation of the G-CSF/Stat3/BATF-dependent differentiation checkpoint by IR, lymphoid-biased HSCs were more sensitive to the differentiation induction than myeloid-biased HSCs, which leads to myeloid skewing in irradiated mice. Therefore, the HSC differentiation via the G-CSF/Stat3/BATF pathway not only a causal factor for IR-induced myeloid lineage skewing but also plays an important role in mediating IR-induced HSC injury. Even though inhibiting the G-CSF/Stat3/BATF-pathway can significantly decrease IR-induced HSC injury due to the suppression of IR-induced HSC differentiation, it also causes the accumulation of DNA damage in HSCs (132), which may increase the risk of HSC transformation and leukemia development after IR. Therefore, targeting this pathway may have limited utility as radiation protectants.

IR-induced cell senescence. Senescence is a term used to describe a condition of permanent cell cycle arrest (133). Senescence commonly occurs in normal cells that have reached their proliferative limit as a consequence of telomere shortening. Telomere attrition is recognized as damaged DNA and initiate growth arrest referred to as replicative senescence. Senescent cells display characteristic phenotypic traits as they become enlarged and flattened with an increased granularity (133). Senescence has also been reported to occur in tumor cells in vitro and in experimental tumors *in vivo* following extensive cellular stress induced by a number of DNA damaging agents including radiation (134). Some clinical evidence of prolonged cytostatic arrest in prostate cancer and

desmoids tumors following radiation therapy also indicate senescence as a major mechanism for regression of patient's tumors. Accordingly, cellular senescence remains of significance as a radiation-induced mechanism to inhibit tumor cell growth.

The most accepted and used marker for senescence is the staining for senescence-associated β-galactosidase of lysosomal compartments in the perinuclear region of senescent cells (135). However, molecules involved in the DNA damage response (DDR) as well as novel markers obtained from microarray studies have also been used as surrogate markers of this process (136). In response to low doses of radiation, a DDR is induced. This continuous DDR and the consequent activation of senescence prevent damage from being propagated to the next cell generation. This type of damage-induced senescence has been referred to as accelerated senescence and is not dependent on telomere erosion.

The earliest evidence of HSCs undergoing senescence comes from the observation of *Bmi1* inactivation mice. It was found that *Bmi1* deficient mice developed progressive BM hypoplasia and died early (< 2 months) after birth (137), and HSCs from $Bmi1^{-/-}$ mice express increased levels of p16 and Arf. Replicative senescence has been reported to depend on the activation of two major tumor suppressor pathways controlled by p16/pRB (138,139) and p53/p21 (140,141). Both these signaling pathways can initiate but are also important for the maintenance of the senescence associated growth arrest. More studies demonstrated that IR can selectively induce HSC senescence (142).

Damage to the HSC niche. The HSC niche significantly contributes to the maintenance of HSC self-renewal capacity and reserves (143-145). IR-induced damage to the HSC niche not only causes HSC injury but also affects the recovery of HSCs after IR. IR-induced BM stromal cell damage is at least in part attributable to the induction of senescence because Carbonneau et al. reported recently that exposure of mice to IR induced senescence in BM stromal cells in a p16/Arf-dependent manner (146). The induction of BM stromal cell senescence contributes to IR-induced residual damage to BM environment that can influence hematopoiesis.

IR damage to the HSC niche and HSCs were also underwent intensive studies. It was reported that BM endothelial cells (ECs) are highly sensitive to IR (147). Exposure of a sublethal dose of TBI resulted in regression of ECs while exposure to a lethal dose of TBI induced severe damage to ECs in mice and required BM transplantation to regenerate. In contrast, transplantation of endothelial cells into lethally irradiated mice improved their survival by promoting HSC regeneration and hematopoietic recovery. Similarly, transplantation of the endothelial progenitor cells into irradiated mice not only accelerated the recovery of the vascular niche but also promoted HSC reconstitution(148). Compared to BM ECs, endosteal osteoblasts, a major component of the osteoblastic niche, are relatively radioresistant. After BM myeloablation, endosteal osteoblasts underwent rapid expansion in response to megakaryocyte-derived mesenchymal growth factors and basic fibroblast growth factor to promote hematopoietic reconstitution and HSC engraftment

after BM transplantation by restoring the damaged HSC niche (149). Also, it has still to be determined whether IR can also cause damage to other cells in the HSC niche.

1.5 Radiation Induced Tumorigenesis

IR is a complete carcinogen that is capable to initiate and promote neoplastic progression (150). Exposure of mice to four weekly doses of 1.5 to 2 Gy γ-irradiation elicits thymic lymphoma due to oncogenic mutations resulting from DNA double strand breaks (151). The transformation of oncogenesis begins from hematopoietic stem/progenitor cell in the bone marrow, not necessary thymocyte (151). So shielding part of bones or transplanting healthy hematopoietic stem/progenitor cells subsequently could ablates the tumorigenesis (152,153). However the mechanism of promotion is poorly understood.

The thymic lymphomagenesis induced by γ-irradiation is markedly enhanced by deficiency in p53 (154). Permanent loss of p53 prior to, concurrently, or post total-body irradiation all accelerated thymic lymphoma development. (155). However, it was later shown that blocking p53 during TBI significantly prevented lymphoma development as compared with wild type mice (156). Lee et al. provided the evidence to explain this phenotype in their report. They proposed that temporary knockdown of p53 during TBI improved the function of hematopoietic stem/progenitor cells to suppress lymphoma development via a non-cell-autonomous mechanism. Consistent with this study, another

group found that temporarily and reversibly blocking p53 during radiation resulted in significantly suppression of lymphoma development, which depends on DNA damage-activated p53 pathways (157). Similarly, loss of *Puma*, a downstream target gene of p53, was also found to ablate γ-irradiation-induced thymic lymphoma (158). Together, these studies indicate that the p53 response to acute damage promotes the development of radiation-induced lymphoma.

The effect of thymic microenvironment on radiation induced tumorigenesis have been subjected to investigations (159). Thymic lymphoma cells, like normal thymocytes, reside in a complex microenvironment that includes the extracellular matrix, diffusible growth factors and cytokines, and the heterogeneous stromal cells comprising the cortex and medulla. The molecular interplays between tumor initiating cells and normal thymocytes gained more attention. Molecules such as Notch ligands may modulate this process by determining T cell versus B cell fate (160). It was reported that toll-like receptor (TLR)-4 inactivation protects mice from thymic lymphoma by downregulating pro-tumor cytokine IL6 and miR-21 (161).

1.6 Gene Targeting in Mice

Genetic investigations in mice have played a major role in current understanding of mammalian biology. The genetic manipulation of mouse has provided a powerful tool for

the *in vivo* analysis of gene function in mammals. Gene targeting, defined as targeted modification of an endogenous genomic locus, takes advantage of homologous recombination (HR) to replace a part of an endogenous gene with a modified DNA fragment. Briefly, the targeting vector is introduced in the ES cells and replaces the endogenous locus by HR. This targeting vector contains expression cassettes for positive selection of recombined ES clones. Often used selection makers are expression cassette conferring resistance to neomycin. Selection against G418 is applied to enrich ES clones with HR. After verification, the ES cell can be used to develop knockout mice. In addition, the use of site-specific DNA recombinase opened a new era for manipulation of mouse genome. The most widely used recombinase in gene targeting studies include Cre and Flp. Cre recombinase recognizes and mediates site-specific recombination between 34-bp recognition sequence referred as loxP sites. While Flp can recognizes 48-bp sequences called FRT sites. Cre usually serves as a preferred recombinase in gene targeting since it performs higher efficiency than Flp. However, the combination of Cre/loxP and Flp/FRT systems provides more flexibility in the use of site-specific DNA recombination for modification of mouse genome, such as conditional gene targeting.

Conditional gene targeting utilizes the Cre/loxP system to achieve tissue-specific and/or inducible expression of Cre to spatially and temporally silencing genes *in vivo*. Generally speaking, two transgenic mice are required in this method. One mouse carrying a loxP-flanked but fully functional allele is generated by HR using ES clones. The other

mouse line carries Cre transgene under the control of a tissue-specific and/or inducible promoter. By crossing these two mice, the loxP-flanked allele is inactivated only in cells expressing Cre recombinase. In this study, I use LoxP based approach to induce conditional Setd4 knockout in mice.

1.7 Mouse Setd4 Gene

To date, there have been no genetic studies on the function of Setd4 *in vivo*. It is necessary to generate loss of function mouse model so that we gain insights about the function of this novel gene in mouse development and tumorigenesis. As illustrated in **Figure 4**, the mouse genomic region at chromosome 16 C4 harbors the Setd4 gene, which contains 12 exons. The mouse carbonyl reductase 1 (Cbr1) is "head-to-head" with the Setd4 gene, but no overlap between these two genes, which have about 4kb apart. Through the examination of Setd4 gene on Vega (Havana group at the Welcome Trust Sanger Institute), we deduced that Setd4 gene has 7 transcripts, and only one transcript gives rise to a coding protein of 439 amino acids. The translation start codon is located in at exon 3 and translation ends at exon 12 (**Figure 5**). Sequence alignment with human SETD4 protein (**Figure 6)** shows that the mouse SETD4 protein shares 77% identity and 93% similarity with human SETD4, with 100% identity at the critical catalytic motifs on N-terminal SET domain. Thus, studies in mouse SETD4 protein will likely provide evidence about function of this gene in

mammals.

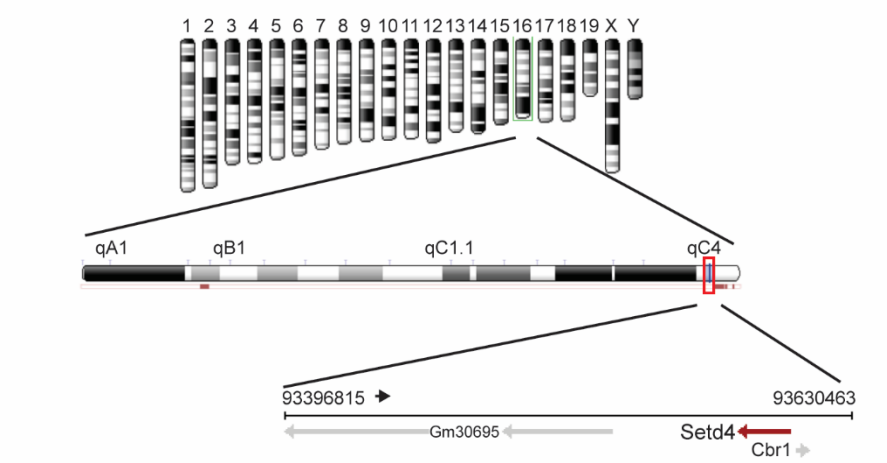

Figure 4. Mouse genomic location of Setd4 gene.

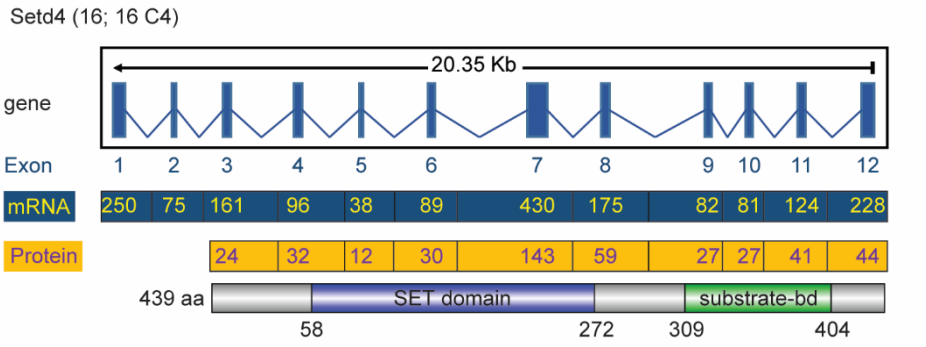

Figure 5. Domain structure of mouse SETD4. Schematic representation of the mouse Setd4 gene and primary protein structures of mouse SETD4 protein. Blue boxes in the genes and mRNA denote exons. The numbers below each gene are exon numbers. The numbers within the exons indicate their sizes in nucleotides. The numbers within the protein indicate their sizes in amino acids. Thin lines in the genes indicate the introns. Blue and green boxes indicate SET and substrate binding domain (substrate-bd), respectively.

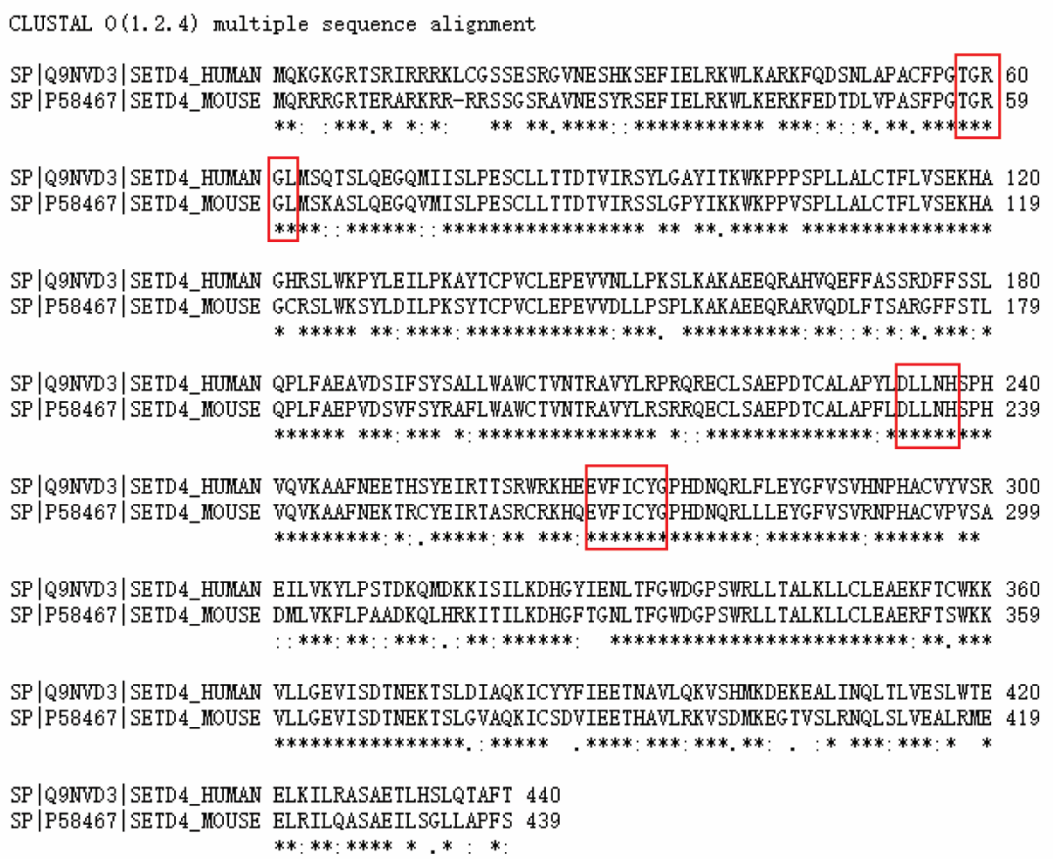

Figure 6. Sequence alignment of mouse and human SETD4 protein. Alignment was analyzed by CLUSTAL. Red boxes represent catalytic motifs on SET domain.

Chapter 2, Rationales and Hypotheses

Other work in Shen lab has shown that upon DNA damage, SETD4 is recruited to DNA damage sites within 30 minutes (Jinjiang Fan, Shen lab unpublished data). This DNA damage can be induced either by micro UV radiation, or Killer-Red induced ROS species (Shen Lab, unpublished data). This suggests a potential role of SETD4 in DNA damage response.

To the best of our knowledge, very little is currently known about the functions of SETD4. A recent study reported that SETD4 can inhibit the cell cycle quiescent Artemia diapause embryos (55). On the contrary, in the breast cancer, SETD4 was found to promote cell cycle and tumor development (81). All of these conclusions are based on studies of human cancer cell lines or Artemia. Therefore, it is necessary to develop a SETD4 knockout mice model to uncover the function of SETD4 *in vivo*.

In my thesis research, I hypothesize that loss of SETD4 could affect mouse development and tumorigenesis. I first establish an inducible Setd4 conditional deficient mouse model, and then challenge both Setd4 floxed mice and deficient mice with different doses of ionizing radiation to investigate the injury response induced by IR.

Exposure to IR at moderate or high dose could result in a significant IR-induced normal tissue damage. Most mammalian adult tissues are quite resistant to IR, including kidney, heart, lung, liver, due to the termination differentiation feature. When acute high

doses of IR cause death to the organism, it is mainly induced by a failure of one or few sensitive tissues, such as hematopoietic system and gastrointestinal system. I therefore focus on the role of the Setd4 gene in the recovery of bone marrow (BM) damage after irradiation, and its potential role in modulation of radiation induced tumorigenesis. These findings will provide new opportunities and insights for developing novel strategies to prevent IR-induced BM suppression.

Chapter 3, Materials and Methods

3.1 Mouse Strains

The animal works presented in this study were approved by the Institutional Animal Care and Use Committee at Rutgers Robert Johnson Medical School. We adhered to and followed our institutional guideline regarding to animal welfare issues. The nomenclature and designation of mouse strains used in this study are summarized in **Table 2.**

Table 2. Summary of mouse lines

Line designation	Description	Background	Source of the line
Setd4$^{flox/flox}$ *Setd4*$^{flox/wt}$	Conditional Setd4 mouse strain, exons 6 of Setd4 in this mouse line has been floxed	B6. 129	Shen Lab, unpublished
EIIaCre$^{+/+}$	Cre-expressing cassette under the control of EIIa promoter	B6. FVB	Jackson Laboratory Stock No 003724
Rosa26-CreERT2$^{+/+}$	CreERT2 is expressed under the control of a universal promoter at the Rosa26 locus, and Cre recombination can be induced by tamoxifen	B6. 129	Jackson Laboratory Stock No 008463
Tp53$^{flox/flox}$ *Tp53*$^{flox/wt}$	Conditional Tp53 mouse strain, exons 2-10 of Tp53 in this mouse line has been floxed	B6. 129	Jackson Laboratory Stock No 008462

3.2. Breeding of Setd4 conditional knockout mice with EIIa-Cre transgenic mice

The homozygous B6.FVB-Tg(EIIa-Cre)C5379Lmgd/J mice were purchased from The Jackson Laboratory (Stock No 003724). It carries a Cre-expressing cassette under the

control of the adenovirus EIIa promoter. We first bred the *Setd4*$^{flox/flox}$ mice with *EIIaCre*$^{+/+}$ mice to generate double transgenic mice (*Setd4*$^{flox/wt}$;*EIIaCre*$^{+/-}$), and then bred *Setd4*$^{flox/wt}$;*EIIaCre*$^{+/-}$ with *Setd4*$^{flox/flox}$;*EIIaCre*$^{-/-}$ mice to generate *Setd4* knockout mice.

3.3. Breeding of Setd4 conditional knockout mice with Rosa26 transgenic mice

The *Rosa26-CreERT2* mice were kindly provided by Dr. Arnold B. Rabson (Child Health Institute of New Jersey). This mouse was originally obtained from Jackson Laboratory (Stock No 008463) with B6 background (162). The CreERT2 is expressed under the control of a universal promoter at the Rosa26 locus, and it is normally distributed in the cytoplasm, but can be relocated to the nucleus upon binding with tamoxifen. This strain enables temporal control of flox-recombination upon tamoxifen induction *in vivo*.

3.4. Breeding of Tp53 mice with Setd4 knockout mice

The mice carrying homozygous Tp53-floxed alleles (163) were purchased from The Jackson Laboratory (Stock No 008462). The exons 2-10 of Tp53 in this mouse line has been floxed (from here on referred as *Tp53*^{flox}) and were crossed with *Setd4*$^{flox/flox}$*; ROSA26-CreERT2*$^{+/+}$ to generate *Setd4*$^{flox/flox}$*; Tp53*$^{flox/wt}$*; ROSA26-CreERT2*$^{/+}$ and *Setd4*$^{flox/flox}$*; Tp53*$^{flox/flox}$*; ROSA26-CreERT2*$^{/+}$. The primer pair of 5′-GGTTAAACCCAGCTTGACCA (1F) and 5′-GGAGGCAGAGACAGTTGGAG (2R) was used to amplify the 390-bp *Trp53*$^{floxExon2–10}$ and the 270-bp *Trp53*^{wt} alleles respectively. The primer pair of 5′-GGTTAAACCCAGCTTGACCA (1F) and 5′-GAAGACAGAAAAGGGGAGGG (10R)

were used to identify a 612-bp product of the LoxP-recombined *Tp53*$^{\Delta Exon2–10}$ allele.

3.5. PCR genotyping

For ES clone selection, PCR amplification 95℃ for 2 min initial strand separation, 38 cycles at 94℃ for 30 s, 58℃ for 30 s and 72℃ for 30 s, and a 5 min final elongation step at 72℃.

For mouse screen, genomic DNA was extracted from 2 mm tail biopsy by 6 h digestion in digestion buffer, then followed by standard DNA extraction protocol. 2 μl of the DNA was transferred to 10 μl PCR reactions. Amplification conditions were 95℃ for 2 min initial strand separation, 38 cycles at 94℃ for 30 s, 60℃ for 30 s and 72℃ for 30 s, and a 5 min final elongation step at 72℃. A PCR premix solution (Syd labs, MB067-EQ2B-L) was used in the PCR reaction.

3.6. RNA extraction and qRT-PCR

RNA was extracted from mouse organs or purified cell populations with RNA purification kit (Thermo Scientific, K0731). cDNA was prepared with random primers and Superscript II reverse transcription (Thermo Scientific, K1691) and assayed by quantitative real-time PCR using SYBR Green Master Mix reagents (Applied Biosystems, 4309155). Reactions were run on Stratagene Mx3005P. PCR amplifications were performed in triplicates for each gene of interest along with parallel measurements of β-actin cDNA (internal control). To confirm the specific amplification of the desired PCR product, melting curves were

analyzed, and PCR products were separated on a 2.5% agarose gel. The primers used for the amplification of each gene are mouse Setd4: forward, 5'-GGCTGATGAGCAAAGCG-3', reverse, 5'- TTCCAGAGGGACCGACA-3'; mouse beta-actin: forward, 5'-CGCCACCAGTTCGCCATGGA -3', reverse, 5'-TACAGCCCGGGGAGCATCGT -3'.

3.7. Western blot

Tissue proteins were lysed in RIPA buffer (10 mM Tris-Cl (pH 8.0), 1 mM EDTA, 1% Triton X-100, 0.1% sodium deoxycholate, 0.1% SDS, 140 mM NaCl) and normalized (DC™ Protein Assay, BIO-RAD, USA) for western blot detection. SETD4 antibodies will be described in Chapter 4 in details**.** Commercial antibodies for western blot are: p53 (sc-393031, SANTA CRUZ), β-Actin (A5441, Sigma-Aldrich).

3.8. Tamoxifen treatment

To cause a translocation of the CreERT2 from cytoplasm to the nucleus, and then trigger LoxP recombination, we injected mice with 5 daily tamoxifen. Tamoxifen (Sigma-Aldrich, T5648) was dissolved at a concentration of 25 mg/ml, in a mixture of 98% corn oil (Santa Cruz, sc-214761A) and 2% ethanol. Totally 160 μl per 25 g (160 mg/kg) of body weight was injected intraperitoneally into 6 to 8 weeks old mice once per day for 5 days.

3.9. Whole body irradiation of mice

Mice were retained in a Rodent RadDisk and then exposed to various doses of whole body irradiation in Gammacell 40 Extractor (MDS Nordion) γ-irradiator at a dose rate approximately 91.6 cGy/min. The specific radiation doses will be given when describing the experiemnts in results.

3.10. Histological and immunohistochemically (IHC) analysis

Tissue specimens were removed surgically, washed in cold PBS, and fixed overnight in 10% formalin at 4°C. After fixation, the tissue was transferred to 70% ethanol before submitting to Rutgers Cancer Institute Biospecimen Repository and Histopathology Service for tissue processing and paraffin embedding. All formalin-fixed paraffin-embedded tissue sections were cut at 5 μM. These tissue sections were stained with hematoxylin and eosin (H&E) following standard procedures. For immunohistochemically (IHC) analysis of tissue sections, antigen retrieval was carried in 0.05% citraconic anhydride (pH 7.4) by steaming the immersed slides in a kitchen steam cooker for 40 min after the temperature of the buffer reached 98 °C. After retrieval, slides were washed in PBS and permeabilized with 0.1% Triton X-100 in PBS for 10 min followed by quenching of endogenous peroxides with 3% hydrogen peroxide for 15 min. BSA 3% in PBS was used for blocking and dilution of primary and secondary antibodies. Incubation was carried out in a humidified chamber following standard procedures for IHC stains. Immunoreactivity was visualized with 3,3′-diaminobenzidine (DAB) (D5637; Sigma). Positive staining is visualized as a brown color precipitate that can be distinguished from the hematoxylin counterstain seen as a blue color.

Commercial antibodies are: CD3 (1:500; Dako, Glostrup, Denmark), B220/CD45R (1:500; Biolegend, San Diego, CA), Ki67 (1:300; Abcam, Cambridge, MA).

3.11. Flow cytometric analysis and antibodies

Bone marrow (BM) single-cell suspensions were prepared either from 1 tibia and femur or from 2 tibias, femurs, pelvis, humerus, radius, and shoulder plates for HSC subset analysis after radiation treatment. Single-cell suspensions from hematopoietic organs were incubated with Fc receptor-blocking antibody (clone 2.4G2) before being stained on ice with specific antibodies conjugated to different fluorophores. Data were acquired on a LSR II cytometer (BD) and analyzed using FlowJo software (Tree Star). Cell doublets were excluded from all analyses and, when possible, dead cells were excluded by the use of DAPI. For BM and splenocyte preparations, RBCs were lysed (Sigma-Aldrich, R7757) before antibody staining. Collection media was RPMI1640 with 10% FBS, 1% Glutamine, 1% Peicillin/Streptomycine, 0.01% 2-Mercaptoethanol. FACS buffer is PBS supplemented with 1% FBS.

To obtain sorted cells for bone marrow transplantation experiments, Lin^- BM cells were firstly stained with Lineage cocktail, following anti-Biotin microbeads (MACS Miltenyi Biotec, 130-090-485), and then sorted by autoMACS separation operator (MACS Miltenyi Biotec).

Antibodies (**Table 3**, all from eBioscience or BD) conjugated to FITC, Alexa Fluor 488, PE, PE-Cy7, APC, Alexa Fluor 647, APC-Alexa Fluor-780, PercpCy5.5, Alexa Fluor

700 were used for the flow cytometric analyses. **Table 4** lists all antibodies, lineage cocktails, and combinations of mAbs used to identify each progenitor population. Some of the lineage cocktail was kindly provided by Dr. Lisa K Denzin lab at Rutgers University.

Table 3. List of antibodies used in bone marrow study

	Antibody name	**Color**	**Clone**	**Catalog**	**Suppliers**
BM progenitors	Lineage-Biotin	Streptavidin-P			Denzin Lab
	Sca-1	A700	D7	56-5981-82	eBiosciences
	c-kit	A780	ACK2	47-1172-82	eBiosciences
	CD34	APC	Ram34	50-0341-82	eBiosciences
	Flt-3	PE	AZF10	12-1351-82	eBiosciences
	CD127	PE-Cy7	SB/199	560733	BD Pharmingen
	CD16/32	PerCP-Cy5.5	94	45-0161-82	eBiosciences
	Dead cell exclusion	DAPI			
Splenocyte	CD3	A700	500A2	557984	BD Pharmingen
	CD19	PE-Cy7	1D3	552854	BD Pharmingen
	CD4	APC-Cy7	L3T4	47-0042-82	eBiosciences
	CD8	PerCP-Cy5.5	53-6.7	45-0081-82	eBiosciences
	MHCII	A594	212.A1		Denzin Lab
	TER-119	PerCP-Cy5.5	TER-119	560512	BD Pharmingen
	CD71	FITC	C2	561936	BD Pharmingen
BM Chimeras	CD45.1	FITC	A20	553775	BD Pharmingen
	CD45.1	APC	A20	110720	Biolegend
	CD45.2	PE-Cy7	104	109829	Biolegend
	CD45.2	FITC	104	109805	Biolegend
	CD11b	A700	M1/70	557960	BD Pharmingen
	TER-119	PerCP-Cy5.5	TER-119	560512	BD Pharmingen
	CD3	A700	500A2	557984	BD Pharmingen
	CD45R/B220	PE	RA3-6B2	553090	BD Pharmingen
	CD19	PE-Cy7	1D3	552854	BD Pharmingen

Table 4. Antibody cocktails and their compositions

Cell Population	Full description of cell population	Marker composition	Lineage cocktail
LSK	$Lin^{-}Sca\text{-}1^{+}c\text{-}kit^{High}$	Lin^{-} Sca-1^{+} c-kit^{+}	CD3ε, CD4, CD8α, NK1.1, CD19, CD11c, CD11b, TCRβ, TCRγ, Gr-1, and Ter119
$LS^{-}K$	$Lin^{-}Sca\text{-}1^{-}c\text{-}kit^{High}$	Lin^{-} Sca-1^{-} c-kit^{+}	
LT-HSC	Long-term HSC	LSK Flt-3^{-} $CD34^{-}$	
ST-HSC	Short-time HSC	LSK Flt-3^{-} $CD34^{+}$	
HSC	Hematopoietic stem cell	LSK Flt-3^{-}	
MPP	Multipotent progenitor	LSK Flt-3^{Int} $CD34^{+}$	
LMPP	Lymphoid-primed MPP	LSK Flt-3^{Bright} $CD34^{+}$	
CLP	Common lymphoid progenitor	Lin^{-} Sca-1^{low} c-kit^{low} $CD127^{+}$ Flt-3^{Bright}	
MEP	Megakaryocyte-erythroid progenitor	$LS^{-}K$ CD16/32^{-} $CD34^{-}$	
GMP	Granulocyte-macrophage progenitor	$LS^{-}K$ CD16/32^{+} $CD34^{+}$	
CMP	Common myeloid progenitor	$LS^{-}K$ CD16/32^{-} $CD34^{+}$	

3.12. Isolation of lymphocytes from mouse peripheral blood

Mouse peripheral blood was collected with Calibrated Micropipets coated with Heparin (VWR 53507-296). And then separated by Lymphocyte Separation Medium (MPBio 0850494). Mononuclear layer (lymphocytes) will be collected and following for blocking and staining steps as shown before.

3.13. Competitive repopulation assay

Lin^{-} BM cells (>95% Lin^{-}) from *Setd4*$^{\Delta/\Delta}$ mice (CD45.2) were mixed at a ratio of 1:1 with WT competitor Lin^{-} BM cells from B6 x B6.SJL F1 mice (CD45.1/CD45.2), and 1×10^{6}

total cells were injected i.v. into lethally irradiated B6.SJL recipients (CD45.1) (B6.SJL-Ptprc^{a} Pepc^{b}/BoyJ; stock no 002014; The Jackson Laboratory Stock). Mouse blood was collected every 4 weeks for analysis.

3.14. Serial competitive bone marrow transplantation

Lin^{-} BM cells (>95% Lin^{-}) from *Setd4*$^{\Delta/\Delta}$ mice (CD45.2) were mixed at a ratio of 1:1 with WT competitor Lin^{-} BM cells from B6 x B6.SJL F1 mice (CD45.1/CD45.2), and 1×10^{6} total cells were injected i.v. into lethally irradiated B6.SJL recipients (CD45.1). 4 months later, bone marrow cells will be isolated from euthanized these recipients and transferred into lethally irradiated B6.SJL recipients. The same procedure will repeat another round after 4 months. Mouse blood were collected every 4 weeks.

3.15. Non-competitive bone marrow reconstituted survival assay

Lin^{-} BM cells (>95% Lin^{-}) from *Setd4*$^{flox/flox}$ or *Setd4*$^{\Delta/\Delta}$ mice (CD45.2), were isolated and 1×10^{6} total cells were injected i.v. into lethally irradiated B6.SJL mice (CD45.1). 16 weeks post transplantation, all the fully-reconstituted recipients were exposed to 8 Gy irradiation. The irradiated mice were observed daily totally for 30 days.

3.16. Non-competitive HSC dilution survival assay

Lin^{-} BM cells (>95% Lin^{-}) from B6.SJL mice (CD45.1), were isolated and specific number of cells were injected i.v. into lethally irradiated *Setd4*$^{flox/flox}$ or *Setd4*$^{\Delta/\Delta}$ recipients (CD45.2).

Survival of the recipients were observed daily totally for 30 days.

3.17. Mouse cytokine protein assay analyses

Bone marrow plasma were collected from littermates *Setd4*$^{\Delta/\Delta}$ and *Setd4*$^{flox/flox}$ mice 24 h and 10 days respectively post IR 8 Gy. Plasma levels of cytokines and chemokines were measured using a Mouse Cytokine Panel A kit (R&D, Catalog # ARY006) following manufacturer's instructions. Images of the blots were acquired by Bio-Rad ChemiDoc Chemiluminescence, and quantitative analyses of cytokine and chemokine spots were performed by Bio-Rad Image Lab.

3.18. Necropsy analysis

All the mice were inspected at least daily. Mice suspected to be ill (because of weight loss, poor grooming, or visible tumor) were observed more closely and euthanized for necropsy before death, and it involved both gross inspection and histological examination. Mice dying of lymphoma, hepatocarcinoma, pulmonary adenocarcinoma, fibrosarcoma, as well as some forms of malignant neoplasm, were considered to have died from "neoplastic" illnesses. The category "nonneoplastic illnesses" included a miscellany of diagnoses, including congestive heart failure, inflammation, renal amyloidosis, and others (164).

3.19. RNA-seq

Total RNA was isolated from mouse *Setd4*$^{\Delta/\Delta}$ and *Setd4*$^{flox/flox}$ LK cells (165) followed by

RNA library preparation with the Illumina HiSeq strand-specific mRNA sample preparation system. All RNA-seq libraries were sequenced with a read length of single-end 150 bp using the Illumina NextSeq 500 and final of over 30 million reads per sample.

3.20. RNA-Seq data analysis

RNA-seq reads were aligned to the mouse genome reference sequence and TPM value (transcripts per kilobase million) were calculated by Dr. Subhajyoti De from Rutgers CINJ. Deferentially expressed genes (DEGs) were selected with a fold change > 2 for further pathway analyses. KEGG pathway signatures and Gene Ontology signatures were performed.

Chapter 4, Establishment of Setd4 Deficient Mouse Models

4.1. Isolation of conditional Setd4 knockout ES clones by *in vitro* FLP-recombination.

A pre-made C57BL/6N JM8.N4 ES clone (EPD0225_5_D10) with a copy of trapped Setd4 (**Figure 7**) allele was generated by the trans-NIH Knock-Out Mouse Project (KOMP). In this clone, one copy of the *Setd4* was inactivated by splicing of upstream endogenous exons to a splice acceptor in the targeting cassette flanked by two FRT recombination sites (**Figure 7**). We obtained this ES clone from the KOMP Repository (www.komp.org).

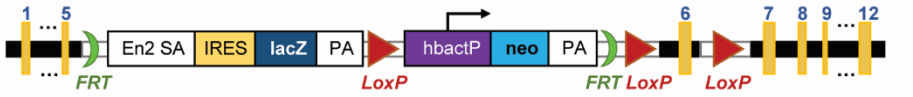

Figure 7. Genomic structure of the trapped *Setd4* allele in an ES clone (C57BL/6N JM8.N4). This clone was obtained from the trans-NIH Knock-Out Mouse Project (KOMP) Repository. The insertion of the FRT site flanked signaling cassette of EN2 SA-IRES-lacZ disrupts the structure of the *Setd4* gene upstream of exon 6. In addition, the exon 6 is flanked by a pair of loxP signal sequences. FRT: Flippase (FLP) recombination site, 48bp(5'GAAGTTCCTATTCcGAAGTTCCTATTCtctagaaaGtATAGGAACTTC3'); loxP: Cre-recombination site, 34bp(5'ATAACTTCGTATAA TGTATGCTATACGAAGTTAT3'). The grey backbone only presents in the trapped allele but not in the wild type *Setd4* genome.

To convert this trapped allele into a version of LoxP/Cre based conditional knockout, the gene-trapping cassette between the two FRT sites has to be removed by flippase (FLP) mediated recombination. Thus, we conducted an *in vitro* FLP-recombination assay to delete the trapping signal cassette between the FRT sequences (**Figure 8A**). The ES cell culture was electroporated with 20 μg of pCAGGS-FLPe-IRES-puro (Gene Bridge,

Germany) plasmid that transiently expresses the flippase (FLP). The electroporation was conducted with 5-million of ES cells in 800ul of medium at 250V, 500uF. Then, the cells were incubated for 20 min at room temperature, diluted 500-fold, and plated into 10cm dishes. Eight days after culture, single clones were picked up and transferred into 96-well plates. After 5 additional days of culture, the culture in the 96 well plate was split into 3 96-well plates: one plate for X-gal staining, one for PCR genotyping, and one for culture expansion. **Figure 8B** shows the X-gal staining of a few representative clones. The X-gal negative clones represent a potential success of FLP-recombination. Two independent β-gal negative sub-clones (D5, E1) were obtained, and then confirmed to contain an allele of floxed *Setd4*-exon 6 and a wild type *Setd4* allele based on PCR genotyping as illustrated in **Figure 8C.** We further performed a metaphase chromosome analysis to confirm that the putative ES clones have normal karyotypes before they can be used to generate transgenic mice (**Figure 8D**). As summarized in **Table 5**, more than 90% of the metaphase spreads of these ES clones have the normal number of 40 chromosomes. The PCR genotype strategy, primer sequences and locations are summarized in **Figure 9**, and **Tables 6** and **7**. Thus, we successfully performed FLP-recombination assay and obtained ES clones containing a copy of the floxed Setd4-exon 6, and these clones may be used to generate chimera mice.

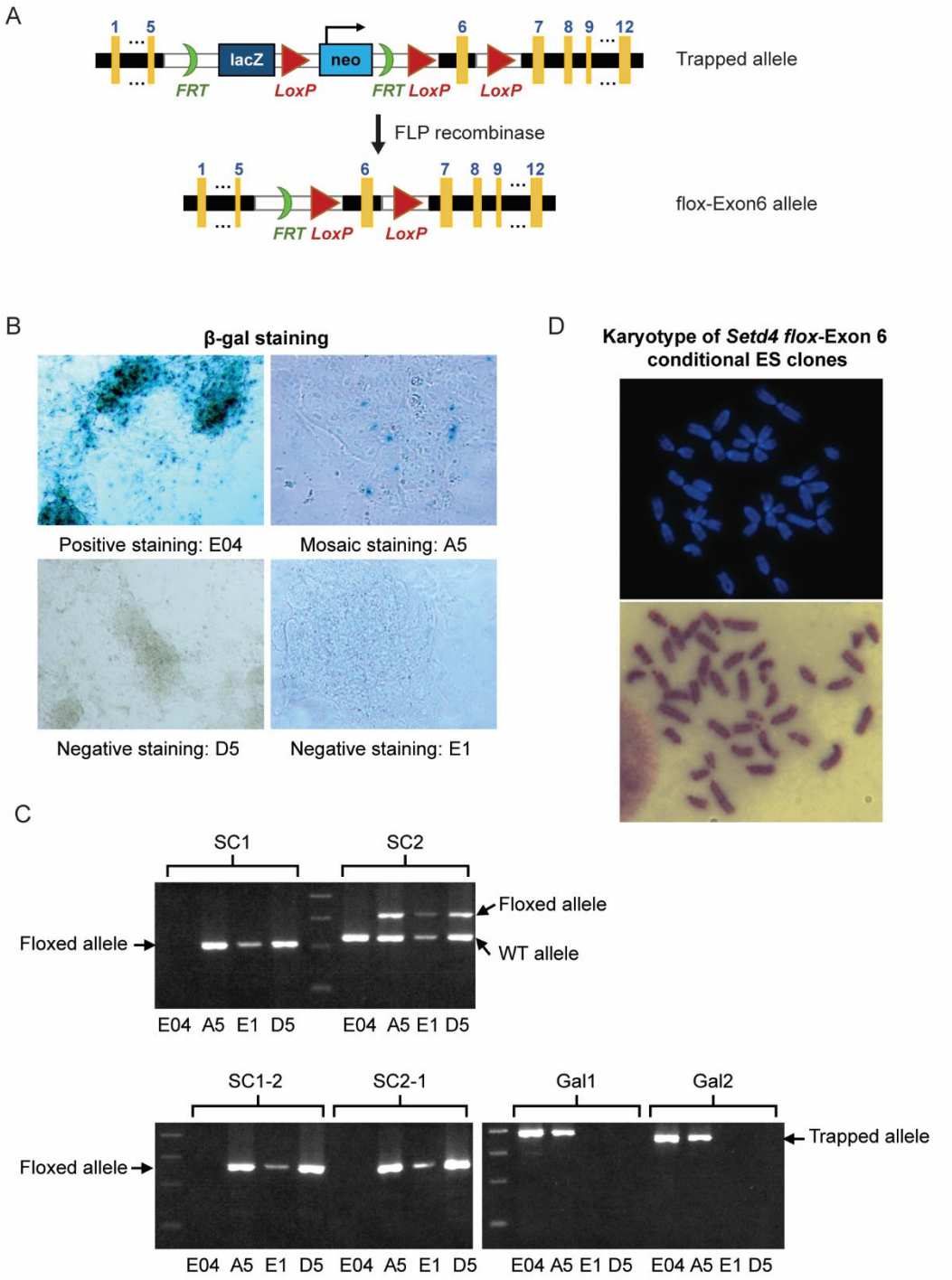

Figure 8. Generation of LoxP-flanked conditional *Setd4*-exon 6 (*flox*-Exon6) allele from the trapped Setd4 allele by FLP-mediated recombination in ES cells. (A) Plasmid pOS was transiently transfected into the ES cells. A copy of the duplicated clone set isolated from 96 wells were used to determine the β-gal expression by LacZ staining. The lacZ negative clones were grown-up used for genotyping. **(B)** Identification of candidate clones with a successful FLP-recombination. Representative clones were stained for β-gal activities, including the parental clone

(E04), a mosaic clone (A5), and 2 β-gal activities clones (D5 and E1). (Data provided by Dr. Jingyin Yue) **(C)** PCR genotype verification of Setd4-exon 6 conditional clones. The primers used in the genotyping are shown on the top of the panel. E04: Parental ES clone with the targeted allele before FLP recombination. A5: mosaic clone with partial FLP recombination. D5, E1: two clones after successful FLP-recombination. (Data provided by Dr. Jingyin Yue) **(D)** Giemsa staining of representative metaphase chromosome spreads of derived *Setd4 flox*-Exon6 conditional clones (data provided by Dr. Jingyin Yue).

Table 5. Number of chromosomes on metaphase spreads of *Setd4*-exon 6 conditional clones

Number of chromosomes in a single cell	**Number of cells with the specified chromosome number (ES clone D5)**	**Number of cells with the specified chromosome number (ES clone E1)**
40	28	29
39	4	2
38	1	1
Average number of chromosomes per cell	39.82	39.88

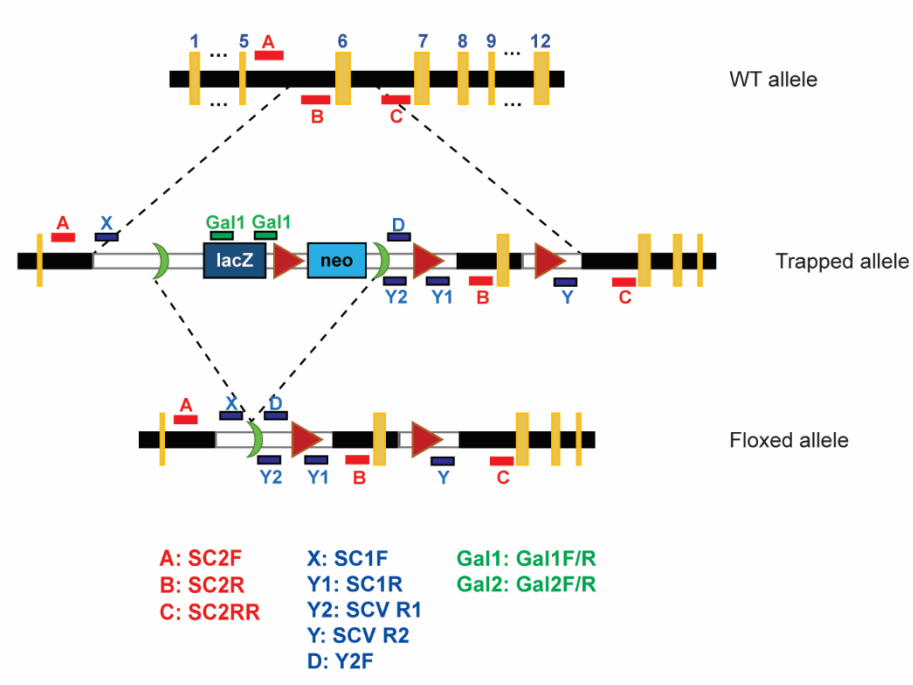

Figure 9. PCR genotyping strategy and primer location for ES clone screen. Primer codes and names are shown in the figure index. Full name and sequence of the primers, and the expected size of PCR products can be found in the text and the referred **Tables 6** and **7**.

Table 6. Primers used for SETD4 genotyping

Code	Primer name	Primer Sequence	Location in reference genome of the gene targeted allele	Primer location
X	SC1F	5'AGGCGCATAACGATACCACGA	P15051	5’ side of left FRT site (present in targeting vector but not in wt genome)
Y1	SC1R	5'TCCGCCTACTGCGACTATAG	P22173	3’ side of the 1st loxP (present in targeting vector but not in wt genome)
A	SC2F	5'TCCTGGGCTCTGCCATCCATG	P15001	Intron 5, ~50bp from the end of 5’-Arm
B	SC2R	5'CTGTTGCAATGGAAATGCCAG	P22223	Intron 5, 3’-side of 1st loxP site
C	SC2RR	5'CTAAAGCTCTGCCCTAAGGTC		Intron 6, 3’-side from the end of the 3’-Arm of the targeting vector.
D	Y2F	5'GAAAGTATAGGAACTTCGTCG		Sequence from knout out vector, 5’-side of the 1st LoxP (present in KO vector but not in wt genome)
Y2	KO-SCV R1	5'CGACGAAGTTCCTATACTTTCTAG		Sequence from knout out vector, 5’-side of the 1st LoxP (present in KO vector but not in wt genome)
Y	KO-SCV R2	5'GAACTGATGGCGAGCTCAGAC		Sequence from knout out vector, 3’-side of the 2st LoxP (present in KO vector but not in wt genome)
Gal1	Gal1F	5’-ctg gcg taa tag cga aga ggc	P16907	
	Gal1R	5’-cga ctg tcc tgg ccg taa ccg	P17300	
Gal2	Gal2F	5’-atc gtg cgg tgg ttg aac tgc	P17728	
	Gal2R	5’-cat cgg tca gac gat tca ttg	P18008	

Tables 7. Primer pairs and anticipated PCR products for different genotypes of ES clones

Primer pair	Trapped allele	FLP-recombined, and exon 6-Floxed allele	WT allele
SC1F:SC1R (SC1)	7122bp	218bp	N/A
SC2F:SC2R (SC2)	7222bp	318bp	234bp
SC1F:SC2R (SC1-2)	7172bp	268bp	N/A
SC2F:SC1R (SC2-1)	7172bp	268bp	N/A
Gal1F:Gal1R (Gal1)	393bp	N/A	N/A
Gal2F:Gal2R (Gal2)	361bp	N/A	N/A

4.2. Generation of a conditional founder mouse lines with floxed Setd4 exon-6 (*Setd4*$^{flox/wt}$, and *Setd4*$^{flox/flox}$).

In the beginning, the original *Setd4*-trapped clone (**C57BL/6N JM8.N4, Figure 7**) was used to generate chimera mice. Although five chimera mice were obtained, they failed to convey a single germ-line transmission among a total of 337 offsprings (see **Table 8** for details). Subsequently this approach was abandoned. Then, we used the FLP-recombined D5 and E1 subclones to inject Albino (white) blastocysts at our transgenic core facility, and implanted to foster mice. Both D5 and E1 clones that contain a wild type and a loxP-*Setd4*-exon 6 conditional allele. D5 clone failed to generate any chimeras, but the E1 clone generated 8 chimeras, 6 males, and 2 females. We bred these male chimeras with C57BL6 female mice (1:2 per cage), germline transmission of the floxed allele was screened by PCR with tail DNA from the offsprings. Among the first 167 offsprings, 6 viable mice were found to have germ-line transmissions of the floxed allele, as identified with the same PCR screen strategy as with ES clone (see **Figure 10** for representative PCR results). Thus, the first generation (F0) of founder heterozygous conditional *Setd4* knockout mice,

designated *Setd4*$^{flox/wt}$, was obtained. By breeding *Setd4*$^{flox/wt}$ male mouse with the *Setd4*$^{flox/wt}$ females, we can then generate homozygous conditional *Setd4* mouse (*Setd4*$^{flox/flox}$).

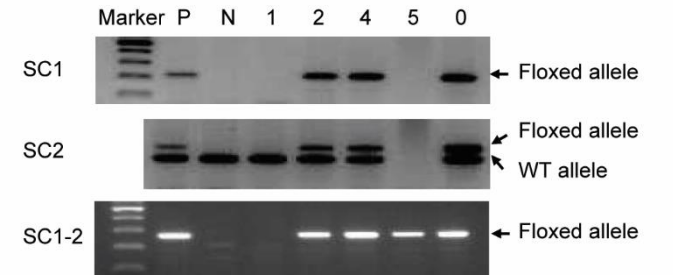

Figure 10. Representative PCR result of germ-line transmission of *Setd4* flox-Exon6 allele. The primers used in the genotyping are shown on the left of the panel. No. 2, 4, 0 mice had successful transmission of the Flox-Exon6 allele, while No. 1, 5 had not. See **Table 9** for primer information. (Data provided by Dr. Huimei Lu)

Table 8. Number of screened newborns of chimera mice generated from trapped *Setd4* ES clone (C57BL/6N JM8.N4)

chimera	Chimeric percentage	Total No. of litters	Total No. of newborns	Average litter size	Positive offsprings
Male #1	~80%	9	69	7.7	0
Male #2	~30%	6	35	5.8	0
Male #3	~20%	10	88	8.8	0
Male #4	~20%	13	122	9.4	0
Female	~20%	4	23	5.8	0
Total		42	337	8	0

Tables 9. Primer pairs and anticipated PCR products with different mouse genotypes

Primer pair	WT allele (wtExon6)	Floxed Exon 6 Allele (flox-Exon6)	Deleted Exon 6 Allele (ΔExon6)
SC2F:SC2R (AB)	234	318	N/A
SC2F: SCV R2 (AY)	N/A	937	223
SC2F: SCV R1 (AY2)	N/A	165	165
Y2F:SC2R (DB)	N/A	174	N/A
Y2F:SC2RR (DC)	N/A	942	204
SC2F:SC2R:SC2RR (ABC)	234	318	369

4.3. Verification of the conditional *Setd4*$^{flox/wt}$ and *Setd4*$^{flox/flox}$ mouse line.

The *Setd4*$^{flox/wt}$ founder line mice were crossed with C57BL6 mice to obtain heterozygous and homozygous LoxP-*Setd4*-6 mice, *Setd4*$^{flox/wt}$ and *Setd4*$^{flox/flox}$. The genotyping of the bred mice was conducted according to the PCR strategy outlined in **Figure 11A** and **Table 9**. To verify whether the conditional allele in the mice is susceptible for *Setd4*-exon6 deletion upon expression of Cre-recombinase, the mouse embryo fibroblasts (MEF) were established from the conditional mice using previously reported procedures (166). The MEF were then infected with retroviruses that express Cre-recombinase. As shown in **Figure 11B**, expression of Cre resulted in the emergence of the *Setd4*-ΔExon 6 allele and the disappearance of the loxP-*Setd4*-Exon 6 allele.

To further verify whether the deletion of Setd4 exon 6 can result in the expected RNA alteration, we performed RT-PCR to amplify the mRNA using primers overlapping exon 5 and exon 7 of Setd4 (see **Figure 11C** for the primer location and sequences). As shown in **Figure 11C**, a short mRNA species that can be detected by RT-PCR. Upon sequencing of this RNA species, we found that *Setd4* mRNA transcript had lost exon-6 and caused a frame-shift of the coded protein, and a premature stop codon at 845 bp. Thus, the exon-6 deletion effectively disrupted the SETD4 protein. These characterizations confirm that the newly established conditional Setd4-Exon6-Flox mice are authentic, the Setd4 exon 6 can be deleted upon expression of Cre-recombinase, and this would cause the loss of functional Setd4 protein.

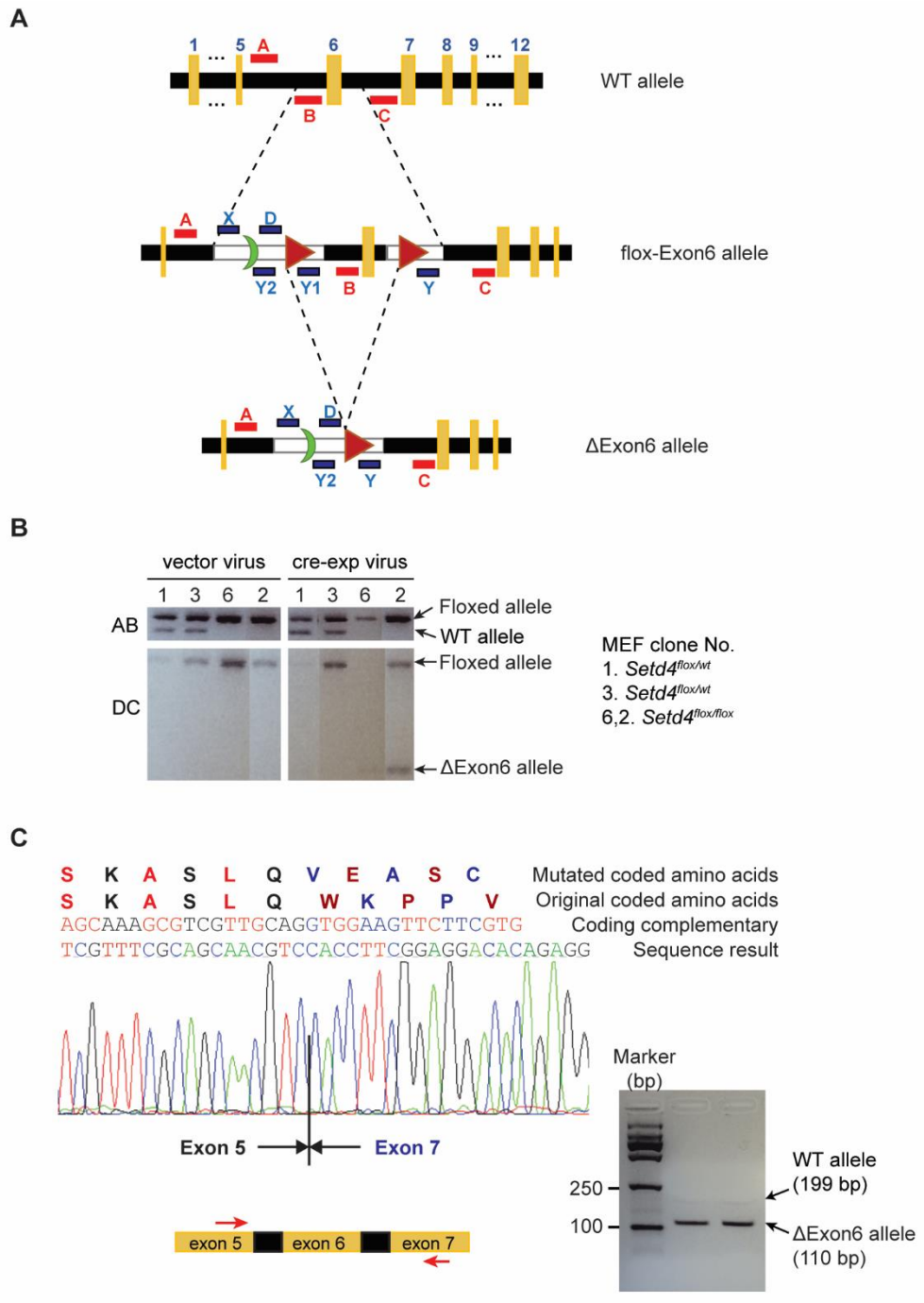

Figure 11. Verification of Setd4 exon 6 deletion. (A) PCR strategy to genotype mice bred from the loxP-Exon 6 conditional *Setd4* mice. See text and **Table 9** for primer information. **(B)** Cre recombinase cause deletion of exon 6 in conditional Loxp-*Setd4*-exon 6 MEFs. **(C)** Sequence of the truncated Setd4 mRNA species in the *Setd4*-ΔExon 6 mice. Wild type allele is resulted in 199bp fragment, while loxP excision allele is supposed to amplify 110bp fragment due to deletion of exon 6 (89 bp). Forward primer: 5'-GGCTGATGAGCAAAGCG-3'; Reverse primer: 5'-TTCCAGAGGGACCGACA-3'. The 110 bp band was recovered from gel and subjected to

sequencing. The sequence result was shown.

4.4 EIIa-Cre mediated whole body conditional *Setd4* knockout in mice.

The *EIIa-Cre* mice carry a Cre transgene under the control of the adenovirus EIIa promoter. The EIIa promoter driving the expression of Cre is known to be restricted to oocytes and preimplantation stages of the embryo (167). In an attempt to generate mice with whole body *Setd4* knockout, we bred the *Setd4*$^{flox/flox}$ mice with *EIIaCre*$^{+/+}$ mice to generate mice *Setd4*$^{flox/wt}$*;EIIaCre*$^{+/-}$. Theoretically, the pups will inherit one wild type allele of *Setd4* from *EIIaCre*$^{+/+}$ mice, and one allele with partial or total germline excision of the loxP flanked sequence.

Next, we sought to generate constitutive *Setd4* knockout mice by crossing *Setd4*$^{flox/wt}$*;EIIaCre*$^{+/-}$ with *Setd4*$^{flox/flox}$*;EIIaCre*$^{-/-}$ mice using three strategies. The representative PCR screens of the offspings of this crossing are shown in **Figure 12**.

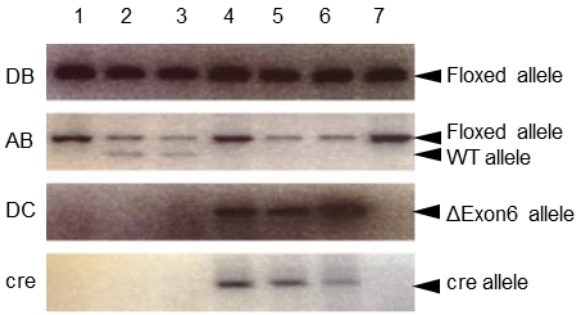

Number	Genotype
1	*Setd4*$^{flox/flox}$*; EIIaCre*$^{-/-}$
2	*Setd4*$^{flox/wt}$*; EIIaCre*$^{-/-}$
3	*Setd4*$^{flox/wt}$*; EIIaCre*$^{-/-}$
4	*Setd4*$^{\Delta/flox}$*; EIIaCre*$^{+/-}$
5	*Setd4*$^{\Delta/flox}$*; EIIaCre*$^{+/-}$
6	*Setd4*$^{\Delta/flox}$*; EIIaCre*$^{+/-}$
7	*Setd4*$^{flox/flox}$*; EIIaCre*$^{-/-}$

Figure 12. Representative PCR genotyping of EIIa-Cre mating. Combinations of three primers (see **Table 9**) are used to amplify and identify each allele of *Setd4*. The name of primers are listed on the left and the band identity is illustrated on the right. The genotyping results are summarized in the chart.

First, two male *Setd4$^{flox/wt}$;EIIaCre$^{+/-}$* mice were mated with *Setd4$^{flox/flox}$;EIIaCre$^{-/-}$* females. This resulted in a total of 38 pups, whose genotype distributions is summarized in **Table 10.** It was surprising that this cross did not produce mice with the *Setd4$^{\Delta/\Delta}$;EIIaCre$^{+/-}$* genotype, but only *Setd4$^{\Delta/flox}$;EIIaCre$^{+/-}$*. Second, we mated two female *Setd4$^{flox/wt}$;EIIaCre$^{+/-}$* with *Setd4$^{flox/flox}$;EIIaCre$^{-/-}$* males. We genotyped 24 pups, and again we found no complete elimination of floxed allele (**Table 11**). Lastly, we mated *Setd4$^{flox/wt}$;EIIaCre$^{+/-}$* males with *Setd4$^{flox/wt}$;EIIaCre$^{+/-}$* females. This generated 71 pups, yet again we failed to obtain any mouse with homozygous *Setd4* loss (**Table 12**).

Table 10. Genotype distribution of newborns (Male: *Setd4$^{flox/wt}$;EIIaCre$^{+/-}$*; Female: *Setd4$^{flox/flox}$;EIIaCre$^{-/-}$*)

Genotype		No. (%) of newborns	Expected % of newborns
Setd4$^{\Delta/\Delta}$; EIIaCre$^{+/-}$	*Setd4$^{\Delta/\Delta}$; EIIaCre$^{+/-}$*	0	25%
	Setd4$^{\Delta/flox}$; EIIaCre$^{+/-}$	11 (29%)	
Setd4$^{\Delta/flox}$; EIIaCre$^{-/-}$		4 (11%)	25%
Setd4$^{flox/flox}$; EIIaCre$^{-/-}$		7 (18%)	0%
Setd4$^{\Delta/wt}$; EIIaCre$^{+/-}$	*Setd4$^{\Delta/wt}$; EIIaCre$^{+/-}$*	1 (3%)	25%
	Setd4$^{\Delta/flox/wt}$; EIIaCre$^{+/-}$	7 (18%)	
Setd4$^{flox/wt}$; EIIaCre$^{-/-}$		8 (21%)	25%
		38	100%

Table 11. Genotype distribution of newborns (Male: *Setd4$^{flox/flox}$;EIIaCre$^{-/-}$*; Female: *Setd4$^{flox/wt}$;EIIaCre$^{+/-}$*)

Genotype		No. (%) of newborns	Expected (%) of newborns
Setd4$^{\Delta/\Delta}$; EIIaCre$^{+/-}$	*Setd4$^{\Delta/\Delta}$; EIIaCre$^{+/-}$*	0	25%
	Setd4$^{\Delta/flox}$; EIIaCre$^{+/-}$	5 (21%)	
Setd4$^{\Delta/flox}$; EIIaCre$^{-/-}$		5 (21%)	25%
Setd4$^{flox/flox}$; EIIaCre$^{-/-}$		0	0%
Setd4$^{\Delta/wt}$; EIIaCre$^{+/-}$	*Setd4$^{\Delta/wt}$; EIIaCre$^{+/-}$*	1 (4%)	25%
	Setd4$^{\Delta/flox/wt}$; EIIaCre$^{+/-}$	9 (37%)	

Setd4$^{flox/wt}$; EIIaCre$^{-/-}$	4 (17%)	25%
	24	100%

Table 12. Genotype distribution of newborns (Male: *Setd4$^{flox/wt}$;EIIaCre$^{+/-}$*; Female: *Setd4$^{flox/wt}$;EIIaCre$^{+/-}$*)

Genotype	No. (%) of newborns
Setd4$^{\Delta/\Delta}$; EIIaCre^{+}	0
Setd4$^{\Delta/flox}$; EIIaCre^{+}	14 (20%)
Setd4$^{\Delta/wt}$; EIIaCre^{+}	25 (35%)
Setd4$^{\Delta/flox/wt}$; EIIaCre^{+}	8 (11%)
Setd4$^{wt/wt}$; EIIaCre^{+}	13 (18%)
others	11 (16%)
	71

To further test the possibility of embryo lethality due to *Setd4* loss, two pregnant females were sacrificed at E10.5, and one pregnant female was sacrificed at E18.5. Totally 21 embryos were genotyped, and we did find two embryos with complete excision of loxP sites from two litters respectively, about 10% out of total (**Table 13**). This indicates that Setd4 may not be essential during early embryogenesis, but *Setd4* loss might cause late or early postnatal death.

Table 13. Genotype distribution of embryos (Male: *Setd4$^{flox/wt}$;EIIaCre$^{+/-}$*; Female: *Setd4$^{flox/wt}$;EIIaCre$^{+/-}$*)

genotype	No. (%) of newborns
Setd4$^{\Delta/\Delta}$; EIIaCre^{+}	2 (10%)
Setd4$^{\Delta/flox}$; EIIaCre^{+}	3 (14%)
Setd4$^{\Delta/wt}$; EIIaCre^{+}	6 (28%)
Setd4$^{\Delta/flox/wt}$; EIIaCre^{+}	2 (10%)
Setd4$^{wt/wt}$; EIIaCre^{+}	3 (14%)
Others	5 (24%)
	21

Although these breeding produced difficult data to interpret (see Chapter-7 for more

discussion), the above analyses suggested that: 1) the EIIa-Cre mediated complete or homozygous Setd4 deletion is late embryogenic or postnatal lethal to mice, and 2) incomplete or mosaic Setd4 deletion can occur when using EIIa-Cre. Nevertheless, we kept *Setd4*$^{\Delta/wt}$ and *Setd4*$^{\Delta/flox}$ mice from the above breeding for long-term observation. The overall survival of these two groups displayed a marginal difference (P=0.046), with a slight longer median survival in *Setd4* mosaic knockout mice (*Setd4*$^{\Delta/flox}$*;EIIaCre*$^{+/-}$) comparing with *Setd4* heterozygous *(Setd4*$^{\Delta/wt}$*;EIIaCre*$^{+/-}$) mice (**Figure 13**). These mice mainly died from tumor, inflammation (such as dermatitis), neoplasm, ocular lesion, etc.

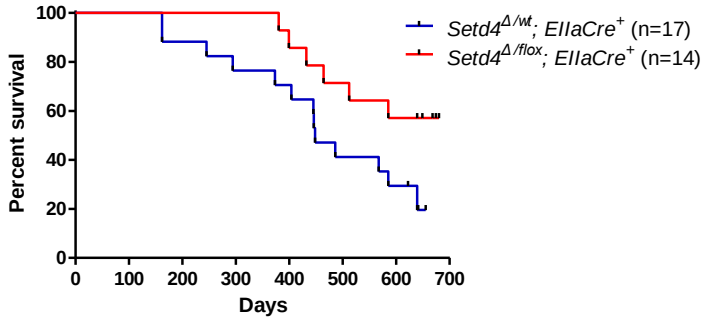

Figure 13. Kaplan-Meier survival curves of *Setd4*$^{\Delta/flox}$*;EIIaCre*$^{+/-}$ and *Setd4*$^{\Delta/wt}$*;EIIaCre*$^{+/-}$ mice. P = 0.046 (log-rank Mantel–Cox test). The median survival of *Setd4*$^{\Delta/wt}$ mice is 448 days.

4.5. Generation of Rosa26-CreERT2 Mediated Inducible *Setd4* Knockout Model.

Since the crossing of *EIIa-Cre* transgenic mice failed to generate whole body *Setd4* knockout, we decided to shift to a different Cre-transgenic mouse model and adapted an inducible approach. We utilized the *Rosa26-CreERT2* mouse strain. In this strain, a fusion gene, CreERT2, had been knocked-into a ubiquitously expressed Rosa26 locus of the

mouse genome. The CreERT2 fusion protein is a fusion product between a mutant estrogen hormone-binding domain (ERT2) and the Cre-recombinase. This fusion restrains the CreERT2 protein in the cytoplasm. Upon binding of ERT2 with the non-steroidal estrogen analog 4-hydroxytamoxifen (OHT) or tamoxifen, the CreERT2 fusion protein can be translocated into the nucleus and exert a recombinase activity toward the LoxP sites. Thus, exposure of the mice (or cells) with tamoxifen can effectively activate Cre recombination (168,169).

Homozygous *Setd4*$^{flox/flox}$*;Rosa26-CreERT*$^{-/-}$ mice were crossed with *Setd4*$^{wt/wt}$*;Rosa26-CreERT2*$^{+/-}$ mice to generate *Setd4*$^{flox/wt}$*;Rosa26-CreERT2*$^{+/-}$ and *Setd4*$^{flox/flox}$*;Rosa26-CreERT2*$^{+/-}$ mice. With this mouse line, administration of tamoxifen can cause the translocation of the CreERT2 protein to nuclease and gain the access to the LoxP sites, can then cause recombination to delete exon-6 of Setd4 gene. As a result, whole body *Setd4* deficient mouse (*Setd4*$^{\Delta/\Delta}$*;Rosa26-CreERT2*$^{/+}$) can be obtained.

To efficiently and reliably distinguish the genomic alleles of wild type exon 6, floxed exon 6, and the deleted exon 6 (ΔExon 6), we first developed a multiplex PCR strategy using the primers sets displayed in **Figure 14A**. A PCR product of 234 bp between the primers A and C indicates the presence of wild type allele, a 318 bp product between primers A and B represent the floxed exon 6 allele, and a 369 bp product between primers A and C represent the deleted exon 6 allele. This is also summarized in **Table 9.**

We injected *Setd4$^{flox/flox}$;Rosa26-CreERT2$^{+/-}$* mice with tamoxifen or oil (as the negative control), and collected the tissues using the multiplex PCR strategy (**Figure 14A**). As represented in **Figure 14B** (top panel), all tissues of oil-injected mice contain the floxed exon 6 allele, although there were weak signals of the ΔExon6 allele in some tissues such as such as liver, small intestine or spleen, indicating that there was detectable amount of the Cre-mediated recombination in these tissues as reported before (170,171). Upon tamoxifen injections (**Figure 14B**, bottom panel), there were significant induction of the signals from the ΔExon6 allele. In bone marrow, spleen, thymus, liver, intestine and pancreas, tamoxifen caused almost a complete elimination of the floxed allele, suggesting a complete deletion of the exon 6 in these tissues. However, there remains some undeleted floxed allele in brain, heart, lung, liver, and kidney (**Figure 14B**, bottom panel). These data suggest that Tamoxifen can effectively induce exon 6 deletion in the mice, but the completeness varies depending on the tissues.

Next, we sought to determine whether the mRNA level of Setd4 is downregulated using Real-time quantitative reverse transcription PCR (qRT-PCR). Fresh tissues RNA were extracted and followed by cDNA preparation. We designed a pair of primer that spans exon 5 and 6 junction to prevent the amplification of genomic DNA, and can only amplify the 83bp Setd4 mRNA when exon 6 is not deleted (see **Figure 14C**, bottom panel). As shown in **Figure 14C**, the Setd4 mRNA level is significantly reduced in bone marrow, spleen, thymus, and small intestines, while moderately reduced in liver, lung, and cerebellum. These RNA expression data are in general agreement with the efficiency of

genomic deletions (**Figure 14B**).

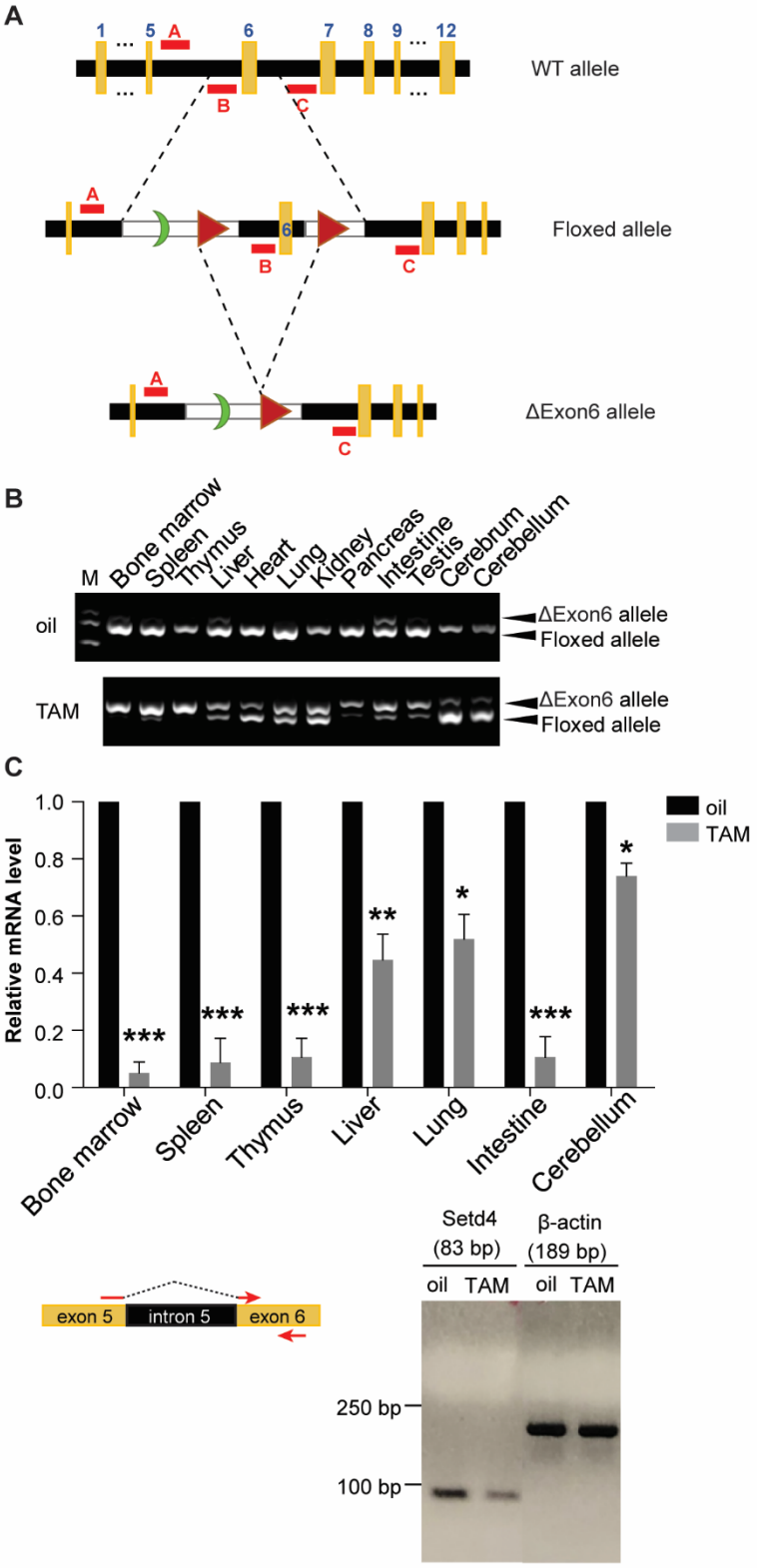

Figure 14. Strategy and verification of Cre-mediated Setd4 exon 6 deletion in mice. (A) Genomic structure of three mouse Setd4 alleles. Exon 6 was flanked by two LoxP sites inserted into introns 5 and 6 (Floxed allele). Cre mediated excision of exons 6 would render exon 7 out of frame and result in a functionally null Setd4 gene (ΔExon6 allele). Three primers were designed (A, B and C) for Setd4 allele PCR analysis. **(B)** Representative PCR result of different mouse tissue DNA with (TAM) or without (oil) tamoxifen treatment. The upper band represents ΔExon6 allele (369 bp, primer A and C), while the lower band is Floxed allele (318 bp, primer A and B). (**C**) qRT-PCR verification of downregulated mRNA of Setd4. The primer location was shown in red arrow. The PCR product at the end of cycles was run on gel to verify the correct sizes of Setd4 and β-actin amplification. Bar graph represents the relative mRNA levels in tested tissues. Error bars represent SD of the mean, with three independent repeats. All experiments were repeated at least three times and only representative figures are shown. Forward primer: 5'-GCGTCGTTGCAGGAGGG-3'; Reverse primer: 5'-AGGGAGCTTCGAATCAC-3'.

The variation of recombination efficiency in different tissues may reflect the varied tissue specific accumulation of tamoxifen, effectiveness of tamoxifen induced nuclear translocation of the CreERT2 in different tissues. In the case of brain, it may also reflect the limited permeability of tamoxifen to pass through the blood-brain-barrier (168). However, it cannot been ruled out that different tissues may have district local chromatin status at Setd4 locus, which cause variable sensitive to LoxP-mediated recombination.

The mouse SETD4 protein was predicted to be 439 amino acids, and weights about 46kD. Next, we attempted to confirm the Setd4 reduction on protein levels using several commercial and customary made antibodies as listed in **Table 14**. Despite of attempting different antibodies, the size of the positive band(s) from western blots varied among different tissues, and often differs between different antibodies. Among these antibodies, only SETD4C3 gave rise to a relatively specific band (**Figure 15A**). In thymus and spleen

samples, the major band is around 30kD, but in liver, a ~46kD band was apparent, which is approximately the full length SETD4 protein. However, the protein levels of these bands in livers and spleen did not match with the detected mRNA level in the same tissue, raising a doubt whether they represent the authentic SETD4 protein.

The five mouse SETD4 antibodies were also used to perform IHC to determine the expression level of SETD4 in formalin-fixed paraffin-embedded tissues, but only two of them (PA5-5 and SETD4C3) gave rise to distinct signals. As shown in **Figure 15B**, the staining pattern of spleen tissues leads us to suspect that mSETD4 is not universally expressed in all the cells, but only a small amount of cell populations had positive signals.

Table 14. SETD4 antibodies tested in this study

Name	**SETD4 Species**	**Antigen regions**	**Rabbit/Mouse**	
h25	Human	hSETD4 aa25-100	Rabbit	Shen Lab
SETD4C3	Mouse	mSETD4aa81-97 (exon 6)	Rabbit	Shen Lab
SETD4C4	Mouse	mSETD4aa81-97 (exon 6)	Rabbit	Shen Lab
F-3	Human	hSETD4 aa24-51	Mouse	Santa Cruz sc-514060
PA5-5	Mouse	hSETD4 aa332-435	Rabbit	Thermo Fisher
PA5-6	Mouse	hSETD4 aa188-258	Rabbit	Thermo Fisher

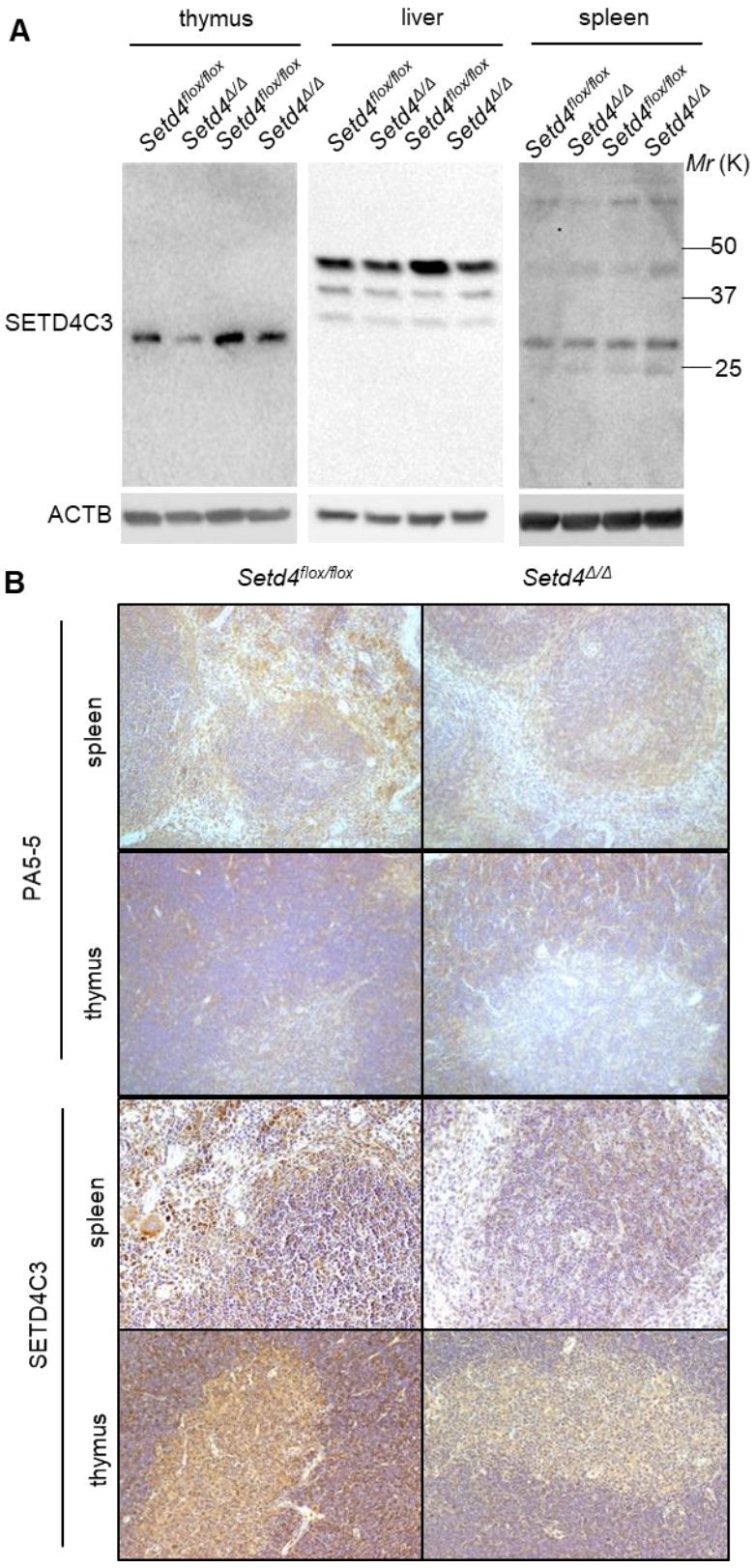

Figure 15. Confirmation of Setd4 knock out after tamoxifen treatment. (**A**). Representative western blot of thymus, liver and spleen tissues before and after tamoxifen treatment. The SETD4

protein level was detected by SETD4C3 antibody. (**B**). Two different antibodies, PA5-5 and SETD4C3, were used for IHC staining and assess the expression of mouse SETD4 in formalin-fixed paraffin-embedded tissues, spleen (top) and thymus (bottom).

Therefore, I unfortunately do not have a reliable method to detect mouse SETD4 protein by either western blot or IHC, despite my multiple attempts with several antibodies. I speculate that this could be due to several causes. First it is possible that the endogenous SETD4 level in mouse tissues are extremely low, and conventional western blot approach is not sufficiently sensitive. It is also possible that the mouse SETD4 protein is heavily modified or alternatively spliced in the tissues. The current Setd4 antibodies were produced with synthetic peptides or recombinant proteins purified from E Coli, and may not be able to detect the endogenous SETD4. Therefore, in my future study to be presented, I heavily rely on DNA genotyping and/or quantitative RT-PCR to verify the effectiveness of Setd4 deletion.

4.6. Induced whole body *Setd4* knockout mice were viable and not susceptible to spontaneous tumorigenesis.

The littermates *Setd4*$^{flox/flox}$*;Rosa26-CreERT*$^{+/-}$ mice were divided into two groups, and injected with tamoxifen or oil (Control) for 5 times. The tamoxifen injected mice were viable and didn't demonstrated any growth defects compared with oil treated mice. During the first 19 months, 45% of the oil treated *Setd4*$^{flox/flox}$*;Rosa26-CreERT*$^{+/-}$ (*Setd4*$^{flox/flox}$) mice died from inflammation (including dermatitis, hepatitis), congestive heart failure, and tumor based on necropsy of available cases, while 38% of tamoxifen treated

Setd4$^{flox/flox}$*;Rosa26-CreERT*$^{+/-}$ (*Setd4*$^{\Delta/\Delta}$) mice died during this time period (**Figure 16A**). However, there was no significant difference of the overall survival rate between *Setd4*$^{\Delta/\Delta}$ mice and *Setd4*$^{flox/flox}$ mice prior to 585 days (19 months) of life (p = 0.55). There was also no gender difference of death between the groups, nor significant difference in terms cause of death.

When aged mice (older than 19 months) were euthanized between 19 to 23 months, the overall neoplastic and nonneoplastic events were similar in both groups (**Table 15**). The subtle difference of hepatocarcinoma and lymphoma incidences between *Setd4*$^{\Delta/\Delta}$ and *Setd4*$^{flox/flox}$ mice was not statistically different (p=0.27) (**Table 15** and **Figure 16B**).

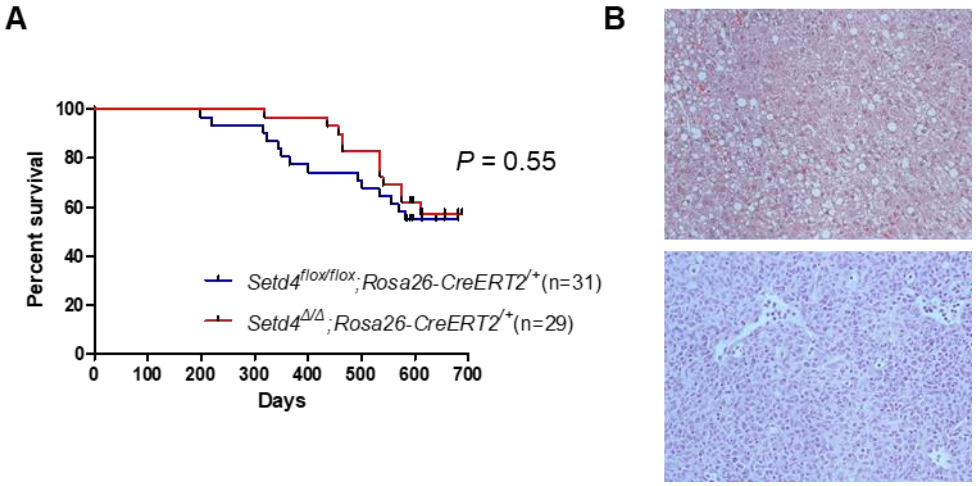

Figure 16. Survival of *Setd4*$^{flox/flox}$ and *Setd4*$^{\Delta/\Delta}$ mice. (A). Kaplan-Meier survival curves of o*il treated Setd4*$^{flox/flox}$*; Rosa26-CreERT*$^{+}$ (*Setd4*$^{flox/flox}$, n = 31) and tamoxifen treated *Setd4*$^{flox/flox}$*; Rosa26-CreERT*$^{+}$ (*Setd4*$^{\Delta/\Delta}$, n = 29) mice. p = 0.55 (log-rank Mantel–Cox test). (B). Representative histopathology of hepatocarcinoma from aged *Setd4*$^{flox/flox}$ mice (top) and lymphoma from aged *Setd4*$^{\Delta/\Delta}$ mice (bottom).

Table 15. Synopsis of Aged Mice (>19 months) Necropsy Outcomes

Cause of Death	**No. (%) of Diagnosable Cases**	
	Virgin *Setd4*$^{flox/flox}$ mice	Virgin *Setd4*$^{\Delta/\Delta}$ Mice
Inflammation(Dermatitis, hepatitis)	4 (24%)	4 (22%)
Pulmonary adenocarcinoma	1 (6%)	1 (6%)
Hepatocarcinoma	3 (18%)	1 (6%)
Lymphoma	0	2 (11%)
Neoplastic	4 (24%)	4 (22%)
Nonneoplastic	4 (24%)	4 (22%)
No visible lesions	9 (53%)	10 (56%)
Total cases	17	18

Chapter 5, Roles of Setd4 in Radiation Sensitivity and Bone Marrow Regeneration

With increasing doses of radiation exposure, mice can develop several well-defined acute radiation syndromes: hematopoietic syndrome when the mice usually die within 30 days (peaks at about 2 weeks), gastric-intestinal (GI) syndrome when the mice die within 10 days (peak at about 5 days), and neurological syndrome when the mice die around 1-2 days after the exposure (85,172-174). As described in Chapter 4, after using several approaches, I was able to establish a tamoxifen-inducible *Setd4* knockout mouse model, which can be used as a platform to investigate the potential role of Setd4 in mouse sensitivity to whole body radiation. In this chapter, I describe the findings with this approach.

5.1 Deletion of Setd4 protects mice from IR induced bone marrow failure.

A preliminary study had showed that both endogenous and exogenous SETD4 is recruited to DNA damage sites upon laser micro-irradiation and oxidative DNA damage (Shen lab, unpublished data). This prompted me to investigate whether Setd4 deficiency modulates the survival of animals upon whole body exposure to γ-irradiation. I injected the 8-week old adult *Setd4*$^{flox/flox}$;*Rosa26-CreERT2*$^{/+}$ and *Setd4*$^{flox/wt}$;*Rosa26-CreERT2*$^{/+}$ mice with tamoxifen once per day for 5 days to induce Setd4 deletion, resulting in *Setd4*$^{\Delta/\Delta}$ and *Setd4*$^{\Delta/wt}$ mice respectively. At the same time, half of the sex-matched littermates were injected with oil, resulting in *Setd4*$^{flox/flox}$ and *Setd4*$^{flox/wt}$ mice. These mice were exposed to 8 Gy of total body γ-irradiation (TBI), a dose lethal to approximately 50% of the wild type

mice with the same background (LD_{50}). The mice were monitored for 42 days. As can be seen from **Figure 17A**, 16 of the 28 control mice died with a median survival of 18 days, but only 1 of 16 *Setd4*$^{\Delta/\Delta}$ mice died during the same time period (*Setd4*$^{\Delta/\Delta}$ vs. control, p = 0.0015). Loss of one copy of *Setd4* also improved the survival of the *Setd4*$^{\Delta/wt}$ mice, with 3 deaths out of 13 exposed (*Setd4*$^{\Delta/wt}$ vs control, p = 0.039). These data indicate that loss of Setd4 has a protective effect against radiation-induced mortality in mice. To verify this result, mice were exposed to a slightly higher dose of 9 Gy that is lethal to ~90% of the mice. As shown in **Figure 17B**, 22 of the total 24 control mice died with survival of a median 13 days, while *Setd4*$^{\Delta/\Delta}$ mice again displayed a significantly prolonged survival (*Setd4*$^{\Delta/\Delta}$ vs control, p = 0.007). However, the *Setd4*$^{\Delta/wt}$ mice were equally sensitive as the control mice (*Setd4*$^{\Delta/wt}$ vs control, p = 0.32).

In the above experiments, the mice were exposed to irradiation 3 days after the last injection of tamoxifen. Although tamoxifen has not been shown to affect mouse sensitivity to irradiation, we performed experiments to rule out any possible role of tamoxifen in the radiation sensitivity using additional control mice. *Setd4*$^{flox/flox}$*;Rosa26CreERT2*$^{-/-}$, *Setd4*$^{flox/wt}$*;Rosa26CreERT2*$^{-/-}$ and *Setd4*$^{wt/wt}$*; Rosa26-CreERT2*$^{/+}$ mice were treated with either oil (n = 9) or tamoxifen (n = 12), and then exposed to 8 Gy TBI. As shown in **Figure 18**, no significant difference of survival was observed between these oil and tamoxifen treated groups after 8 Gy (p = 0.5) or 9 Gy exposures (p=0.8). These results ruled out any potential effect of tamoxifen on the survival difference as observed in **Figure 17**.

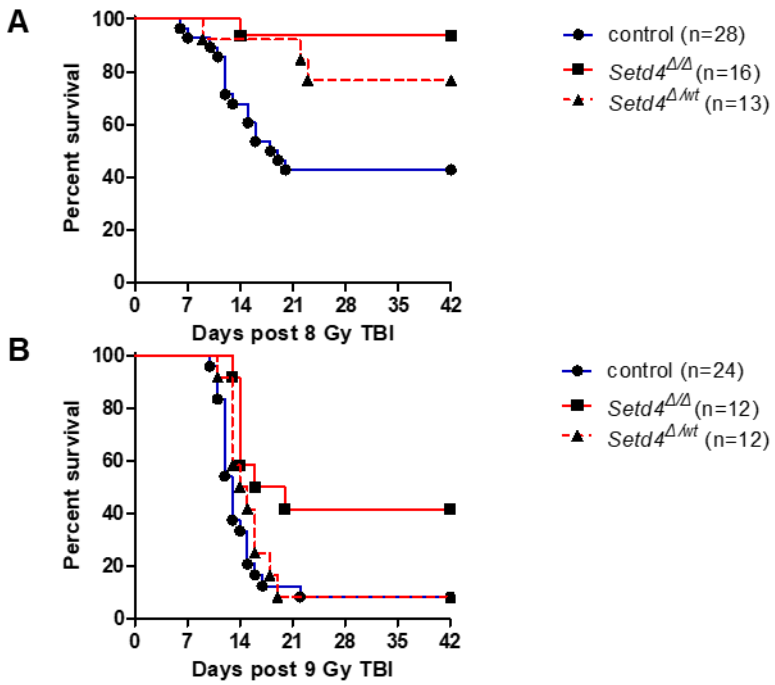

Figure 17. Kaplan-Meier survival of conditional mice treated with tamoxifen before total-body γ-irradiation. Littermates of *Setd4*$^{flox/flox}$ and *Setd4*$^{flox/wt}$ treated with oil or tamoxifen were given an 8 Gy (panel A) or 9 Gy (panel B) of TBI. The animal survival was monitored for 42 days. **A**. Control: littermates of *Setd4*$^{flox/flox}$ and *Setd4*$^{flox/wt}$ treated with oil (n = 28); *Setd4*$^{\Delta/\Delta}$: tamoxifen treated *Setd4*$^{flox/flox}$ (n = 16); *Setd4*$^{\Delta/wt}$ tamoxifen treated *Setd4*$^{flox/wt}$ (n = 13). *Setd4*$^{\Delta/\Delta}$ vs control, p = 0.0015; *Setd4*$^{\Delta/wt}$ vs control, p = 0.039.

B. Control: littermates of *Setd4*$^{flox/flox}$ and *Setd4*$^{flox/wt}$ treated with oil (n = 24); *Setd4*$^{\Delta/\Delta}$: tamoxifen treated *Setd4*$^{flox/flox}$ (n = 12); *Setd4*$^{\Delta/wt}$: tamoxifen treated *Setd4*$^{flox/wt}$ (n = 12). *Setd4*$^{\Delta/\Delta}$vs control, p = 0.007; *Setd4*$^{\Delta/wt}$ vs control, p = 0.32.

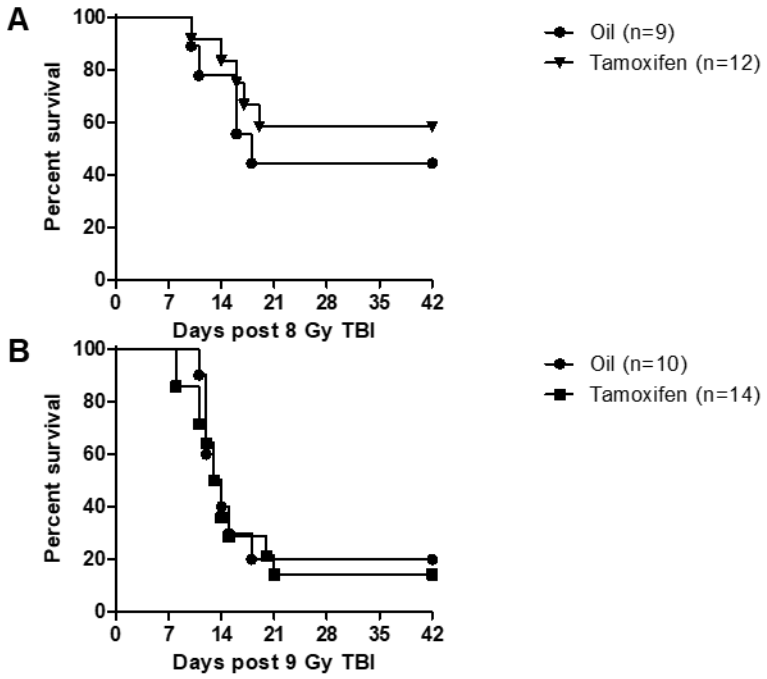

Figure 18. Kaplan-Meier survival of control mice treated with tamoxifen. Oil and tamoxifen treated control mice were exposed to 8 Gy (panel A) or 9 Gy (panel B), and the animal survival was monitored for 42 days.

A. Oil: the combined mice of oil-treated *Setd4$^{flox/flox}$;Rosa26CreERT2$^{-/-}$* (n = 4), *Setd4$^{flox/wt}$;Rosa26CreERT2$^{-/-}$* (n = 3), and *Setd4$^{wt/wt}$; Rosa26-CreERT2$^{/+}$* (n = 2). Tamoxifen: the combined mice of tamoxifen treated *Setd4$^{flox/flox}$;Rosa26CreERT2$^{-/-}$* (n = 4), *Setd4$^{flox/wt}$;Rosa26CreERT2$^{-/-}$* (n = 4), and *Setd4$^{wt/wt}$; Rosa26-CreERT2$^{/+}$* (n = 4). P=0.5 (Oil vs Tamoxifen).

B. Oil: the combined mice of oil-treated *Setd4$^{flox/flox}$;Rosa26CreERT2$^{-/-}$* (n = 6), *Setd4$^{flox/wt}$;Rosa26CreERT2$^{-/-}$* (n = 2), and *Setd4$^{wt/wt}$; Rosa26-CreERT2$^{/+}$* (n = 2). Tamoxifen: the combined mice of tamoxifen-treated *Setd4$^{flox/flox}$;Rosa26CreERT2$^{-/-}$* (n = 6), *Setd4$^{flox/wt}$;Rosa26CreERT2$^{-/-}$* (n = 4), and *Setd4$^{wt/wt}$; Rosa26-CreERT2$^{/+}$* (n = 4). P=0.8 (Oil vs Tamoxifen).

The time course of mouse fatality as described in **Figures 17-18** was consistent with radiation-induced hematopoietic syndrome, suggesting a role of Setd4 deletion in the protection of radiation induced hematopoietic failure. To further address whether Setd4 deletion also protects the mice from radiation-induced gastric-intestinal (GI) syndrome, we irradiated the littermates of *Setd4$^{\Delta/\Delta}$* and *Setd4$^{flox/flox}$* mice with 13 Gy TBI. All the mice

died within 10 days post IR and the median is 6 and 7 days respectively (**Figure 19**), confirming the induction of gastric intestinal syndrome at this dose. However, mice in both groups died of GI syndrome with a similar time course, suggesting that there is little effect of Setd4 loss in protecting the mice from radiation induced GI syndrome.

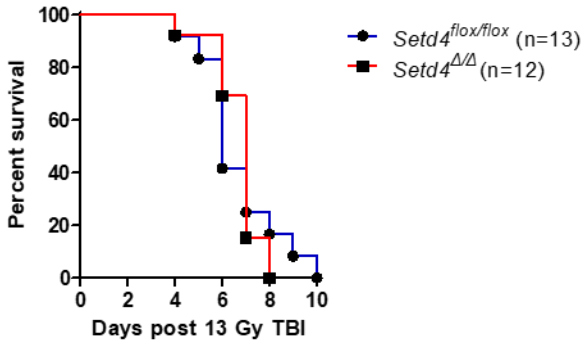

Figure 19. Kaplan-Meier survival of conditional mice treated with tamoxifen before 13 Gy of total-body γ-irradiation. Littermates of *Setd4*$^{\Delta/\Delta}$ (n = 13, tamoxifen treated *Setd4*$^{flox/flox}$) and *Setd4*$^{flox/flox}$ (n = 12, oil treated) were given TBI at a dose of 13 Gy. Their survival was monitored for 12 days. p = 0.96.

As shown in **Figures 17 and 18**, there were sufficient number of mice survived the 8 Gy of single dose irradiation. These mice were kept for long-term observation for up to 600 days. As shown in **Figure 20**, the survived mice have little significant difference in term of long-term survival. They typically developed lymphoma, epicarditis, and myocarditis. The incidences of tumors in irradiated *Setd4*$^{\Delta/\Delta}$ mice (3/15) were comparable with *Setd4*$^{\Delta/wt}$ (2/10) and control mice (3/12). These data suggest that *Setd4* loss does not increase the tendency of tumor development after a single dose 8 Gy TBI once the mice survived the initial hematopoietic syndrome (**Figure 20**).

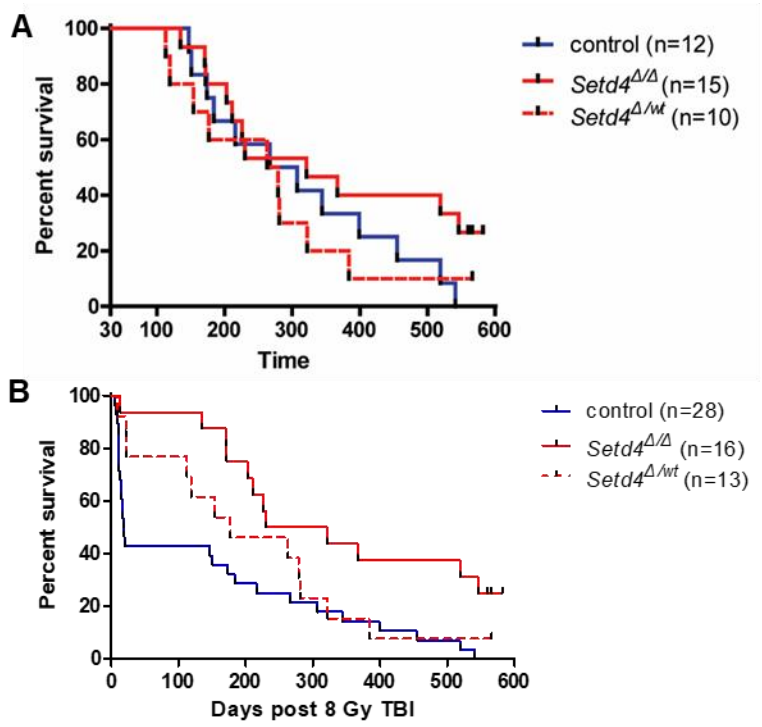

Figure 20. **Kaplan-Meier survival of long-term survival of the *Setd4*$^{\Delta/\Delta}$, *Setd4*$^{\Delta/wt}$, and control mice that survived 30 days after the 8Gy initial irradiation.**
A. The long-term survival of the mice recovered from the initial hematopoietic syndrome from 8Gy of TBI. The median for control mice is 287 days, *Setd4*$^{\Delta/\Delta}$ is 321 days, and for *Setd4*$^{\Delta/wt}$ is 271 days.
B. The overall survival of the mice exposed to 8 Gy TBI from the beginning of the irradiation.

5.2 Setd4 deletion promotes bone marrow recovery from radiation damage.

Since deletion of Setd4 protected the mice from fatality of radiation induced hematopoietic syndrome (**Figure 17**), I hypothesized that Setd4 may modulate bone marrow recovery upon radiation damage. I adapted the well-established methods to quantify the number of different cell types in the hierarchy of the bone marrow regeneration at different times after radiation exposure. In each mouse, I collect all bone marrow cells from one pair of the femur and tibia, isolated and counted the mono-nuclear cells (BM-MNC) (see Chapter 3 for the detailed methods on BM-MNC isolation) from tamoxifen treated *Setd4*$^{flox/flox}$*;Rosa26-CreERT2*$^{/+}$ *(Setd4*$^{\Delta/\Delta}$*)*, and *Setd4*$^{wt/wt}$*;Rosa26-CreERT2*$^{/+}$ *(Setd4*$^{wt/wt}$*)*,

and oil treated *Setd4$^{flox/flox}$;Rosa26-CreERT2$^{-/+}$ (Setd4$^{flox/flox}$)* mice. As shown in **Figure 21A**, shortly after irradiation (4 days), there was equal level of BM-MNC depletion for both knockout and control mice. However, by 14 and 21 days, there were more BM-MNC in the *Setd4$^{\Delta/\Delta}$* mice than the control mice, suggesting an enhanced recovery in the Setd4 knockout mice.

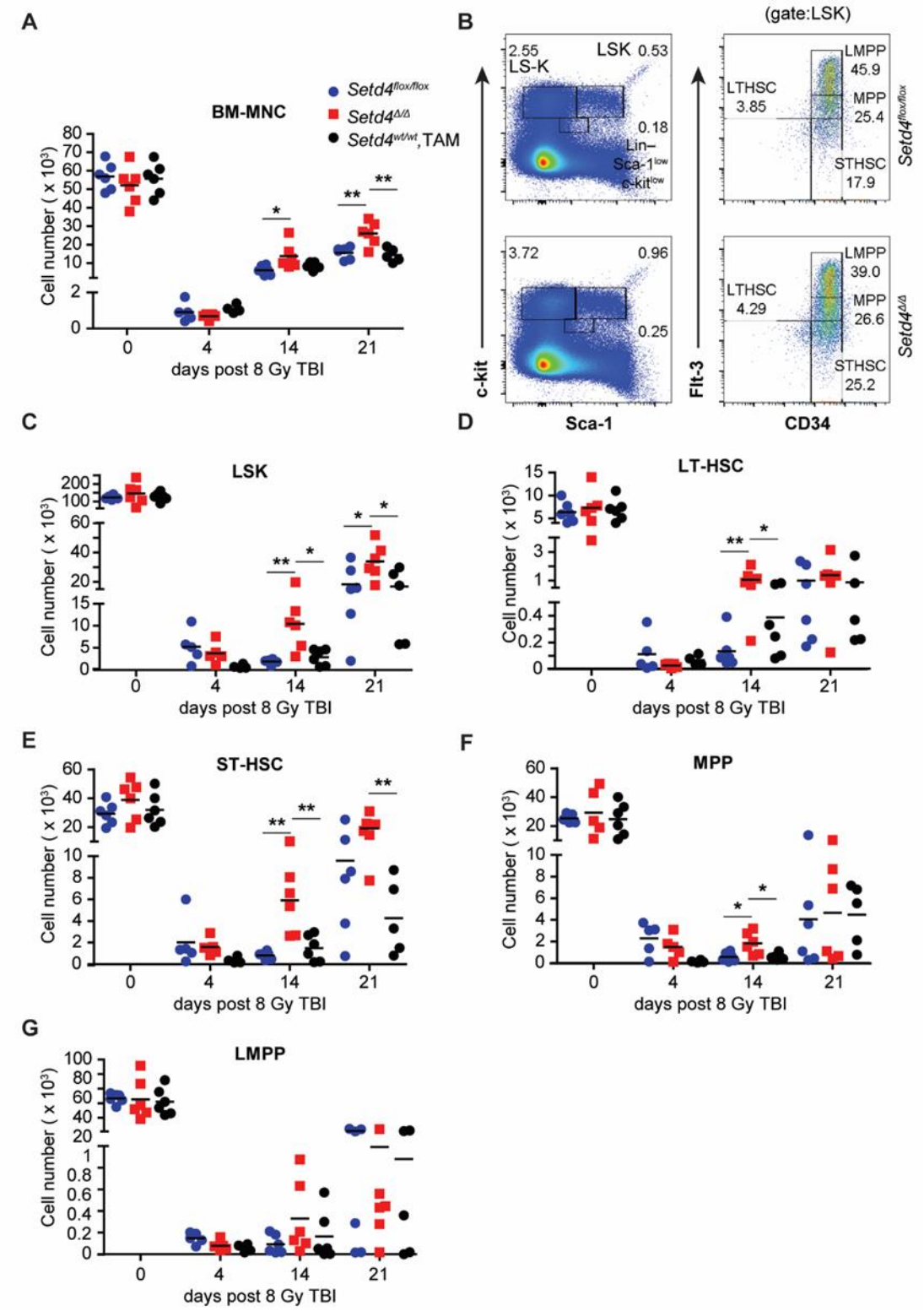

Figure 21. **Bone marrow cell counts of HSCs and HPCs after 8 Gy of irradiation.** The bone marrow cell counts were analyzed at 4, 14, and 21 days after 8Gy of TBI. See Section 3.11 in Chapter 3 for technical details on the surface marker based identification of the cell population.

A. Total bone marrow mono-nuclear cell counts.
B. Representative flow-cytometry staining profiling for HSC and progenitors populations. **C-G**. The numbers of cells recovered from a pair of femur and tibia at each time points for LSK, LT-HSC, ST-HSC, MPP and LMPP.

To compare the kinetics of BM HSCs and HPCs post TBI in *Setd4*$^{\Delta/\Delta}$ and *Setd4*$^{flox/flox}$ mice, we further analyzed the BM sub-populations in a time course after IR. Mice were exposed to TBI and 4, 14, 21 days later, BM cells were isolated and enumerated. Then, the BM-MNC cells were stained with a series of fluorescent antibodies cocktails to determine the relative distribution of various hematopoietic cell populations by multicolor flow cytometry (175-177). A representative flow cytometry profile is shown in **Figure 21B, 22A** and **22E**. HSCs and HPCs were firstly enriched in Lineage negative (Lin$^-$) cell population, which exclude well differentiated cells (data not shown). Then these cells were divided into three cell populations based on different selection markers: LSK (Sca-1$^+$ (S) and c-kit$^+$ (K)), LS$^-$K (Lin$^-$ Sca-1$^-$ c-kit$^+$), and Lin$^-$ Sca-1^{low} c-kit^{low} (**Figure 21B**, left panel). On the basis of CD34 and Flt-3 expression, LSKs were further separated into four groups: long-term HSCs (LT-HSCs; Flt-3$^-$ CD34$^-$), short-term HSCs (ST-HSCs; Flt-3$^-$ CD34$^+$), multipotent progenitors (MPPs; CD34$^+$ Flt-3^{Int}), and lymphoid-primed MPPs (LMPPs; CD34$^+$ Flt-3^{Bright}) (**Figure 21B**, right panel) (177). Further differentiation of MPPs and LMPPs gives rise to common lymphoid progenitors (CLPs) (Lin$^-$ Sca-1^{low} c-kit^{low}) (**Figure 22E**). In addition, LS-K BM population was further divided, based on CD34 and CD16/32 expression, into common myeloid progenitors (CMP; CD16/32$^-$ CD34$^+$), granulocyte-macrophage progenitors (GMP; CD16/32$^+$ CD34$^+$), and megakaryocyte-erythroid

progenitors (MEP; CD16/32^{-} CD34^{-}) (**Figure 22A**).

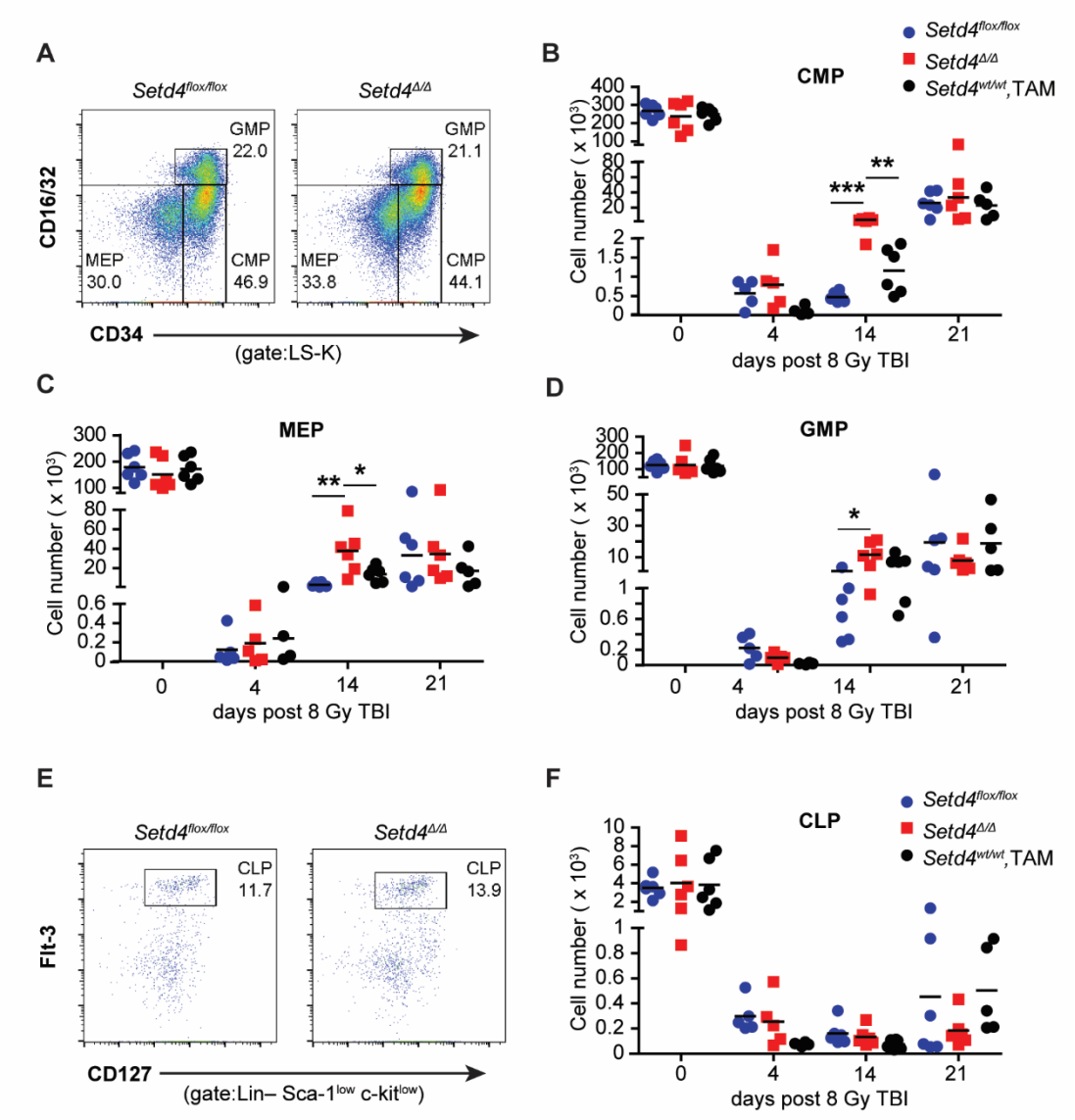

Figure 22. **Myeloid and lymphoid progenitor counts after 8 Gy of irradiation.**
A. Representative staining profiling for BM myeloid progenitors populations.
B-D. Absolute cell numbers in each time points of CMP, MEP, and GMP.
E. Representative staining profiling for BM CLP populations.
F. Total number of cells in each time points of CLP.

As shown in **Figures 21C-21G**, without irradiation, there were no significant difference of LSK, LT-HSC, ST-HSC, MPP, and LMPP populations between Setd4

knockout mice and control mice. Shortly after irradiation, all cell populations were equally depleted at 4 days. However, by 14 days after irradiation, the Setd4 knockout mice have significantly enhanced recovery of these cell populations, except LMPP. Similarly, there were enhanced recoveries of the CMP, MEP, and GMP populations at 14 day (**Figures 22B-22D**), but not CLP (**Figure 22F**). By 3 weeks post IR, the difference among groups are not as dramatic as 2 weeks because at this time point, all the survived mice had passed the most death-susceptible window of hematopoietic failure and likely have succeeded to replenish damaged bone marrow. Collectively, these data indicates that Setd4 inactivation leads a faster recovery of IR induced bone marrow injuries by efficient expansion of LT-HSC, ST-HSC and especially myeloid progenitors.

However, under 6.5 Gy when all mice can survive, all cell subsets had similar recovery rates in both Setd4 knockouts and wild type mice (data not shown), which implied that Setd4 deficiency mediated radiation response is more relevant to lethal dose exposure.

5.3 Enhanced erythropoiesis in Setd4 deficient mice spleen post high-dose ionizing radiation.

Under insult conditions such as radiation, inflammation, anemia and so on, when bone marrow repopulation was impaired, erythropoiesis in other hematopoietic organs such spleen in rodent will take place to support the organism (178). During the course of the study, we observed enlarged spleens more frequently in the *Setd4*$^{\Delta/\Delta}$ mice than the

Setd4$^{flox/flox}$ mice (**Figure 23A**). This prompted us to investigate whether there is any effect of Setd4 loss in splenic erythropoiesis. As shown in **Figure 23B**, there was indeed a significantly enhanced erythropoiesis in *Setd4*$^{\Delta/\Delta}$ spleen than in *Setd4*$^{flox/flox}$ and *Setd4*$^{wt/wt}$ mice 2 weeks post IR 8 Gy. To examine erythroid maturation, we analyzed cell surface markers CD71 and Ter119, which are commonly used to define the maturation stages of erythroid progenitors (179,180) (see **Figure 23C**). At 2 weeks after 8Gy of irradiation, we observed significantly more S3 (CD71^{hi}/Ter119^{hi}) population and correspondingly reduced immature S0 (CD71^{-}/Ter119^{-}) population (**Figure 23D**), indicating a significantly enhanced erythropoiesis in *Setd4*$^{\Delta/\Delta}$ mice (**Figure 23E**). The percentage of erythroid cell population (S1-S5) relative to lymphoid and myeloid cell populations in the spleen is also increased in *Setd4*$^{\Delta/\Delta}$ mice compared to the other groups (**Figure 23F**). This result indicates that loss of Setd4 also enhanced splenic erythropoiesis after irradiation, which would certainly contribute to the better survival post IR.

5.4 Setd4 loss further enhances the survival of p53 deficient mice post IR.

The p53 tumor suppressor is a critical mediator of apoptosis in hematopoietic progenitors exposed to genotoxic damage, and p53 deficient mice can survive otherwise lethal radiation due to their refractory BM-derived hematopoietic progenitors (181). To test the potential genetic interdependence of Setd4 and p53 mediated apoptotic pathway, we generated lines of mice lacking either or both proteins and subjected the sex-matched littermates to 9 Gy TBI. As expected, *p53*$^{\Delta/\Delta}$ mice survived this lethal dose, with a slightly better survival than

Setd4$^{\Delta/\Delta}$ mice, while *Setd4*$^{\Delta/\Delta}$*;p53*$^{\Delta/\Delta}$ mice displayed a further increased survival rate above these groups (**Figure 24**). This result indicates that Setd4-dependent survival pathway might be independent of p53.

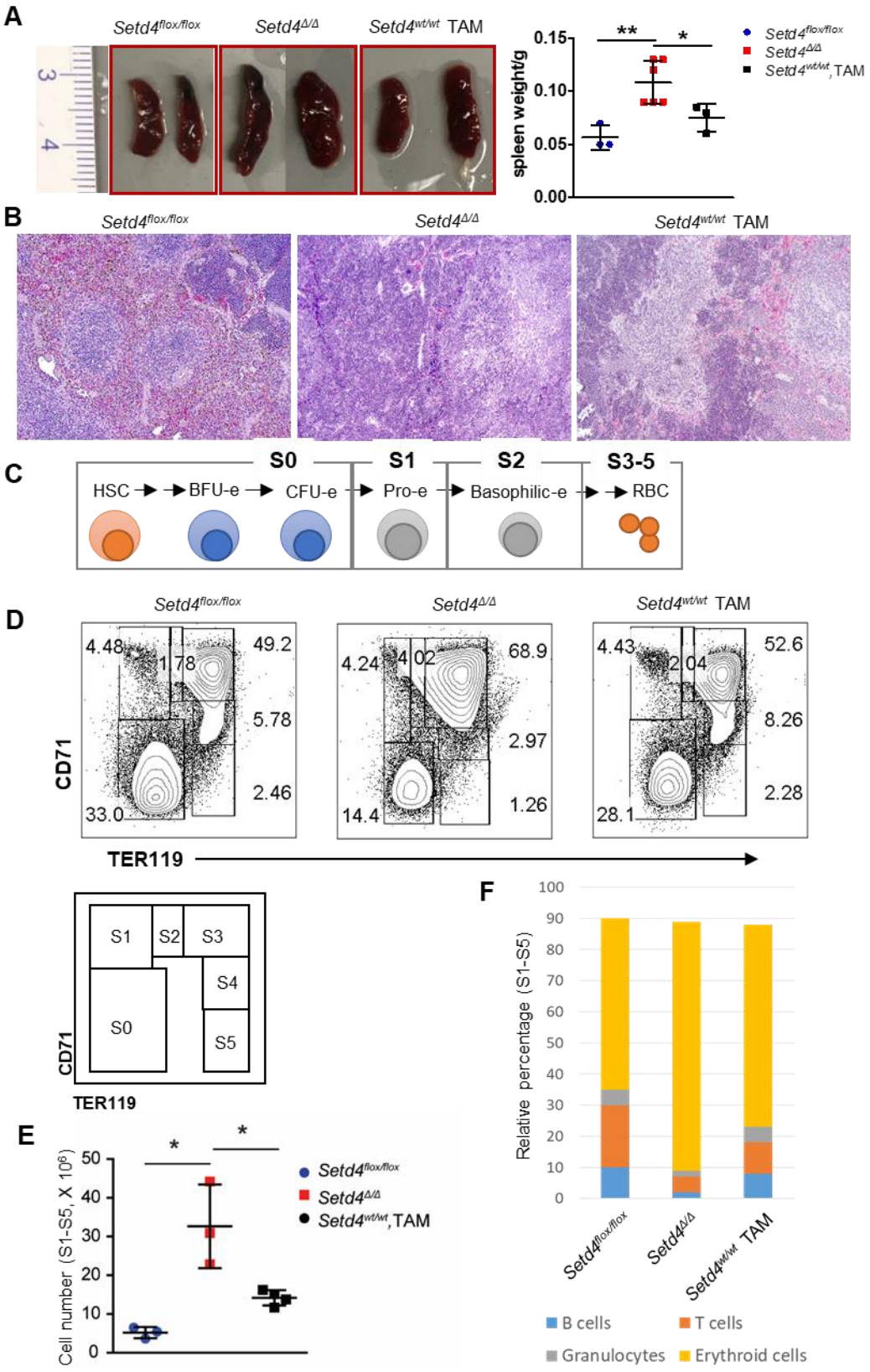

Figure 23. Splenic erythropoiesis post high-dose of ionizing radiation.

A. Representative gross features of spleens and spleen weight at 2 weeks post 8 Gy TBI.
B. H&E staining of spleens at 2 weeks post 8 Gy TBI.
C. Representation of erythroid developmental sequence from S0 to S5. HSC: hematopoietic stem cell; BFU-e: burst-forming unit-erythroid; CFU-e: colony-forming unit-erythroid; Pro-e: pro erythroblast; Basophilic-e: basophilic erythroblast. This panel was modified from (179).
D. Representative staining profiling for spleen erythroid populations.
E. Numbers of splenic erythroid cell populations (S1-S5) at 2 weeks post 8 Gy.
F. Percentage of B, T, granulocytes, and erythroid cells in the spleen at 2 weeks post 8 Gy.

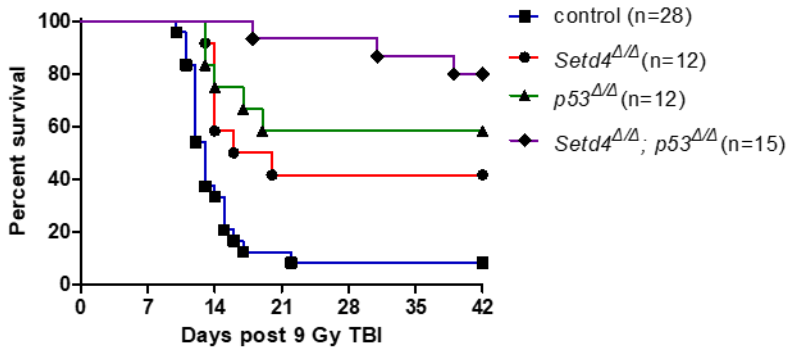

Figure 24. **Comparative survival of *Setd4*$^{\Delta/\Delta}$ and *p53*$^{\Delta/\Delta}$ mice to total-body γ-irradiation.** Three genotypes (*Setd4*$^{\Delta/\Delta}$, n = 12; *p53*$^{\Delta/\Delta}$, n = 12; *Setd4*$^{\Delta/\Delta}$*; p53*$^{\Delta/\Delta}$, n = 15) were given TBI at a dose of 9 Gy. Their survival was monitored for 42 days. *Setd4*$^{\Delta/\Delta}$ vs *Setd4*$^{\Delta/\Delta}$*; p53*$^{\Delta/\Delta}$, p = 0.019; *p53*$^{\Delta/\Delta}$ vs *Setd4*$^{\Delta/\Delta}$*; p53*$^{\Delta/\Delta}$, p = 0.15; *Setd4*$^{\Delta/\Delta}$ vs *p53*$^{\Delta/\Delta}$, p = 0.48. The same survival of wild type mice as shown in **Figure 17B** is included here for comparison.

5.5 Contribution of the HSC hierarchy in radiation sensitivity.

The difference of bone marrow sensitivity to radiation damage may be due to intrinsic effects of Setd4 deficiency on the HSC hierarchy or due to protective effect from bone marrow microenvironment (bone marrow niche). It is generally believed that the fitness of the HSCs and the progenitors in the hematopoiesis hierarchy play a critical role in the recovery of the bone marrow failure. In addition, the microenvironment niche provides essential regulatory and supporting function for hematopoiesis. We first hypothesized that Setd4 deletion in the HSC hierarchy confers a resistance to radiation, which contributes to

an enhanced recovery of these mice from radiation induced bone marrow failure. In addition, Setd4 deficiency may have improved the fitness of the HSC hierarchy. To test these hypotheses, we designed three bone marrow transplantation approaches.

Direct measurement of radiation sensitivity of BM-depleted mice that were supplemented with Setd4 deficient HSCs. First, we irradiated B6.SJL wild type mice with CD45.1 surface marker with two doses of 6.5Gy (2x6.5 Gy) separated by 4 hours. It is well established that this scheme of irradiation can completely deplete the entire HSC driven hematopoiesis, but not the bone marrow niche the mice (182). Within 24 hours after the irradiation, 1 million of Lin^- bone marrow cells from *Setd4*$^{\Delta/\Delta}$ (tamoxifen treated *Setd4*$^{flox/flox}$*;Rosa26-CreERT2*$^{/+}$) or *Setd4*$^{flox/flox}$ (Oil treated *Setd4*$^{flox/flox}$*;Rosa26-CreERT2*$^{/+}$ sex-matched littermates) were transplanted to treat the bone marrow failure (**Figure 25A**). As expected, this procedure completely rescued the lethality of the recipient mice (24 of 24 mice survived the treatment). Eight weeks of after the transplantation, peripheral blood was sampled to analyze the distribution of the CD45 surface marker. As represented in **Figure 25B**, more than 90% of the cells contain the donor surface marker of CD45.2, but not the recipient marker of CD45.1, suggesting that the transplantation was successful. Furthermore, the DNA of ear clips, which contains cells of the recipient wild type and the blood cells from the donor *Setd4*$^{flox/flox}$ or *Setd4*$^{\Delta/\Delta}$ mice, were used for genotype verification. As shown in **Figure 25C**, all the *Setd4*$^{flox/flox}$ mice contain the Setd4 flox-Exon6 allele (as well as the wild type genotype of the recipient mice as expected), and all

the *Setd4*$^{\Delta/\Delta}$ mice contain the Setd4 ΔExon6 allele. These data (**Figure 25B and 25C**) firmly concluded that the transplanted mice have successfully implanted the donor HSC as the source of hematopoiesis, thus they were chimera mice where the HSC-hierarchy was contributed by the donor mice (*Setd4*$^{flox/flox}$ or *Setd4*$^{\Delta/\Delta}$).

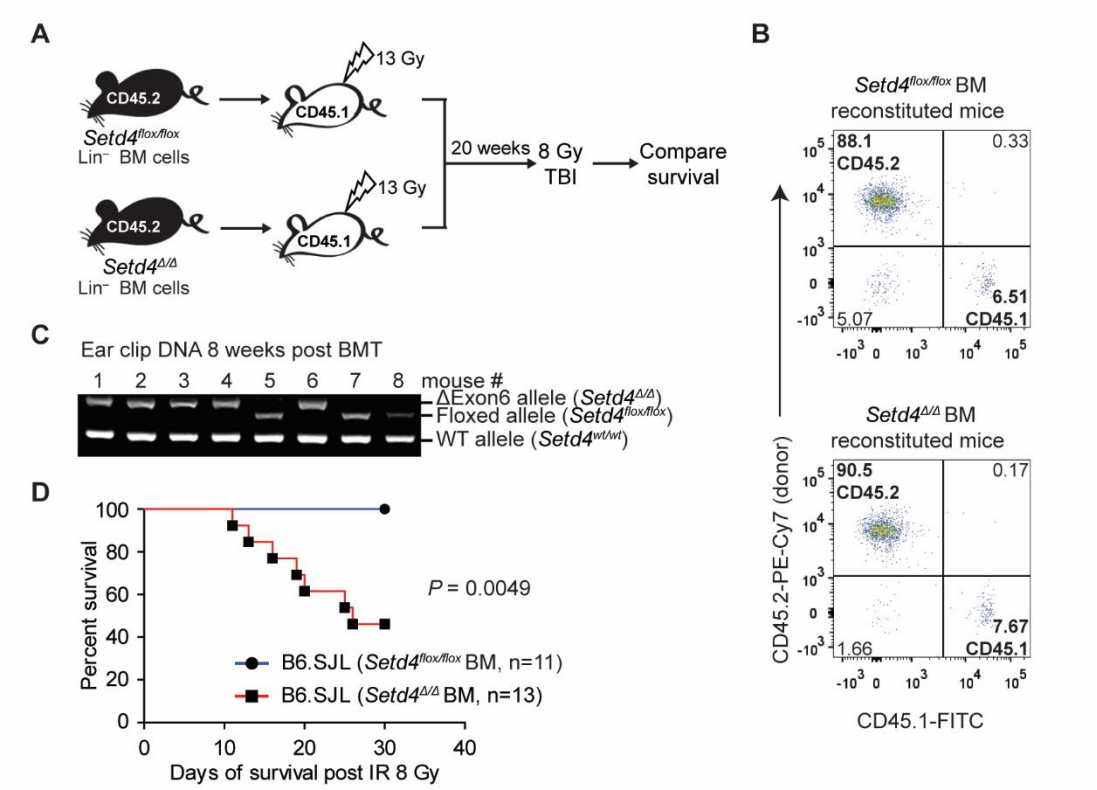

Figure 25. ***Setd4*$^{\Delta/\Delta}$ reconstituted mice are significantly more sensitive than *Setd4*$^{flox/flox}$ reconstituted mice given 8 Gy TBI.**

A. Schema detailing of non-competitive reconstituted survival assay. 1 million Lin^{-} BM cells from either *Setd4*$^{flox/flox}$ or *Setd4*$^{\Delta/\Delta}$ mice (CD45.2) were transferred into lethally irradiated B6.SJL mice (CD45.1). 16 weeks post transplantation, the fully-reconstituted recipients were exposed to 8 Gy irradiation.

B. Flow cytometric analysis of peripheral blood cells from CD45.1 recipients reconstituted with CD45.2 *Setd4*$^{flox/flox}$ BM cells (top panel) or with CD45.2 *Setd4*$^{\Delta/\Delta}$ BM cells (bottom panel). The peripheral blood cells were isolated 8 weeks after lethal TBI and bone marrow transplantation, and then stained with FITC-CD45.1 and PE-Cy7-CD45.2 antibodies.

C. Genotyping of ear snips from reconstituted mice. Genotyping PCR was performed with *Setd4* allele-specific primers. Genomic DNA templates extracted from earsnips of recipients reconstituted with $Setd4^{\Delta/\Delta}$ BM cells (lanes 1 to 4, and 6) or with $Setd4^{flox/flox}$ BM cells (lanes 5, 7, 8).
D. Kaplan-Meier survival curves of reconstituted CD45.1 B6.SJL mice after γ radiation. B6.SJL recipients were given a lethal dose of TBI and reconstituted with 1×10^6 total bone marrow cells from $Setd4^{\Delta/\Delta}$mice or $Setd4^{flox/flox}$ mice ($Setd4^{\Delta/\Delta}$ BM-reconstituted B6.SJL mice, n = 13; $Setd4^{flox/flox}$ BM-reconstituted B6.SJL mice, n = 11). After 16 weeks, the mice were given a single dose of (8.0 Gy) and monitored for survival (p = 0.0049).

Because it takes about 16 weeks for the LT-HSCs to fully refurnish the entire hematopoiesis hierarchy (183), these mice were kept for 20 weeks after the transplantation, and then treated for whole body irradiation (8Gy) to induce hematopoietic syndrome and determine whether there is any difference of radiation sensitive between the $Setd4^{flox/flox}$ and $Setd4^{\Delta/\Delta}$ donors. As shown in **Figure 25D**, the mice transplanted with $Setd4^{\Delta/\Delta}$ HSC died with a typical time-course of hematopoietic syndrome, but they were actually more sensitive than the mice transplanted with the $Setd4^{flox/flox}$ HSC. This is contradictory to prediction of our initial hypothesis of "Setd4 deletion in the HSC hierarchy confers resistance to radiation". As a matter of fact these results suggest that $Setd4^{\Delta/\Delta}$ HSC hierarchy may actually be more sensitive than $Setd4^{flox/flox}$ mice.

Radiation sensitivity of competitively transplanted HSCs. Because of the unexpected finding in **Figure 25D**, we designed a second approach using a competitive transplantation assay as outlined in **Figure 26A.** First, we depleted the bone marrow of wild type recipient mice (CD45.1, B6SJL) with 2x6.5Gy of TBI separated by 4 hours according the procedure as described before (182). Then, Lin^- bone marrow cells of $Setd4^{\Delta/\Delta}$ (CD45.2) and $Setd4^{wt/wt}$

(CD45.1/2, B6xB6.SJL) were mixed at approximately 1:1 ratio, and transplanted into the lethally radiated congenic recipients (CD45.1). The relative contribution of each type of donor cells to hematopoiesis (as represented by peripheral T-cells, B-cells, and granulocytes) was monitored every 4 weeks by flow cytometric analysis for the first 16 week after transplantation. We routinely take blood samples every 4 weeks, because this is considered the shortest period of time for the mice to recover from the blood loss due to sampling without affect its well beings. As presented in **Figure 26B**, this transplantation successfully implanted the CD45.2 and CD45.1/2 donors and there were little recipient CD45.1 cells left in peripheral blood. At 8 weeks after the transplantation, the relative contributions of $Setd4^{\Delta/\Delta}$ (CD45.2) and $Setd4^{wt/wt}$ (CD45.1/2) cell types to the blood cell population were about 45-50% and 50-55% respectively. We reasoned that, if the radiation sensitivities of $Setd4^{\Delta/\Delta}$ (CD45.2) and $Setd4^{wt/wt}$ (CD45.1/2) are similar, then the relative percentage of these populations should remain consistent in the animals after irradiation. During the first 16 weeks post transplantation, the population size between $Setd4^{\Delta/\Delta}$ and $Setd4^{wt/wt}$ was indeed approximately 1:1 as expected (**Figure 26C**), suggesting a relatively even competitiveness of these cell types to regenerate peripheral blood.

For the same reason that it takes about 16 weeks for the mice to refurnish the entire bone marrow and peripheral system with new LT-HSC (183), the reconstituted mice were exposed to 6.5 Gy of gamma-radiation at 20 weeks after the initial transplantation. We then estimated the relative population sizes of the $Setd4^{\Delta/\Delta}$ (CD45.2) and $Setd4^{wt/wt}$ (CD45.1/2)

cells in peripheral blood based on the CD45 markers every 4 weeks after the irradiation, i.e. 24, 28, and 32 weeks after the initial transplantation. We reasoned that if the *Setd4*$^{\Delta/\Delta}$ and *Setd4*$^{wt/wt}$ cells have similar radiation sensitive, their relative contribution to the bone marrow and peripheral blood should remain consistent in the following weeks after irradiation. **Figure 26C** shows the relative population sizes of the irradiated (top panel) and non-irradiated (bottom panel) mice. Remarkably, the size of irradiated *Setd4*$^{\Delta/\Delta}$ population became reduced after irradiation (**Figure 26C**, top panels), while it is gradually increased in the non-irradiated mice (**Figure 26C**, bottom panel). The total ratio of *Setd4*$^{\Delta/\Delta}$ cells to wild type competitor cell dropped from 1.5:1 to 0.5:1 by 4 weeks (24 weeks after transplantation) and couldn't recover later (**Figure 26D**). This lineage analysis also suggested that myeloid lineage was mostly affected, and the ratio decreased significantly from 1:1 to 1:4 12 weeks post IR (**Figure 26D**). The relative ratio of B cells seemed not affected by IR, while T cells also decreased immediately 4 weeks post IR (**Figure 26B**). These data suggest that deletion of Setd4 conferred a radiation sensitivity for the *Setd4*$^{\Delta/\Delta}$ cells when compared with *Setd4*$^{wt/wt}$ competitors.

To further assess the long-term fitness of the bone marrow cells, we measured relative contribution of the Setd4 deficient and wild type bone marrow cells after additional 16 weeks (48 weeks after the initial transplantation, or 28 week after the irradiation) for the same mice used in **Figure 26.** As shown in **Figure 27A**, the ratio of the *Setd4*$^{\Delta/\Delta}$ to *Setd4*$^{wt/wt}$ cells in the bone marrow were significantly reduced at the time of the observation. For

example, the ratio of *Setd4*$^{\Delta/\Delta}$ to *Setd4*$^{wt/wt}$ LT-HSCs decreased from 1:1 to 1:9. This suggests that the Setd4 deficient LT-HSCs and its progenies were more sensitive to radiation, consistent with the conclusion drawn from **Figure 25**.

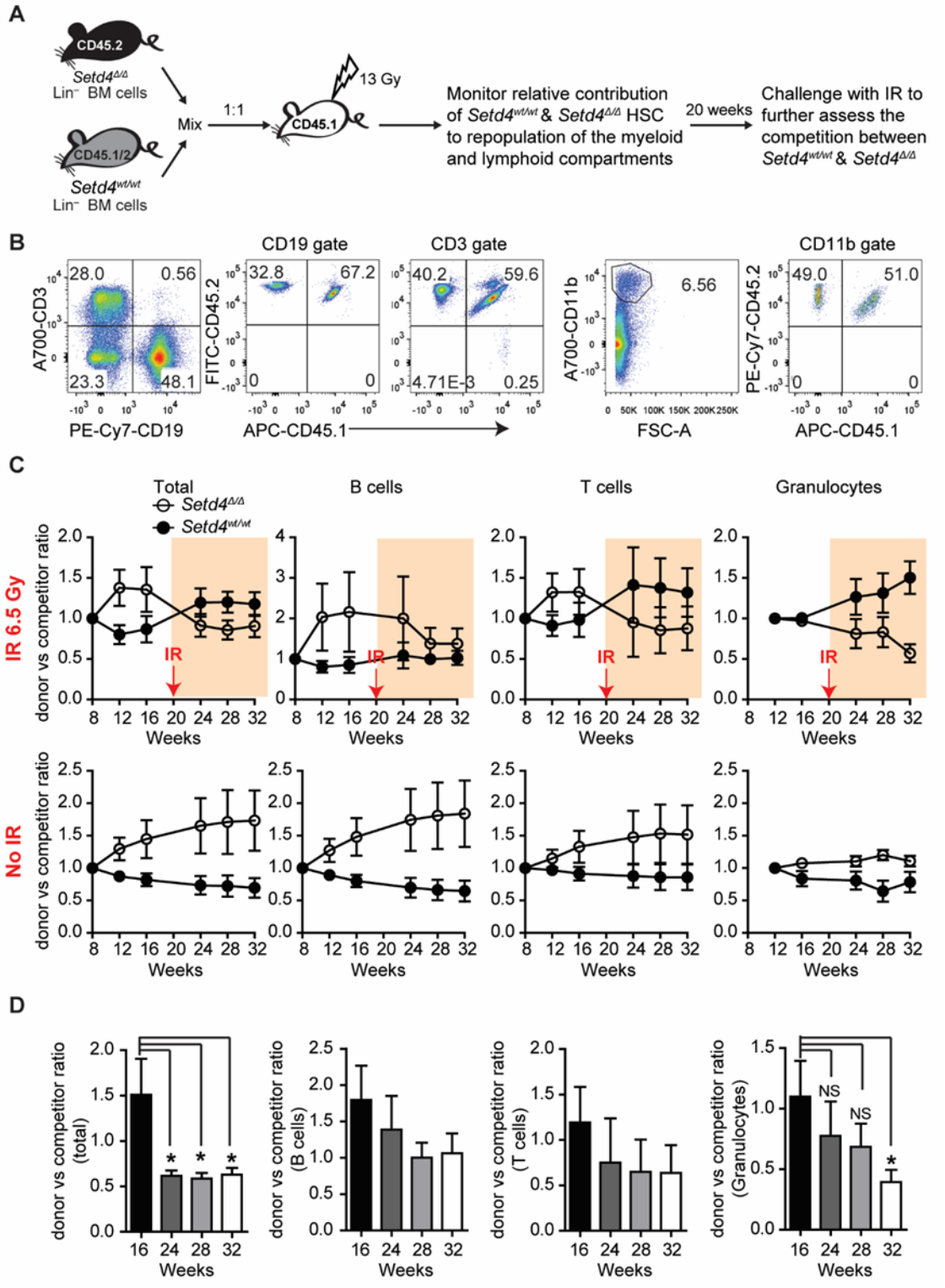

Figure 26. **Radiation sensitivity of engrafted *Setd4*$^{\Delta/\Delta}$ HSCs.**

A. Shema detailing of competitive repopulation assay. Lin⁻ BM cells (>95% Lin⁻) from *Setd4*$^{\Delta/\Delta}$ mice (CD45.2) were mixed at a ratio of 1:1 with WT competitor Lin⁻ BM cells from B6 x B6.SJL

F1 mice (CD45.1/CD45.2), and 1 × 10^6 total cells were injected i.v. into lethally irradiated B6.SJL recipients (CD45.1). The contribution of HSCs to reconstitution of HSCs, progenitors, and lymphoid and myeloid lineages in the transplanted recipients was monitored by flow cytometric analysis for every 4 weeks. 6 out of 11 reconstituted mice were exposed to sublethal irradiation (6.5 Gy) 20 weeks after transplantation (IR: n=6; non-IR: n=5).

B. Representative staining profiling of peripheral blood cells for T, B cells and granulocytes.

C. Peripheral blood from lethally irradiated transplanted mice were monitored for the contribution of HSCs to granulocyte, B and T cell lineages. Data show mean ± SEM and are representative of two identical experiments.

D. The relative contribution ratio of radiated *Setd4*$^{\Delta/\Delta}$ (donor) vs WT (competitor) in total, B, T cells and granulocytes was plotted at 16, 24, 28 and 32 wk post transplantation. *, $P < 0.05$. t test.

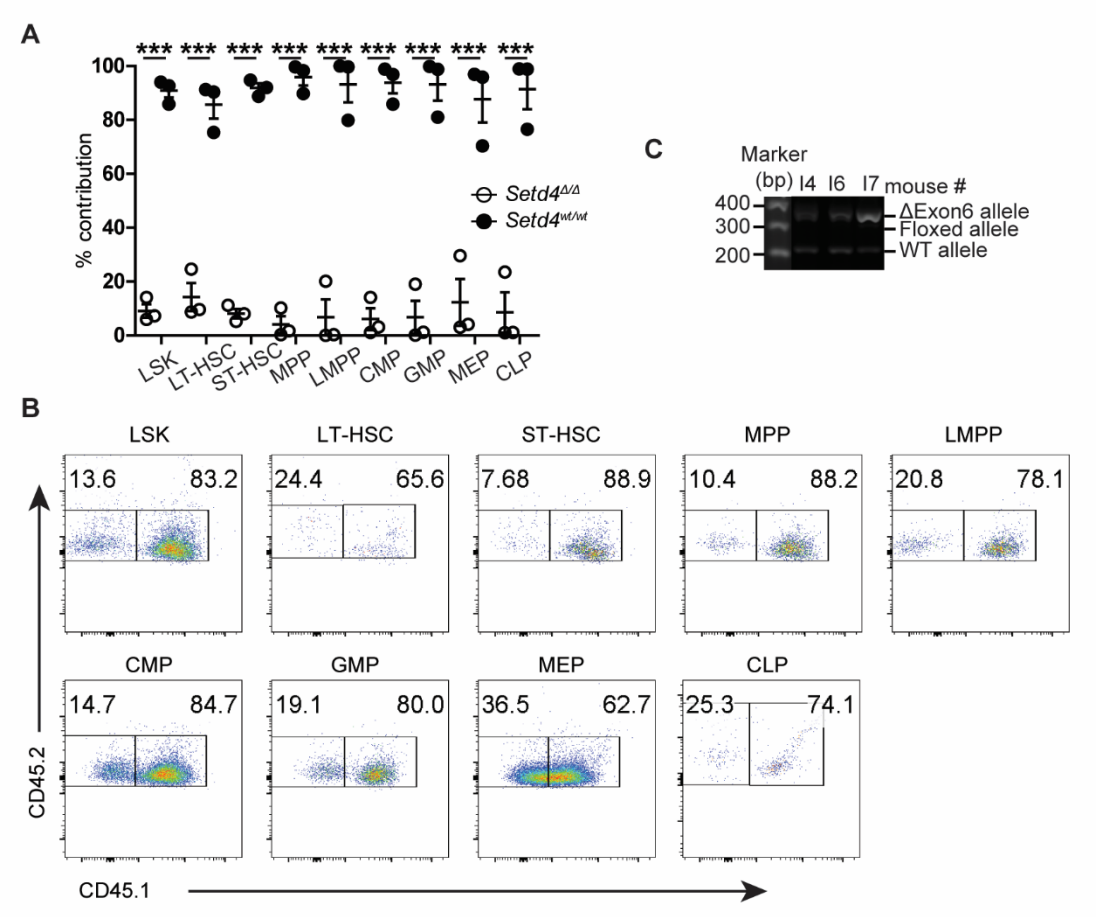

Figure 27. **Radiation sensitivity of engrafted *Setd4*$^{\Delta/\Delta}$ HSCs.**

Representative flow cytometric analysis of BM HSC and HPC populations from irradiated reconstituted mice at 48 wk after transplantation (**B**). Cumulative data from B was plotted in **A**. All the paired group is statistically significant (i.e. $P < 0.001$). Data show mean ± SEM and are representative of two identical experiments. ***, $p < 0.001$. **C**. Genotyping of bone marrow cells from all reconstituted mice whose BM were analyzed by flow cytometric.

Cell proliferation capacity of HSC. In **Figures 26** and **27**, the Setd4 was deleted before transplantation. In addition, **Figure 26B** (bottom panel) seems to indicate that there was a trend of gradual increase of the Setd4-deficient cell population when the mice were not irradiated. To further verify the role of Setd4 deletion on HSC fitness, we designed another competitive assay by performing *in vivo* deletion of Setd4 in the recipient mice. Half million Lin^- of CD45.2 $Setd4^{flox/flox}$ cells were co-transplanted along with approximately equal number of wild type competitor Lin^- bone marrow cells of B6xB6.SJL F1 mice (CD45.1/2) (**Figure 28A**), again into lethally radiated congenic CD45.1 recipient mice. The relative contribution of each type of donor cells to hematopoiesis was monitored every 4 weeks by flow cytometric analysis for the first 16 week after transplantation. Sixteen weeks after the transplantation, at which time the repopulation of the bone marrow and peripheral blood by transplanted LT-HSC should have been completed (183), half of the reconstituted mice were injected with tamoxifen to induce *in vivo* Setd4 deletion in the recipient mice, and the mice were left for observation for additional 16 weeks to determine whether the deletion of Setd4 can alter the fitness or competitiveness of the HSC. As shown in **Figure 28B,** the tamoxifen injection effectively induced the *in vivo* conversion of the flox-Exon6 allele to the ΔExon6 allele in the reconstituted recipient mice. However, there was no significant difference of the relative population sizes between $Setd4^{wt/wt}$ (CD45.1/2) and $Setd4^{\Delta/\Delta}$ (CD45.2, and converted from $Setd4^{flox/flox}$) among both the Oil-treated (Top panels, **Figure 28C**) and tamoxifen treated (lower panels, **Figure 28C**) during the next 16 weeks after the *in vivo* induction of Setd4 deletion in term of total cell population, and

individually in B and T cells (**Figure 26C**). Although there seems to be a slight increase of *Setd4*$^{\Delta/\Delta}$ granulocyte population at 8 weeks post tamoxifen (24-weeks after the original transplantation), this is not statistically significant. These data indicates that there was little lineage bias or a proliferation advantage for the *Setd4*$^{\Delta/\Delta}$ HSCs to generate short-term and long-term hematopoietic repopulation.

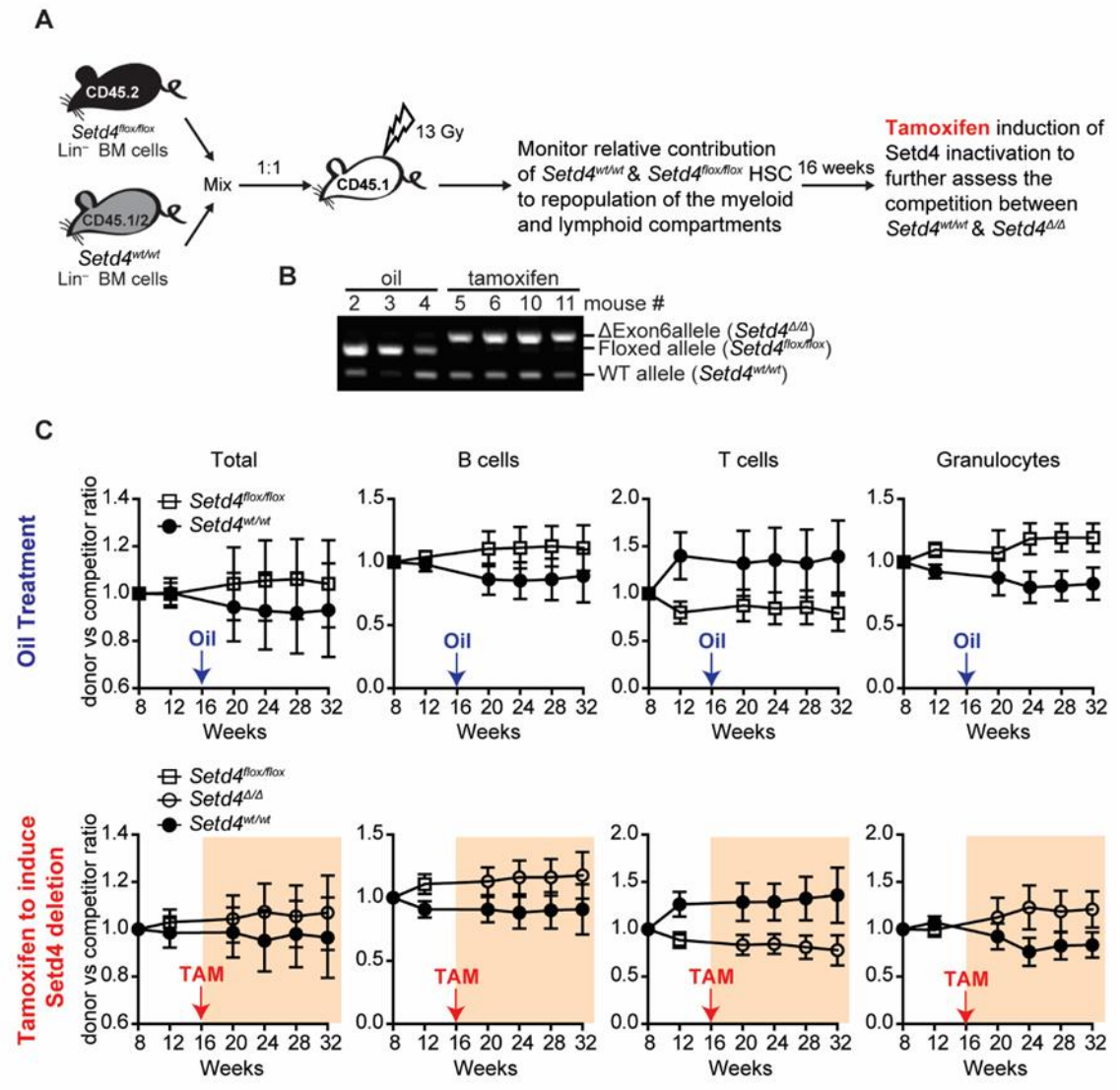

Figure 28. ***Setd4***$^{\Delta/\Delta}$ **HSCs are functionally comparable.**

A. Shema detailing of competitive repopulation assay. Lin⁻ BM cells (>95% Lin⁻) from *Setd4*$^{flox/flox}$ mice (CD45.2) were mixed at a ratio of 1:1 with WT competitor Lin⁻ BM cells from B6 x B6.SJL

F1 mice (CD45.1/CD45.2), and 1×10^6 total cells were injected i.v. into lethally irradiated B6.SJL recipients (CD45.1). The contribution of HSCs to reconstitution of HSCs, progenitors, and lymphoid and myeloid lineages in the transplanted recipients was monitors by flow cytometric analysis for every 4 weeks. 16 weeks after transplantation, 6 out of 12 reconstituted mice were injected with tamoxifen to induce *Setd4* inactivation. Then the contribution was accessed for another 16 weeks (Oil: n=6; TAM: n=6).

B. Representative genotyping of tail snips from reconstituted mice two weeks after oil or tamoxifen treatment. Genotyping PCR was performed with *Setd4* allele-specific primers. Mouse #2, #3, #4 were oil treated mice, while #5, #6, #10, #11 were treated with tamoxifen.

C. Peripheral blood from lethally irradiated transplanted mice were monitored for the contribution of HSCs to granulocyte, B and T cell lineages. Data show mean ± SEM and are representative of two identical experiments.

To further assess the long-term fitness of the stem cells, the same animals used in **Figure 28** were kept for additional 16 weeks, and sacrificed to perform bone marrow analysis at 48 weeks after original transplantation. The relative distribution of each CD45 subtypes among the tamoxifen and oil treated mice are shown in **Figures 29A-29I**, and representative flow cytometry profile for the lineage analysis are shown in **Figure 29J** (Oil treated) and **Figure 29K** (tamoxifen treated). These results suggest that there is little difference of stem cell competiveness (LSK, LT-HSC, and ST-HSC) between Oil treated ($Setd4^{flox/flox}$) and tamoxifen-treated ($Setd4^{\Delta/\Delta}$) when competed with the $Setd4^{wt/wt}$ cells. However, there are some advantages for the $Setd4^{\Delta/\Delta}$ HPCs (MPP, LMPP, CMP, GMP, MEP, and CLP) over the $Setd4^{flox/flox}$ HPCs at 48 weeks after transplantation.

Collectively, these data (**Figures 25-29**) show that Setd4 deletion confers more radiation sensitivity to the cells in the HSC hierarchy. This refuted my initial hypothesis that the radiation protective effect of Setd4 deletion in mice was due to an intrinsic radiation resistance of the cells in the hematopoietic lineages. Rather, these data actually suggest a

radiation sensitization by Setd4 deletion in the cells of HSC hierarchy.

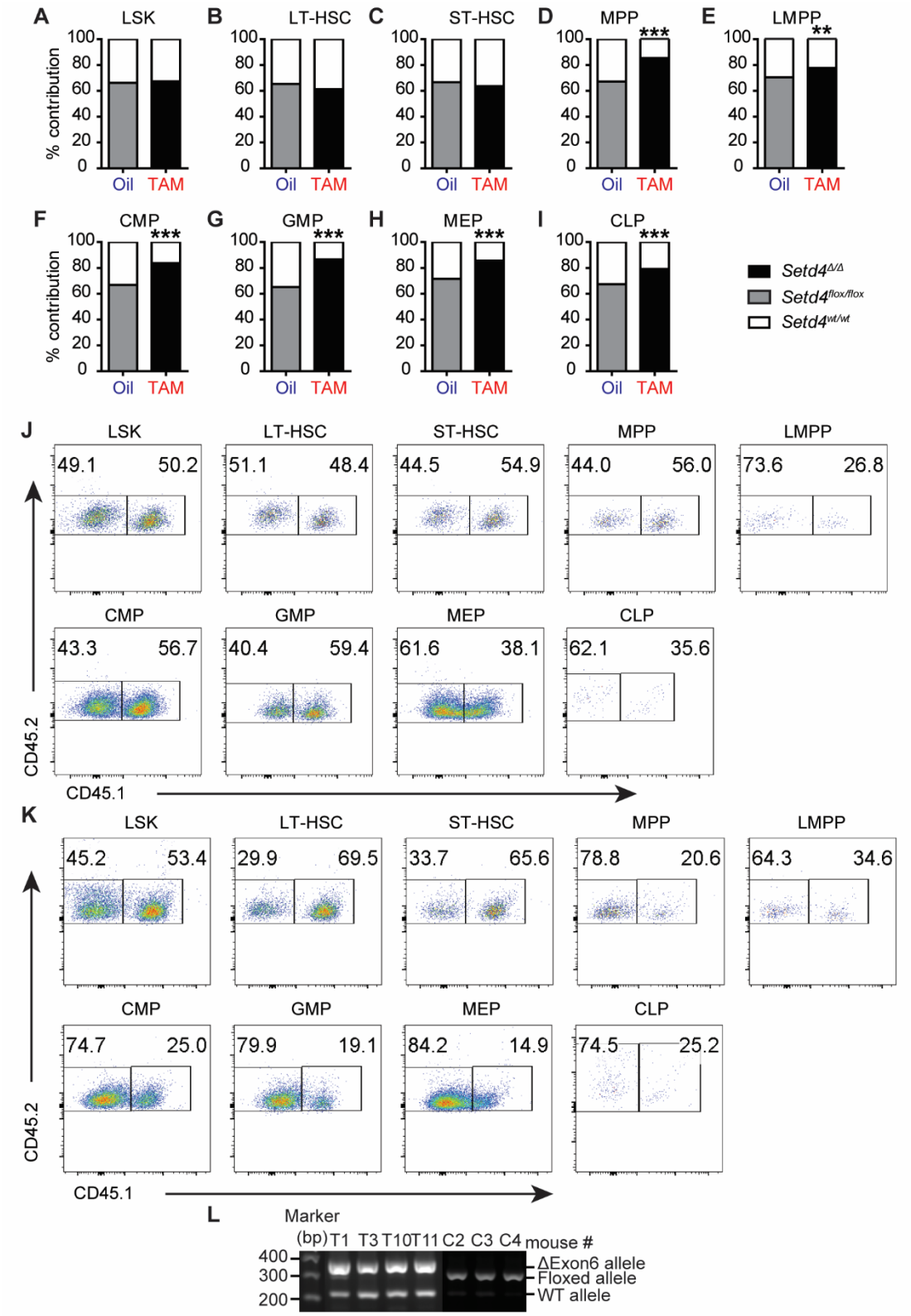

Figure 29. ***Setd4$^{\Delta/\Delta}$*** **HSCs are functionally comparable.** Representative flow cytometric analysis of BM HSC and HPC populations at 48 weeks after the transplantation for the same animals as in Figure 28.
A-I. Contribution of donor and competitors for different cell subtypes in BM. **, $p < 0.01$; ***, $p < 0.001$ (Oil: n=3; TAM: n=4).
J and **K**. Representative staining profiling of BM analysis.
L. Genotyping of bone marrow cells from all reconstituted mice whose BM were analyzed by flow cytometric. C2, C3, C4 were oil treated mice, while T1, T3, T4 and T11.

5.6 *Setd4* deletion confers an improved bone marrow microenvironment to support HSC transplantation.

Setd4$^{\Delta/\Delta}$ HSCs are significantly more sensitive to γ-irradiation than *Setd4$^{flox/flox}$*, yet *Setd4$^{\Delta/\Delta}$* mice are significantly more resistant to lethal dose γ-irradiation. **Figure 25-29** did not support a model that Setd4 deletion enhances the recovery of hematopoietic syndrome through a mechanism of radiation resistance of the HSC and its progenies. This led me to test the alternative hypothesis that the enhanced recovery is mediated by an improved bone marrow environment in Setd4 deficient mice, by using a HSC dilution survival assay **(Figure 30A).**

Age and sex matched *Setd4$^{flox/flox}$;Rosa26-CreERT2$^{/+}$* littermates were divided into two groups: one treated with tamoxifen to induced Setd4 deletion (referred as *Setd4$^{\Delta/\Delta}$*), and the other treated with oil to be used as control (*Setd4$^{flox/flox}$*). Seven days after this, the mice were subjected to lethal doses of radiation (2 doses of 6.5Gy separated by 4 hours), and transplanted with a series numbers of wild type Lin$^-$ bone marrow cells from B6.SJL (CD45.1) mice (**Figure 30A**). The survival of recipients depends on whether the damaged

bone marrow is sufficient to support the transplanted HSCs at diluted concentrations. The total number of the mice used in each group and dilutions are summarized in **Table 15.** **Figure 30B** shows the mouse survival rates at each HSC dilutions. As shown here, the *Setd4*$^{\Delta/\Delta}$ recipient can support transplantation with fewer Lin^{-} cells, and it has significantly higher overall survival than the *Setd4*$^{flox/flox}$ mice. This indicates that *Setd4*$^{\Delta/\Delta}$ mice possess an improved bone marrow environment to support the HSC transplantation, confirming the alternative hypothesis.

As shown in **Figure 30B**, the survival rate increased as the number of transplanted cell increased. The *Setd4*$^{\Delta/\Delta}$ recipients had significantly higher survival rate than the *Setd4*$^{flox/flox}$ mice. Based on a survival calculation (184,185), the number of cells required for 63% survival (or 37% fatality rate) was $40x10^3$ for *Setd4*$^{\Delta/\Delta}$ mice and $69x10^3$ for *Setd4*$^{flox/flox}$ mice, a reduction of 1.7-folds. While the survival rate for the *Setd4*$^{wt/wt}$*;CreERT2*$^{/+}$ (B6. 129) recipient mice is different from the *Setd4*$^{flox/flox}$ mice due to background difference (B6. 129), there is little difference between tamoxifen or oil treated recipients, suggesting that the presence of CreERT2 and tamoxifen treatment had little contribution to the observed protective effect of the Setd4 deficient recipients.

Collectively, these transplantation studies suggest that the radiation-resistance of Setd4 deficient mice is likely mediated by an improved bone marrow niche for the damaged hematopoietic cells to regenerate.

Table 16. Survival of transplanted recipient mice

Number of cells transplanted (x10^3) per mouse	No of mice (Engrafted/Transplanted)			
	***Setd4*$^{flox/flox}$ (Oil)**	***Setd4*$^{\Delta/\Delta}$ (Tam)**	***Setd4*$^{wt/wt}$; *CreERT2*$^{/+}$ (Oil)**	***Setd4*$^{wt/wt}$; *CreERT2*$^{/+}$ (TAM)**
100	6/8	10/10	4/6	3/6
75	9/12	11/12	4/11	3/11
60	8/14	11/14	5/14	3/9
50	5/14	11/14	4/14	5/14
40	5/13	7/13	1/7	1/11
25	1/10	2/10		1/9
10	0/3	0/3		
The fraction of mice represents the survived recipients with successful engraftment 30 days post bone marrow transplantation.				

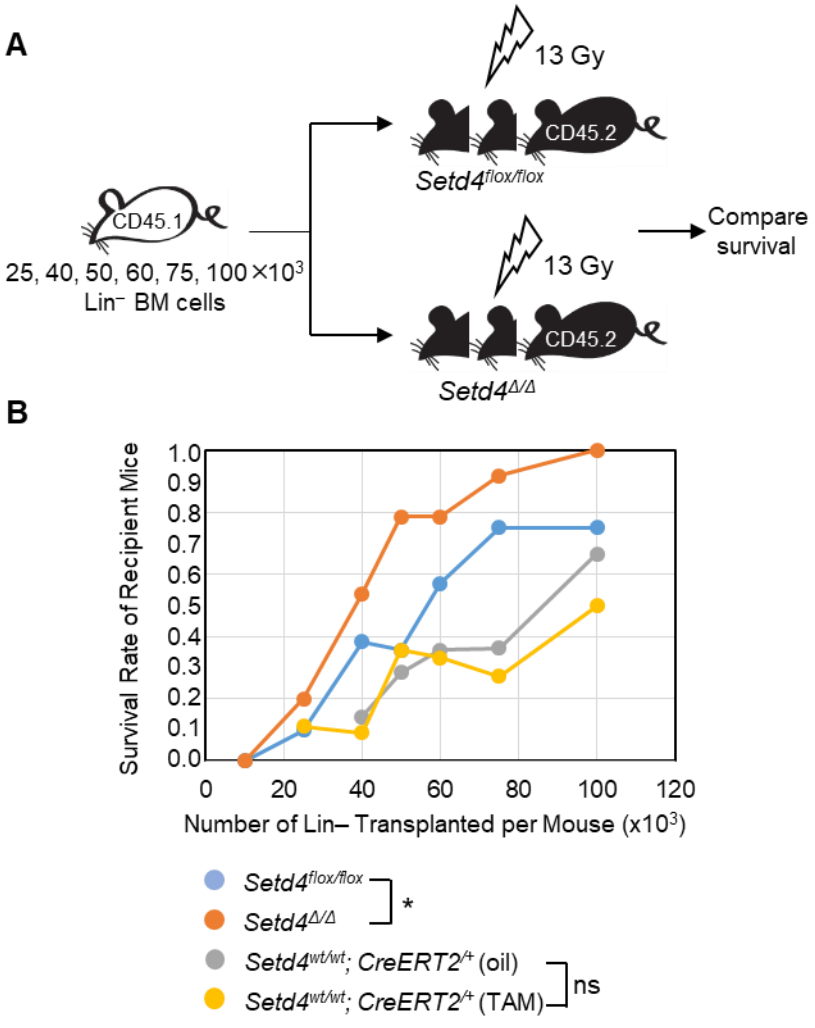

Figure 30. **Survival rate of lethally-irradiated recipient mice after transplantation of Lin$^-$ bone marrow donor cells.**

A. Shema detailing of HSC transplantation to rescue the lethally irradiated recipient mice. Serially diluted donor Lin$^-$ BM cells (10, 25, 40, 50, 60, 75, and 100x10^3) from B6.SJL (CD45.1) mice were transferred into lethally irradiated *Setd4*$^{\Delta/\Delta}$ or *Setd4*$^{flox/flox}$ recipients. The fatality was monitored for 30 days.

B. The survival rate of the transplanted recipient mice as a function of the numbers of transplanted Lin$^-$ cells per mouse. For each experimental point, 6-14 recipients were used (see **Table 15** for the specific number of mice used in each time point). The calculated number of cells for a 63% of survival rate is 69.0x10^3 for *Setd4*$^{flox/flox}$ mice, and 40.5x10^3 for *Setd4*$^{\Delta/\Delta}$ mice. P value was calculated by Chi-Square test.

Chapter 6, Roles of Setd4 in Radiation Induced Tumorigenesis

6.1 Loss of *Setd4* extends the survival of radiation-induced thymic lymphoma.

Despite of an insignificant difference between Setd4 knockout and control mice in terms of life span and spontaneous tumor formation, the studies presented in Chapter 5 revealed a role of Setd4 deletion in protection of acute myeloablaltion and myelosuppresion after a single dose of whole body irradiation. Thus, we became interested in whether Setd4 deletion also modulates radiation-induced tumorigenesis. To address this, we induced Setd4 deletion in the adult *Setd4*$^{flox/flox}$;*Rosa26-CreERT2*$^{/+}$ mice by 5 daily injections of tamoxifen to produce Setd4 knockout (*Setd4*$^{\Delta/\Delta}$). The age and sex matched littermates were injected with oil to serve as the control (*Setd4*$^{flox/flox}$). Five days after the last injection, we irradiated the mice with 2 Gy of gamma-rays weekly for 4 weeks (4x2Gy), which is known to induce thymic lymphoma in mice (151).

As predicted, these mice developed lymphoma mainly in thymus. In some mice, tumor cell infiltrations were observed in the spleen, liver, kidney, lung, and other organs (**Figure 31A**). We characterized the lymphoma by biopsy, H&E staining, and IHC, and found that the lymphoma cells were positive for the T-cell marker CD3 but negative of the B-cell marker B220/CD45R (**Figure 31B**). These analyses confirmed that the tumors were T-cell lymphoma. As shown by a flow cytometric analysis, the tumor cells aberrantly expressed CD4 and CD8 compared with thymocytes from unirradiated mice (**Figure 31C**).

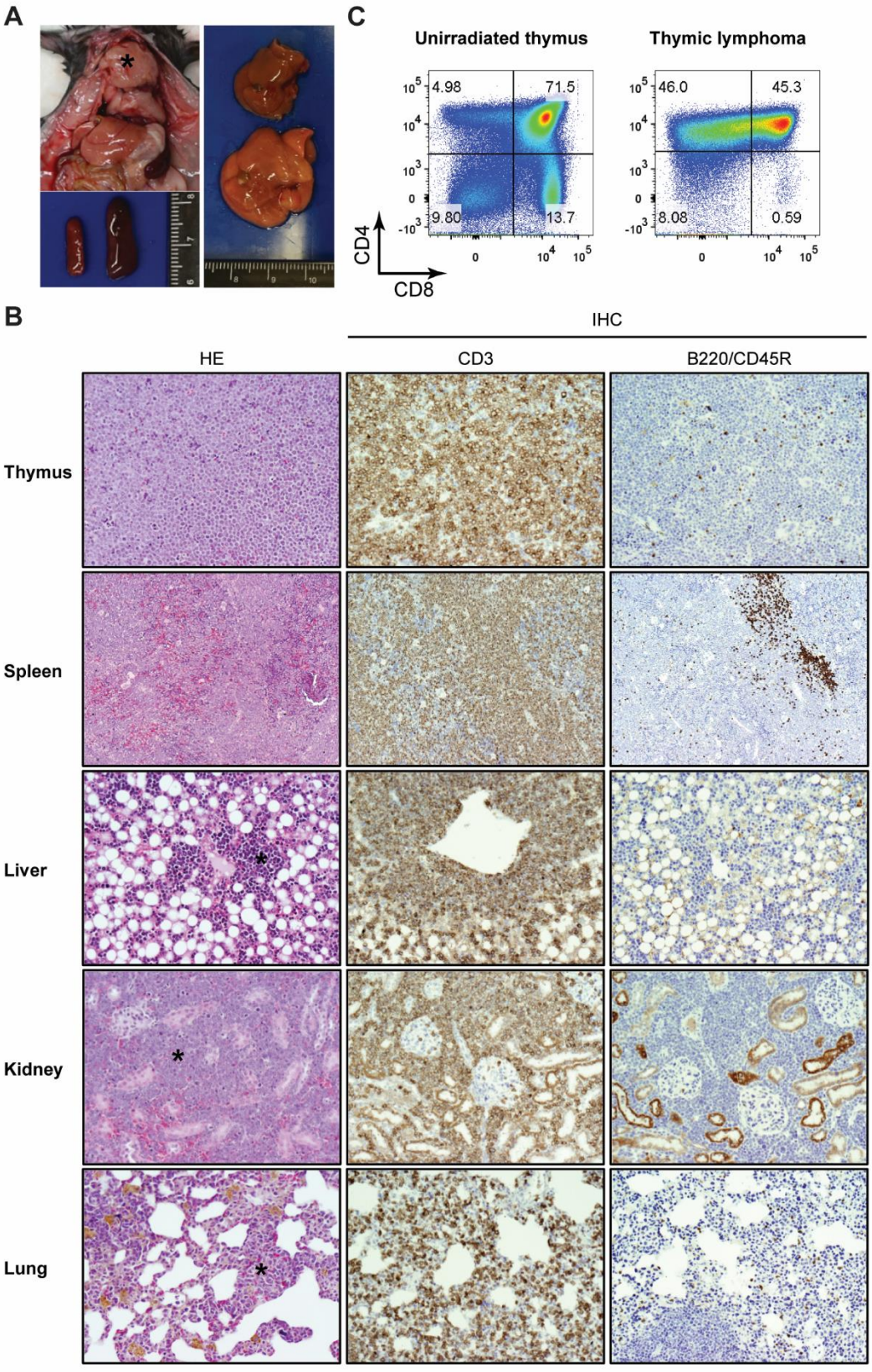
A
C
Unirradiated thymus
Thymic lymphoma
4.98
71.5
9.80
13.7
46.0
45.3
8.08
0.59
CD4
CD8
B
IHC
HE
CD3
B220/CD45R
Thymus
Spleen
Liver
Kidney
Lung

Figure 31. **Characterization of radiation-induced thymic lymphoma.**
A. Representative gross features of thymic lymphoma mouse. Note the mouse usually carried a huge thymic lymphoma and also involved in spleen or liver.
B. H&E and immunohistochemistry (IHC) staining of representative tumor. The tumor cells in thymus and infiltrated organs (spleen, liver, kidney and lung; black asterisk) stain for CD3 positive and B220/CD45R negative. 100x.
C. Representative flow cytometry plots of unirradiated thymocytes and lymphoma cells.

During the initial 100 to 300 days, all died mice had thymic lymphomas with obvious necropsy features. Intriguingly, the loss of Setd4 significantly delayed radiation-induced thymic lymphoma and improved the overall survival (**Figure 32A**). The median survival was 197 days for *Setd4*$^{flox/flox}$ mice, but 278 days for *Setd4*$^{\Delta/\Delta}$ mice. Genotyping of tumor DNA confirmed the Setd4 deletion in the lymphomas and tumor infiltrated organs of the *Setd4*$^{\Delta/\Delta}$ mice (**Figure 32B**). To rule out a potential role of tamoxifen treatment on the time course of tumor development, we treated *Setd4*$^{wt/wt}$*;Rosa26-CreERT2*$^{/+}$ littermates with tamoxifen and oil, and performed the same TBI (4 x 2Gy) as the mice in **Figure 32**. We found that tamoxifen treatment with wild mice did not affect the time course of tumorigenesis (**Figure 33**). Collectively, these data suggest that loss of Setd4 significantly suppressed radiation-induced thymus lymphoma.

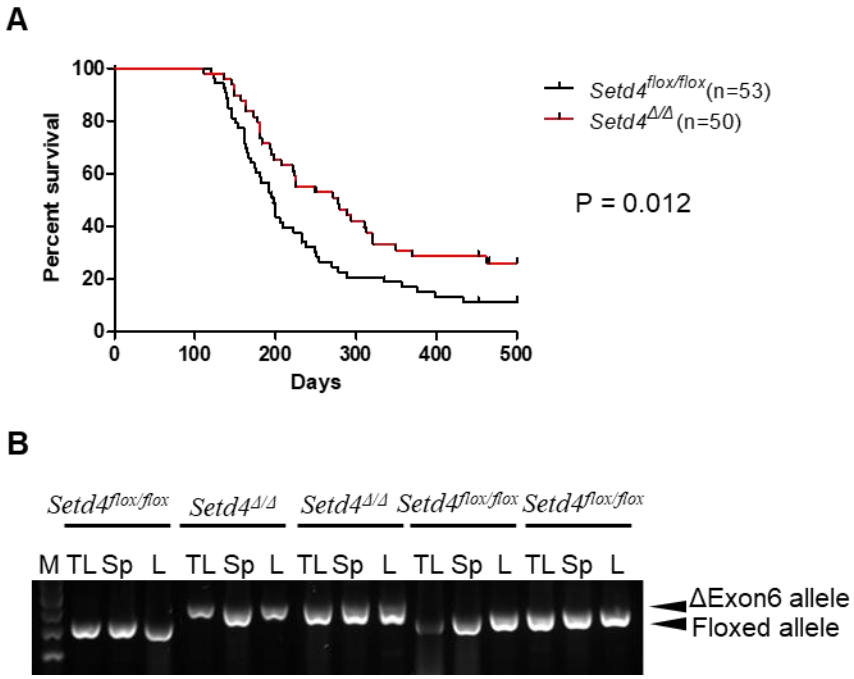

Figure 32. Loss of *Setd4* delays radiation-induced thymic lymphoma. Sex matched littermates of *Setd4*$^{flox/flox}$*;Rosa26-CreERT2*$^{/+}$ were treated with tamoxifen and oil to produce *Setd4*$^{\Delta/\Delta}$ mice (n=50) and *Setd4*$^{flox/flox}$ mice (n=53). These mice were exposed to four weekly 2 Gy doses of γ-irradiation (4x2Gy), and the long term survival were monitored.

A. Kaplan-Meier survival of *Setd4*$^{\Delta/\Delta}$ mice (n=50) and *Setd4*$^{flox/flox}$ mice (n=53) of sex-matched littermates. P = 0.012 (log-rank Mantel–Cox test). The median for *Setd4*$^{\Delta/\Delta}$ is 278 days, and for *Setd4*$^{flox/flox}$ is 197 days.

B. Representative genotypes of tumor DNA obtained from thymic lymphoma (TL), Spleen (Sp), and livers (L) using multiplex PCR that simultaneous detect the wt, Flox-Exon6, and ΔExon6 alleles.

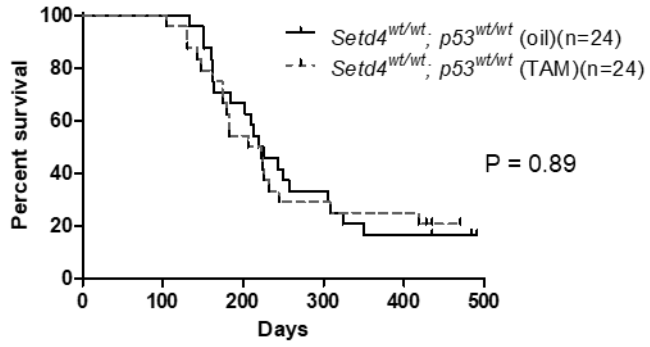

Figure 33. Kaplan-Meier survival of wild type mice treated with tamoxifen. Littermates of *Setd4*$^{wt/wt}$*;Rosa26-CreERT2*$^{/+}$ mice were treated with either oil (n = 24, black line) or tamoxifen (n = 24, grey dash line), and then exposed to four weekly 2 Gy of γ-irradiation (total: 4x2Gy). The

median survival is 222 days for oil treated, and 214 days for tamoxifen treated group. P = 0.89 (log-rank Mantel–Cox test).

6.2 Setd4-deficient thymic lymphomas were more disseminative in peripheral organs.

Next we compare the lymphoma features between the *Setd4*$^{flox/flox}$ and *Setd4*$^{\Delta/\Delta}$ mice. Although both mice have T-lymphoma cell disseminations in peripheral organs such as spleen, liver, kidney, and lungs (**Figure 34A**), the *Setd4*$^{\Delta/\Delta}$ mice had a more widespread and aggressive infiltration of T-lymphoma cells in the peripheral organs in the form of the generalized lymphomas (**Figure 34A**). The IHC based semi-quantification of the lymphoma infiltration in other organs is summarized in **Table 17**. Within 200 days after the radiation exposure, which was the median survival for *Setd4*$^{flox/flox}$ mice, the sizes of *Setd4*$^{\Delta/\Delta}$ thymus tumors were significantly smaller than the *Setd4*$^{flox/flox}$ tumors (**Figure 34B**), as well as more generalized. However, for cases beyond 200 days, the *Setd4*$^{\Delta/\Delta}$ thymic lymphomas were significantly bigger than *Setd4*$^{flox/flox}$ tumor (**Figure 34C**), and more generalized into peripheral tissues.

Table 17. Infiltration of thymic lymphoma in peripheral organs

Genotype	Case ID	Survival days post TBI	Degree of tumor infiltration			
			Spleen	Liver	Kidney	Lung
Setd4$^{flox/flox}$	1825	181	++	++	-	-
	1826	169	++	+	-	+
	1827	138	-	-	-	+
	1828	182	++	+++	++	++
	1829	166	++	++	+	+
	919-1	124	+	+++	-	+

	927-1	141	+	+++	+++	++
	927-2	141	+++	+++	+	+++
	1001-1	145	++	+	+	+
	1026-1	161	+	+++	+	+
	1108	174	+++	+++	+++	+++
	1204-1	200	+	+	+++	+++
	1204-2	200	++	+++	++	+
	1830	270	+	-	-	-
	1831	278	+++	+++	++	-
Setd4$^{\Delta/\Delta}$	1818	289	+++	+++	+++	+++
	1819	279	+++	+++	+++	+++
	1216	221	++	+++	++	+++
	1821	161	+++	+++	+++	+++
	1822	180	++	+	++	++
	1823	177	+	++	+	++
	1824	148	+++	++	++	+
	913/906	111	+++	+++	+++	+++
	1001-2	135	+	+	+	++
	1127	193	+++	+++	+++	+++

The scores were based on IHC staining of CD3.

-: <5% of cells are T-cell marker positive.

+: 5-30% of cells are T-cell marker positive.

++: 30-60% of cells are T-cell marker positive.

+++: >60% of cells are T-cell marker positive.

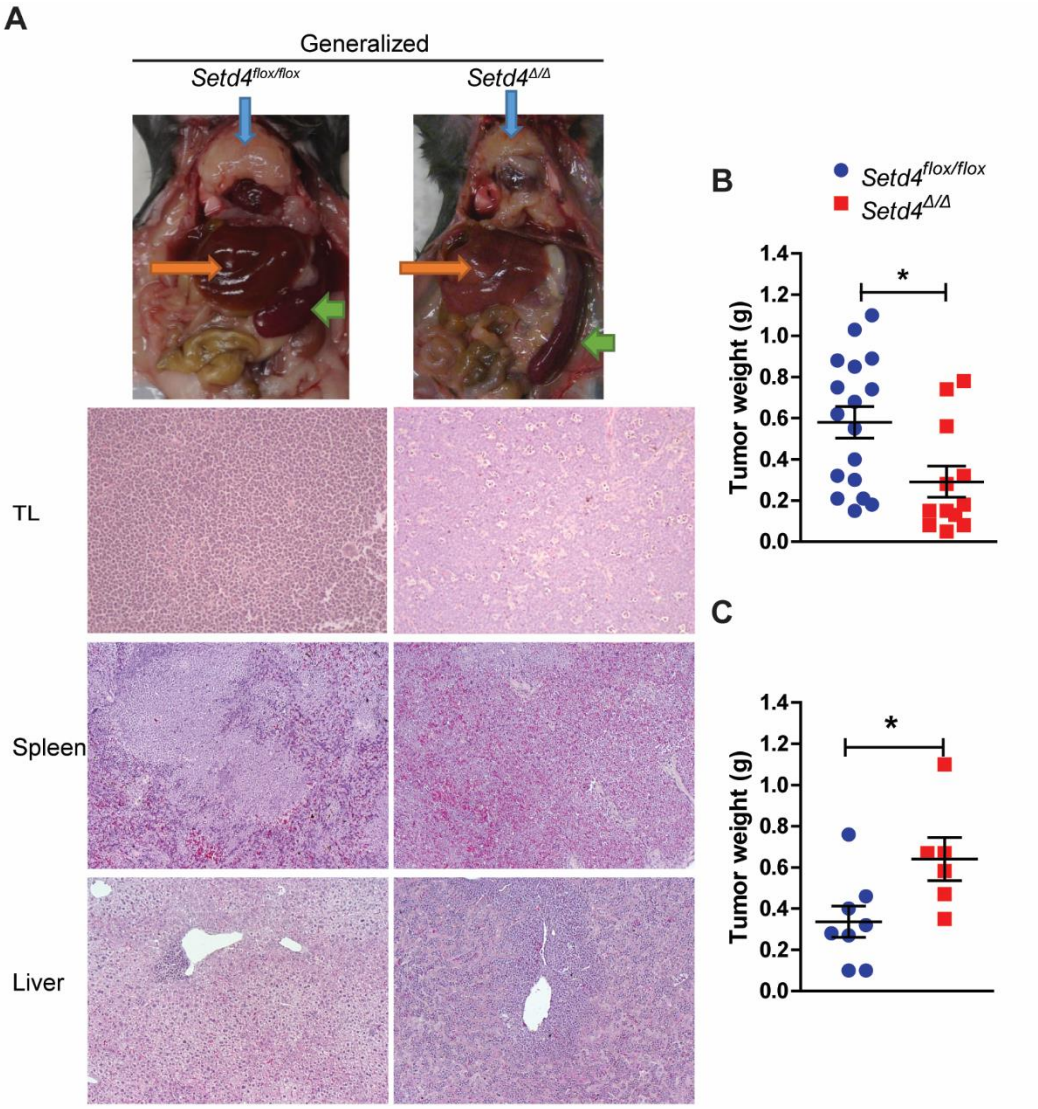

Figure 34. Setd4 deficiency enhances dissemination of thymic lymphoma to peripheral tissues.
A. Representative images of thymic lymphomas (TL; blue arrow) and their dissemination to peripheral tissues, including spleen (green arrow) and liver (yellow arrow). Representative H&E staining in three groups indicate the infiltration of lymphoma in spleen and liver.
B. Plots of tumor weight between *Setd4*$^{\Delta/\Delta}$ and *Setd4*$^{flox/flox}$ mice (Samples were collected within 200 days post fractionated ionizing radiation).
C. Tumor weight between *Setd4*$^{\Delta/\Delta}$ and *Setd4*$^{flox/flox}$ mice. (Samples were collected beyond 200 days post fractionated ionizing radiation). Statistical analysis were performed using the unpaired Student t test. *, $p < 0.05$.

6.3 Distinct subtypes of thymic lymphoma in *Setd4$^{\Delta/\Delta}$* mice.

To investigate cell type of thymic lymphomas (TL), flow cytometric analyses were conducted to measure the distribution of CD8 and CD4 markers with single cell suspension isolated from a limited number of fresh thymic lymphoma tissues. As shown in **Figure 35**, we found that while the *Setd4$^{flox/flox}$* lymphomas were mainly composed of $CD8^+/CD4^-$ cells, the *Setd4$^{\Delta/\Delta}$* thymic lymphomas were majorly composed of $CD8^+/CD4^+$ double positive cells (**Figure 35B**). In the tumor cell infiltrated spleen tissues, there were higher percentage of $CD8^+/CD4^+$ in *Setd4$^{\Delta/\Delta}$* mice than the *Setd4$^{flox/flox}$* mice as well (**Figure 35C**). These data suggest that there were distinct thymic tumor subtypes developed in the *Setd4$^{\Delta/\Delta}$* and *Setd4$^{flox/flox}$* mice**.** Because additional studies on distinct tumor subtypes would hint for the molecular function of Setd4 gene, IHC based approaches are being developed to verify the findings of **Figure 35** with prefixed tissues. In the future, the whole genomic DNA and total RNA will be extracted from thymic lymphoma specimen and subjected to high-throughput sequencing to determine the spectrum of mutagenic changes, with the hope that novel insights will be gained from Setd4 loss to mechanism of thymic lymphoma formation.

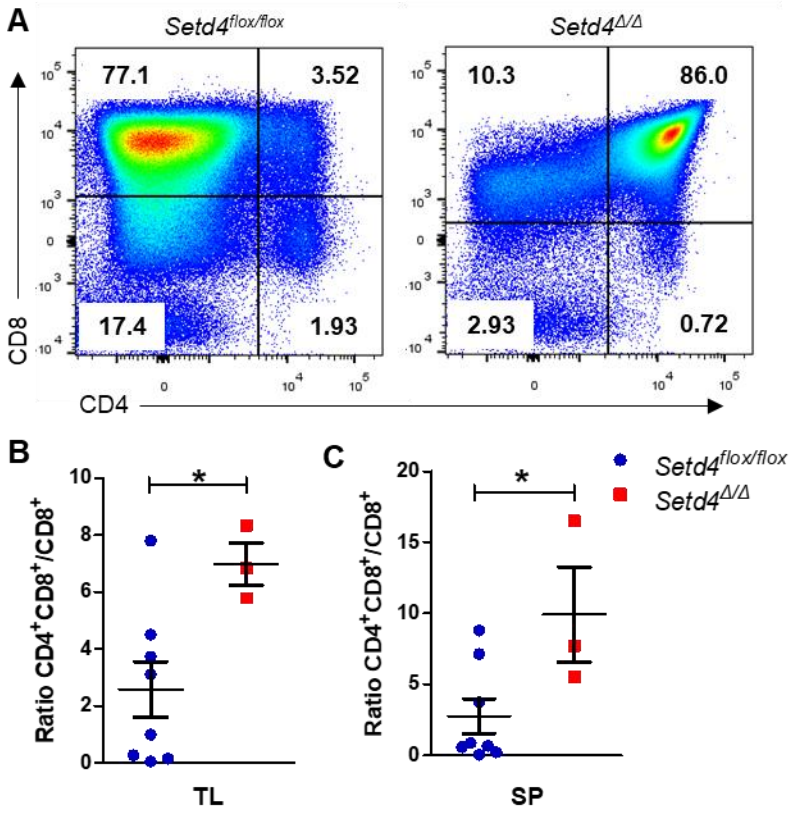

Figure 35. Different subtypes of thymic lymphoma in *Setd4*$^{\Delta/\Delta}$ mice. Cell suspension of fresh tumor tissues were used to stain for the CD4 and CD8 markers and analyzed by flow cytometer.
A. Representative images of flow cytometric profiles of thymic lymphoma with CD4 and CD8 makers in *Setd4*$^{\Delta/\Delta}$ and *Setd4*$^{flox/flox}$ mice**.**
B. Ratio of $CD4^+/CD8^+$ double positive cells vs $CD4^-/CD8^+$ cells in thymic lymphoma of *Setd4*$^{\Delta/\Delta}$ and *Setd4*$^{flox/flox}$ mice.
C. Ratio of $CD4^+/CD8^+$ double positive cells vs $CD4^-/CD8^+$ cells in the spleen of *Setd4*$^{\Delta/\Delta}$ and *Setd4*$^{flox/flox}$ mice. Statistical analysis were performed using the unpaired Student t test. *, $p < 0.05$.

6.4 Insignificant change of the suppressive immunological environment in Setd4 deficient lymphoma.

The immunological tumor microenvironment is a known determinant for tumor infiltration through the regulation of pro-tumor cytokines (186). Our Setd4 deficient mice displayed a similar delayed tumorigenesis as observed in the toll-like receptor 4 (TLR-4) deficient mice

(161). The myeloid-derived suppressor cell (MDSCs) are a heterogeneous population of suppressive innate immune cells that exists only in pathological conditions such as chronic inflammation and cancer (187,188). MDSCs suppress both innate and adaptive immunity within tumor microenvironment via production of various immune-suppressive molecules (187). The presence of MDSC in the tumor tissue is considered an indicator of an immunologically suppressed microenvironment (189) and is strongly associated with metastasis (190). Therefore, we measured the MDSC in the Setd4 deficient infiltrated tumors, which was defined as $CD11b^{+}$, $Gr\text{-}1^{+}$. As shown in **Figure 36**, the contribution of MDSCs in thymic lymphoma mass was less than 1% of total cells, and there was little difference between *Setd4*$^{\Delta/\Delta}$ and *Setd4*$^{flox/flox}$ mice (**Figure 36**). Thus, it is unlikely that the enhanced infiltration of tumor cells in *Setd4*$^{\Delta/\Delta}$ mice was due to an altered immunological environment.

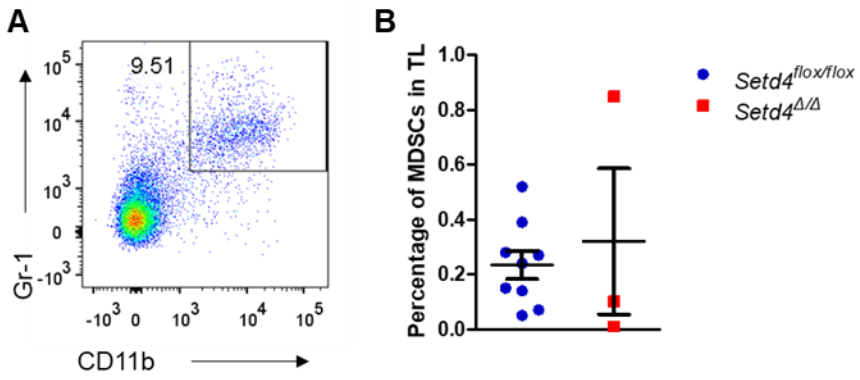

Figure 36. Insignificant MDSC infiltration in thymic lymphoma.
A. Representative images flow cytometric profile of thymic lymphoma with CD11b and Gr-1 makers.
B. Percentage of Gr-1 and CD11b positive MDSCs in *Setd4*$^{\Delta/\Delta}$ and *Setd4*$^{flox/flox}$ thymic lymphomas.

6.5 Generation of Setd4 and Tp53 double deficient mice.

Since loss of p53 markedly accelerate radiation-induced thymic lymphoma (154), and Setd4 loss enhanced mouse survival from radiation induced hematopoietic syndrome (**Figure 24**), we wondered whether Setd4 loss would also delay the tumor development in p53 deficient mice. We used a conditional homozygous Tp53 $^{flox/flox}$ mice, which had the exons 2-10 of Tp53 flanked by LoxP (163). The structure of the Tp53 allele and PCR genotyping strategy are illustrated in **Figure 37A**. A representative genotyping results were shown in **Figure 37B**. After tamoxifen administration, Tp53 was confirmed to being inactivated by both PCR (**Figure 37C**) and western blot (**Figure 37D**). We mated *Setd4*$^{flox/flox}$*;Rosa26-CreERT2*$^{/+}$ mice with *Tp53* $^{flox/flox}$. In this way, both Setd4 and p53 are deleted after Cre recombination.

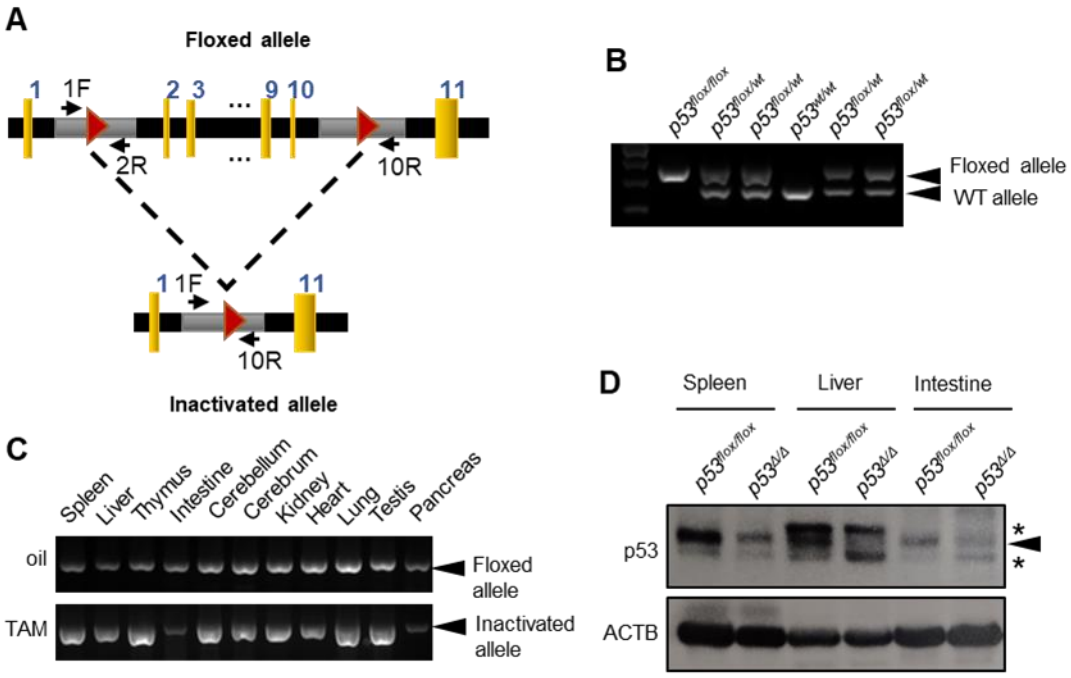

Figure 37. Genomic structure of conditional Tp53 allele.

A. LoxP sites are inserted into introns 1 and 10. Cre mediated excision of exons 2-10 would result in a functionally null p53 gene. The location of three primers (1F, 2R and 10R) for Tp53 PCR genotyping are illustrated.
B. Representative PCR result of Tp53 genotyping. The 390 bp band represents floxed allele, while 270 bp represents wild type allele (primer 1F and 2R).
C. Verification of exons 2-10 deletion upon CreERT2 activation by tamoxifen (Tam). The 612 bp band represents the recombined p53 allele (primer 1F and 10R).
D. Verification of loss of Tp53 protein by western blot. The thick arrow represents the mouse p53 band, while the star bands are non-specific. All tissues were collected 5 days post tamoxifen induction.

6.6. Setd4 deletion does not affect spontaneous tumorigenesis in p53 deficient mice.

As shown in **Figure 38A**, the $Tp53^{\Delta/\Delta}$ mice developed spontaneous tumors before 300 days and the time course of the tumor formation and tumor types are very similar to previously reported by others (191,192). As previously described in Chapter 4 (**Figure 16**), $Setd4^{\Delta/\Delta}$ mice do not have a significantly altered risk of spontaneous tumor formation. However, deletion of Setd4 in $Tp53^{\Delta/\Delta}$ mice resulted in a slight but significant acceleration of tumor development in the $Tp53^{\Delta/\Delta}$ mice (compare **Figure 38A** with **Figure 38B**, and also see **Figure 38C,** p=0.013**)**. Note that there are also cases of lymphomas and osteosarcoma in oil-treated $Setd4^{flox/flox};Tp53^{flox/flox}$ mice, and the median survival for oil-treated $Setd4^{flox/flox};Tp53^{flox/flox}$ was 494 days (**Figure 38B**). This is presumably caused by leaky CreERT2 activity in the nucleus without tamoxifen induction, as noticed before (170,171). By 300 days, all the $Setd4^{\Delta/\Delta};Tp53^{\Delta/\Delta}$ mice have died with obvious tumors and the median survival is 134 days. The predominant tumor type is lymphoma (82% of all cases, **Figure 39A**), which usually affected thymus, similar as reported by others using homozygous p53 mutation (191,192). Many lymphomas also involved with other major visceral organs

including spleen, liver, kidney and lung (**Figure 40A-C**). These lymphomas are T cell lymphoma based on immunohistochemistry characterization (**Figure 40G-I**). Of the sarcomas, three are undifferentiated sarcomas arose from subcutis invading the abdomen wall into the body cavity (**Figure 40E** and **F**), and one is osteosarcoma (**Figure 40D**).

We also observed that heterozygous Tp53 deletion alone did not accelerate spontaneous tumor formation within 420 day (**Figure 41A**, p=0.2), but combined homozygous Setd4 deletion with heterozygous Tp53 deletion mice can accelerate spontaneous tumor development (**Figure 41B,** p=0.015). Currently, we only observed the survival of the p53 heterozygous mice (**Figure 41A**) for 420 days and the mice with combined genotypes had been observed for 700 days (**Figure 41B**), statistical analyses were performed with a cut of 450 days, and we found that there is no effect of Setd4 deletion in modulating tumor risk of heterozygous p53 mice (**Figure 41C**, p=0.57). The $p53^{\Delta/wt}$ mice had a late onset of tumor development compared to $p53^{\Delta/\Delta}$ mice (**Figure 41A**). The tumor spectrum is similar to previously reported (191,192). **Figure 39B** shows the tumor distribution in $Setd4^{\Delta/\Delta};p53^{\Delta/wt}$ mice. The most common tumor types were sarcoma (57%) and lymphomas (43%). In addition, 4 cases seemingly died from unresolved infections, without obvious tumor, 8 cases failed to development any tumor until 18 months post tamoxifen induction. The majority of oil mice died from either inflammation or stayed till the end of the experiment. Thus we conclude that the overall survival and tumor spectrum of Setd4 deletion in heterozygous $p53^{\Delta/wt}$ mice was similar as heterozygous $p53^{\Delta/wt}$ itself.

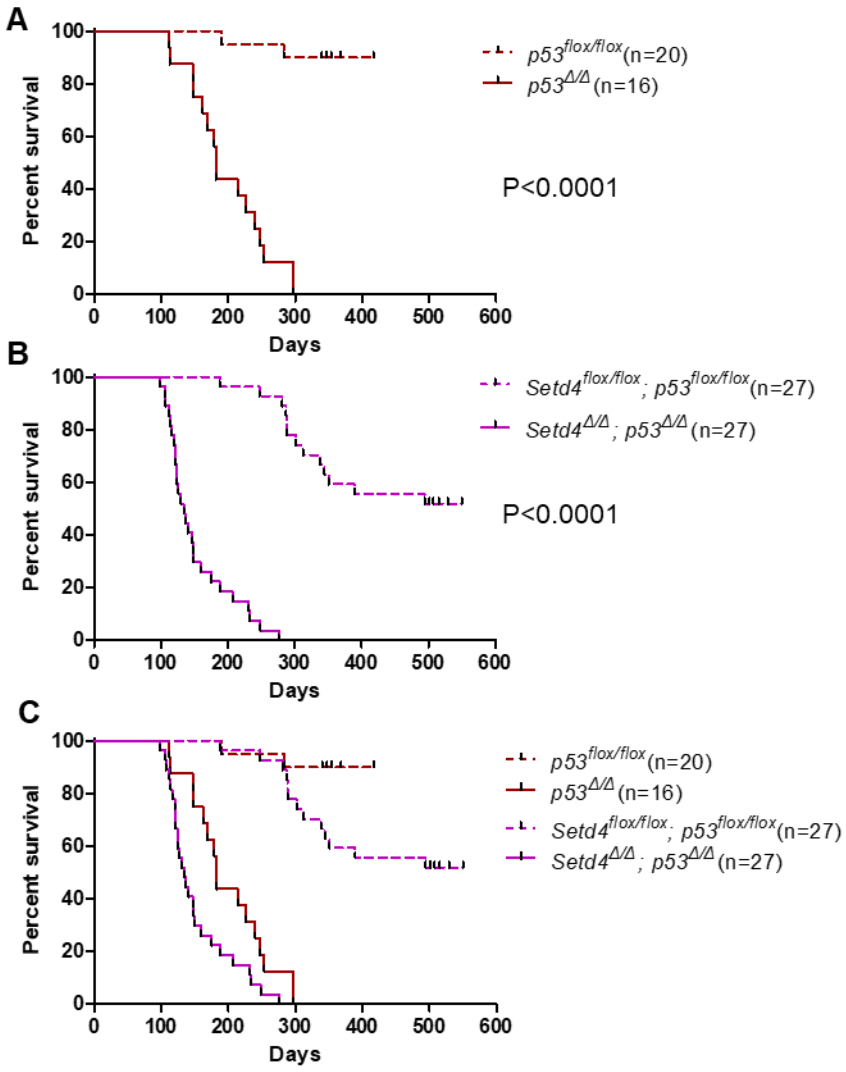

Figure 38. Kaplan-Meier survival of *p53*$^{\Delta/\Delta}$ and *Setd4*$^{\Delta/\Delta}$*; p53*$^{\Delta/\Delta}$ mice. Littermates of *p53*$^{flox/flox}$ and *Setd4*$^{flox/flox}$*; p53*$^{flox/flox}$ treated with oil or tamoxifen were kept for long-term survival observation. Points represent animals that had died or had to be sacrificed owing to illness. Tumors were observed in all *p53*$^{\Delta/\Delta}$ and *Setd4*$^{\Delta/\Delta}$*; p53*$^{\Delta/\Delta}$ mice examined by necropsy.

A. Survival of 20 *p53*$^{flox/flox}$ (brown dash line) and 16 *p53*$^{\Delta/\Delta}$ (brown line) mice. Median survival: 182 d for *p53*$^{\Delta/\Delta}$, $p < 0.0001$ (log-rank Mantel–Cox test).

B. Survival of 27 *Setd4*$^{flox/flox}$*; p53*$^{flox/flox}$ (purple dash line) and 27 *Setd4*$^{\Delta/\Delta}$*; p53*$^{\Delta/\Delta}$ (purple line) mice. Median survival: 134 d for *Setd4*$^{\Delta/\Delta}$*; p53*$^{\Delta/\Delta}$, $p < 0.0001$ (log-rank Mantel–Cox test).

C. Combined plots of A and B. *p53*$^{flox/flox}$ vs *Setd4*$^{flox/flox}$*; p53*$^{flox/flox}$: 0.051; *p53*$^{\Delta/\Delta}$ vs *Setd4*$^{\Delta/\Delta}$*; p53*$^{\Delta/\Delta}$: 0.013

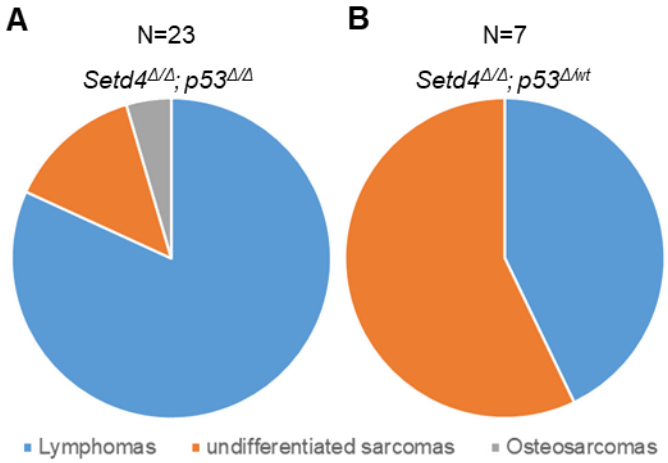

Figure 39. Tumor type distribution in p53 mutant mice. Pie charts show the relative frequencies of tumor types observed in *Setd4$^{\Delta/\Delta}$; p53$^{\Delta/\Delta}$* and *Setd4$^{\Delta/\Delta}$; p53$^{\Delta/wt}$* mice. Frequencies determined from 23 total tumor in *Setd4$^{\Delta/\Delta}$; p53$^{\Delta/\Delta}$* mice, and 7 total tumor in *Setd4$^{\Delta/\Delta}$; p53$^{\Delta/wt}$* mice. Note that the sarcoma is the most common type in *Setd4$^{\Delta/\Delta}$; p53$^{\Delta/wt}$*, whereas lymphomas are the major type in *Setd4$^{\Delta/\Delta}$; p53$^{\Delta/\Delta}$*.

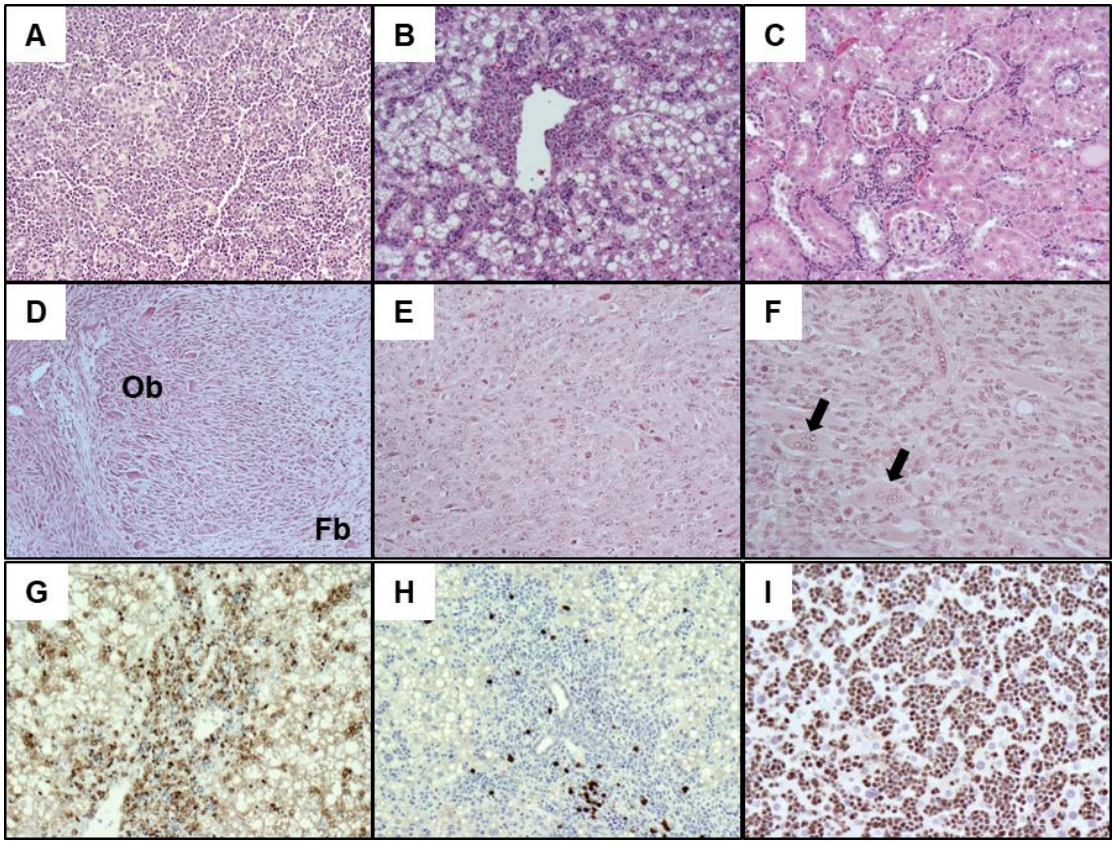

Figure 40. Histopathology and IHC of representative tumors from *Setd4$^{\Delta/\Delta}$; p53$^{\Delta/\Delta}$* mice. Thymic lymphoma (**A**) and lymphoblastic malignance in liver (**B**) and kidney (**C**). Note that solid lymphoma cell infiltration between hepatic cells and in renal cortex.

(**D**). Osteosarcoma from a *Setd4*$^{\Delta/\Delta}$*; p53*$^{\Delta/\Delta}$ animal. Tumor consists of both fibroblastic (Fb) and osteoblastic (Ob) regions.

(**E** and **F**). Cases of undifferentiated sarcomas with pleomorphic spindle cells and atypical nuclei. And occasionally multinucleated giant cells (filled black arrows in **F**).

Immunohistochemistry characterization of lymphoma (**G, H** and **I**). The infiltrated lymphoma cells in (**B**) were stained with CD3 (**G**), B220/CD45R (**H**) and ki67 (**I**) respectively and resulted in CD3 positive and B220/CD45R negative. Note that all tumors were highly cellular and exhibited strong Ki67 positivity (**I**). A-D, G-I, 100x; E and F, 200x.

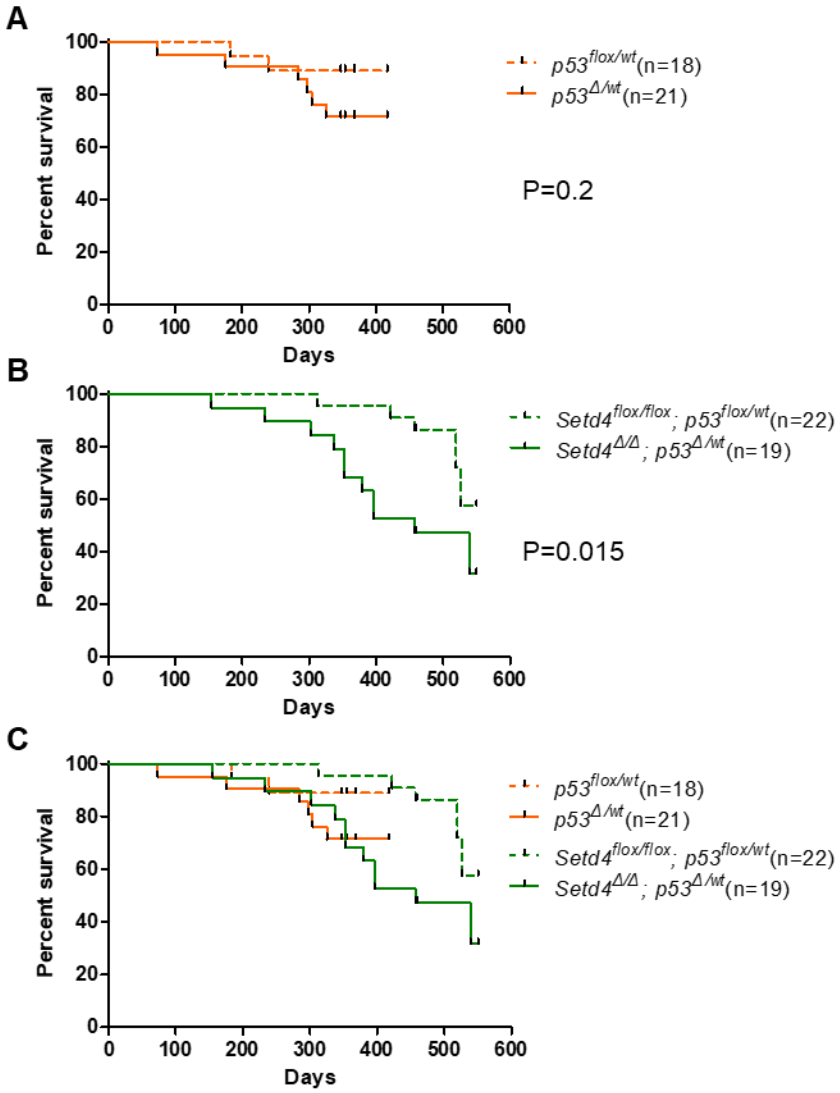

Figure 41. Kaplan-Meier survival of *p53*$^{\Delta/wt}$ and *Setd4*$^{\Delta/\Delta}$*; p53*$^{\Delta/wt}$ mice. Littermates of *p53*$^{flox/wt}$ and *Setd4*$^{flox/flox}$*; p53*$^{flox/wt}$ treated with oil or tamoxifen were kept for long-term survival observation. Points represent animals that had died or had to be sacrificed owing to illness.

A. Survival of 18 *p53*$^{flox/wt}$ (orange dash line) and 21 *p53*$^{\Delta/wt}$ (orange line) mice. p = 0.2 (log-rank Mantel–Cox test).

B. Survival of 22 *Setd4$^{flox/flox}$; p53$^{flox/wt}$* (green dash line) and 19 *Setd4$^{\Delta/\Delta}$; p53$^{\Delta/wt}$* (green line) mice. Median survival: 457 d for *Setd4$^{\Delta/\Delta}$; p53$^{\Delta/wt}$*, p = 0.015 (log-rank Mantel–Cox test).
C. Combined plots of A and B. *p53$^{flox/wt}$* vs *Setd4$^{flox/flox}$; p53$^{flox/wt}$*: 0.42; *p53$^{\Delta/wt}$* vs *Setd4$^{\Delta/\Delta}$; p53$^{\Delta/wt}$* : 0.57.

6.7 Setd4 deletion does not delay radiation-induced tumorigenesis in p53 knockout mice.

We next investigated whether Setd4 deletion suppresses radiation-induced lymphoma in p53 deficient mice using the same 4x2Gy radiation exposure scheme as in **Figure 32.** We found that *p53$^{\Delta/\Delta}$* mice had a greatly enhanced radiation-induced thymic lymphoma within 100 days post TBI (compare **Figure 42A** with **38A**), so as *p53$^{\Delta/wt}$* mice, although a slightly later (compare **Figure 42B** with **Figure 41A**). However, deletion of Setd4 in these mice did not significantly affect the course of tumor development in *Tp53$^{\Delta/\Delta}$* mice (compare **Figure 42C** with **42A**, **Figure 42D** with **42B,** and see **Figure 43**).

As shown in **Figure 43B**, after fractionated γ-irradiation, *Setd4$^{\Delta/\Delta}$;Tp53$^{\Delta/\Delta}$* mice developed thymic lymphoma with greatly higher incidence and accelerated rate compared with *Setd4$^{\Delta/\Delta}$* mice (median survival: 90 d for *Setd4$^{\Delta/\Delta}$; p53$^{\Delta/\Delta}$* vs. 278 d for *Setd4$^{\Delta/\Delta}$*, $p < 0.0001$). There was even a significantly accelerated lymphomagenesis in *Setd4$^{\Delta/\Delta}$;Tp53$^{\Delta/wt}$* mice (median survival: 128 days for *Setd4$^{\Delta/\Delta}$; p53$^{\Delta/wt}$* vs. 278 days for *Setd4$^{\Delta/\Delta}$*, $p < 0.0001$) (**Figure 43B**). Thus, loss of p53 abrogates the delay of radiation-induced thymic lymphoma in Setd4 deficient mice. In another word, Setd4 loss could not rescue the deleterious lymphomagenesis caused by p53 inactivation.

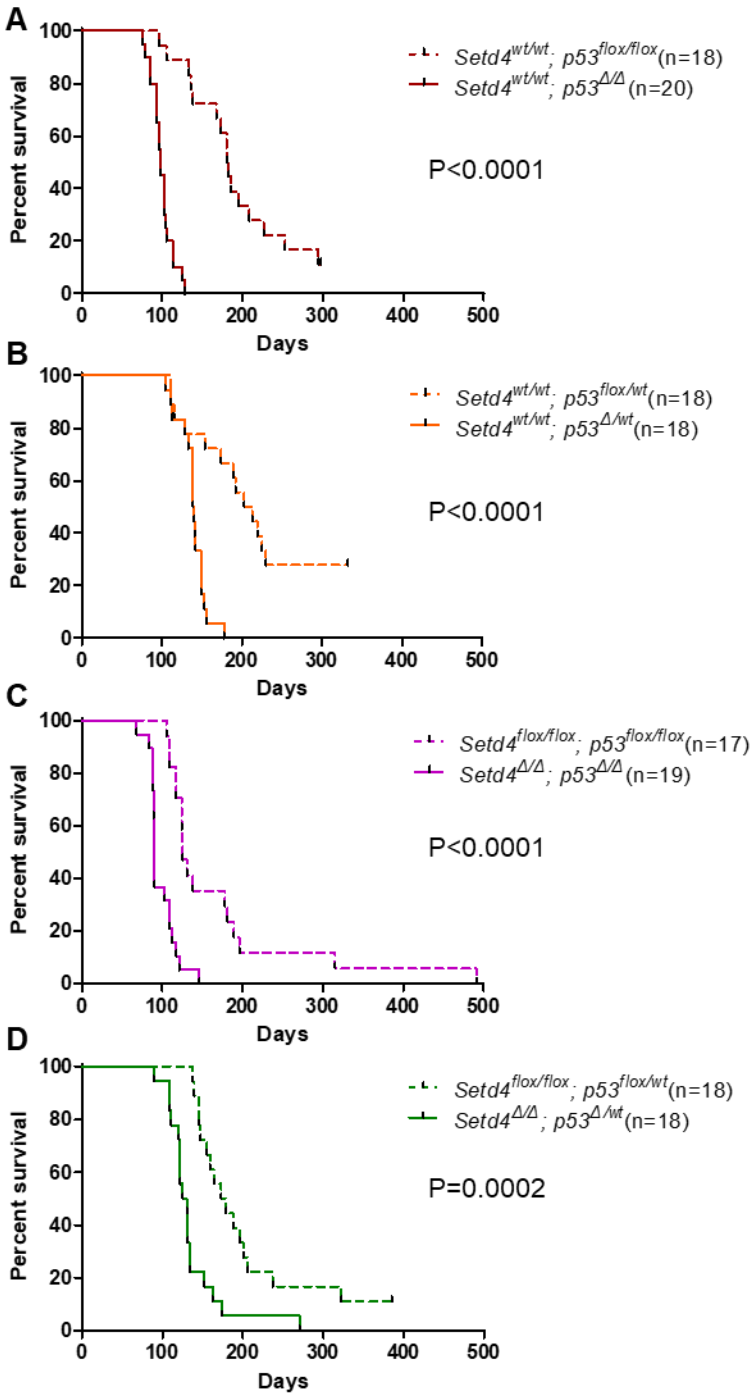

Figure 42. Loss of p53 abrogates the delayed development of radiation-induced thymic lymphoma in Setd4 deficient mice. Sex matched littermates of *p53*$^{flox/flox}$, *p53*$^{flox/wt}$, *Setd4*$^{flox/flox}$; *p53*$^{flox/flox}$ and *Setd4*$^{flox/flox}$; *p53*$^{flox/wt}$ treated with oil or tamoxifen were exposed to four weekly doses of γ-irradiation (2x4 Gy).

A. Kaplan-Meier survival of *p53*$^{flox/flox}$ and *p53*$^{\Delta/\Delta}$. Median survival 182 d vs 98 d, P < 0.0001 (log-rank Mantel–Cox test).

B. Kaplan-Meier survival of *p53*$^{flox/wt}$ and *p53*$^{Δ/wt}$. Median survival 208 d vs 140 d, P < 0.0001 (log-rank Mantel–Cox test).
C. Kaplan-Meier survival of *Setd4*$^{flox/flox}$*; p53*$^{flox/flox}$ and *Setd4*$^{Δ/Δ}$*; p53*$^{Δ/Δ}$. Median survival 125 d vs 90 d, P < 0.0001 (log-rank Mantel–Cox test).
D. Kaplan-Meier survival of *Setd4*$^{flox/flox}$*; p53*$^{flox/wt}$ and *Setd4*$^{Δ/Δ}$*; p53*$^{Δ/wt}$. Median survival 176 d vs 128 d, P = 0.0002 (log-rank Mantel–Cox test).

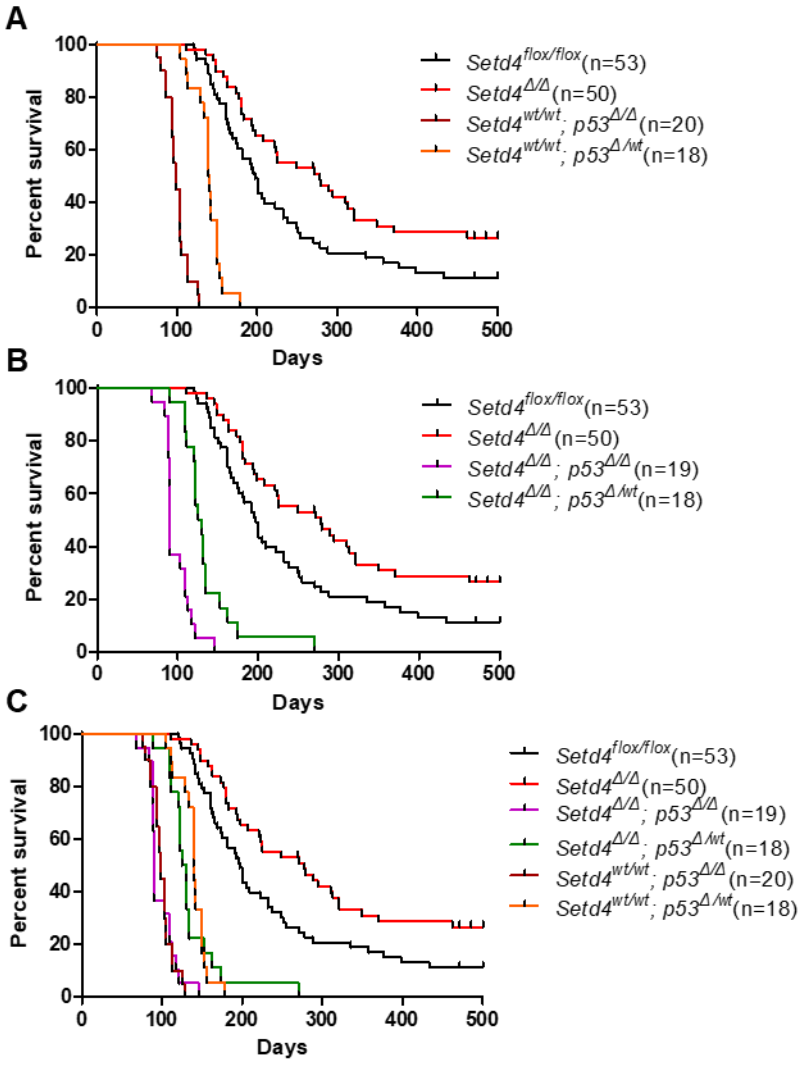

Figure 43. Loss of p53 abrogates the delayed development of radiation-induced thymic lymphoma in Setd4 deficient mice. Kaplan-Meier survival of mice exposed to four weekly doses of γ-irradiation (2x4 Gy).
A. *Setd4*$^{Δ/Δ}$ mice (n=50), *Setd4*$^{flox/flox}$ mice (n=53), *p53*$^{Δ/wt}$ (n=18), and *p53*$^{Δ/Δ}$ (n=20). The median survival: 287 d for *Setd4*$^{Δ/Δ}$, 197 d for *Setd4*$^{flox/flox}$, 140 d for *p53*$^{Δ/wt}$, and 98 d for *p53*$^{Δ/Δ}$. *Setd4*$^{Δ/Δ}$ vs *Setd4*$^{flox/flox}$; P = 0.012; *Setd4*$^{Δ/Δ}$ vs *p53*$^{Δ/Δ}$; P < 0.0001; *Setd4*$^{Δ/Δ}$ vs *p53*$^{Δ/wt}$; P < 0.0001 (log-rank Mantel–Cox test).

B. *Setd4*$^{\Delta/\Delta}$ mice (n=50), *Setd4*$^{flox/flox}$ mice (n=53), *Setd4*$^{\Delta/\Delta}$*; p53*$^{\Delta/wt}$ (n=18), and *Setd4*$^{\Delta/\Delta}$*; p53*$^{\Delta/\Delta}$ (n=19). The median survival: 287 d for *Setd4*$^{\Delta/\Delta}$, 197 d for *Setd4*$^{flox/flox}$, 128 d for *Setd4*$^{\Delta/\Delta}$*; p53*$^{\Delta/wt}$, and 90 d for *Setd4*$^{\Delta/\Delta}$*; p53*$^{\Delta/\Delta}$. *Setd4*$^{\Delta/\Delta}$ vs *Setd4*$^{flox/flox}$; P = 0.012; *Setd4*$^{\Delta/\Delta}$ vs *Setd4*$^{\Delta/\Delta}$*; p53*$^{\Delta/\Delta}$; P < 0.0001; *Setd4*$^{\Delta/\Delta}$ vs *Setd4*$^{\Delta/\Delta}$*; p53*$^{\Delta/wt}$; P < 0.0001 (log-rank Mantel–Cox test).

C. Combined plots of A and B.

Chapter 7, Discussion and Future Directions

In this study, we constructed an inducible Setd4 knockout mouse model and investigated the role of Setd4 in radiation sensitivity and tumorigenesis. We found that *Setd4* deficient mice were significantly more resistant to radiation-induced hematopoietic syndrome than the littermate wild type mice. We found that Setd4 deficient hematopoietic stem cells (HSCs) and progenitor cells (HPCs) have a slight *in vivo* growth advantage than the wild type cells, but are more sensitive to radiation. We found that the Setd4 deficient recipient mice have an enhanced ability to engraft transplanted HSCs, suggesting an improved bone marrow niche for the Setd4 deficient animals. Using a radiation-induced thymic lymphoma model, we also found that Setd4 deletion delayed radiation-induced tumorigenesis. Collectively, our study suggests that Setd4 defect can enhance the recovery of radiation-induced bone marrow damage and suppress radiation-induced thymic lymphoma, and that Setd4 is new gene in regulating bone marrow and hematopoietic functions in mice.

7.1 SETD4 deficient mouse models.

Mouse model is considered one of the most reliable systems to understand the function of a gene in the mammals. Previously, our lab has tried both direct deletion of Setd4 in germline stage and the canonical Cre-LoxP mediated conditional knockout approach, but with no luck. After many years of persistent attempts, we finally established a mouse Setd4 deficient mouse model using the Rosa26CreERT2 mediated inducible method.

During my first attempt of the EIIa-Cre approach, we failed to obtain embryos with Setd4 deletion or carrying a transmitted Setd4 floxed allele (see Chapter 4.4). The majority of the heterozygous *Setd4* loss mice were mosaic, no matter in male or female mating. A careful analysis of the failed attempts can potentially reveal the functional insight of Setd4. Initially, we suspected that the loxP sites on *Setd4* gene were not susceptible to Cre-recombination during embryo stage. This might be due to the facts that *EIIACre* transgene dose develop mosaicism under the most of circumstances due to restricted Cre activity, the frequency and extent of mosaicism completely depend on the target gene (167). However, by comparing pups of mosaic fathers and mothers, it was interesting that we observed that the maternal produce higher efficiency of Cre-recombination than paternal (**Tables 10** and **11**). This is similar to previous reports in the literature (193). In mouse development, the expression of *EIIACre* transgene during oocytes maturation, ovulation, and fertilization is strong enough to completely recombine the floxed segments. Although there is a second peak of expression during the early embryo stage, it is much less active and thus produces mosaic mice with partial excision. This might explain the presence of high percentage of F2 with heterozygous *Setd4* loss, and no birth of $Setd4^{flox/flox};EIIaCre^{-/-}$ pups in female mating scheme (**Tables 11**), but $Setd4^{flox/flox};EIIaCre^{-/-}$ pups were produced in male mating scheme (**Table 10**). Thirdly, there is a possibility that loss of *Setd4* might cause oocyte lethality. Based on the genotyping results of female mosaic pups (**Table 11**), even if the maternal Cre causes completed the excision of loxP during oogenesis, the frequency of maternally transmitted *Setd4* deleted allele was less than expected. Gallardo et al reported

a list of 348 ovarian factors involved in female infertility and are evolutionally conserved between human and mouse (194). Interestingly, *Setd4* was among those factors (194). They validated the expression pattern of *Setd4* by qRT–PCR and found it is highly expressed during postnatal day 1 to day 14 in adult ovaries. By means of RNA *in situ* hybridization, they further confirmed that mouse *Setd4* is mainly expressed from primary follicles to antral stages during follicle maturation. Thus, it is possible that our failed attempt to generate constitutive Setd4 deletion was due to a function of Setd4 in oogenesis. Fourthly, a potential neonatal death of embryonic *Setd4* knockout can also explain the lack of *Setd4* knockout pups. Nevertheless, further analyses of the failed generation of constitutive Setd4-null mice with EIIa-Cre suggest the possibility of oocyte lethality in Setd4 deficient mice. Additional studies should be devoted to address if *Setd4* is critical for female fertility and characterize at which stages of follicle assembly and development.

7.2 Detection of Setd4 protein in mouse tissues

In our study, although DNA genotyping and qRT-PCR analyses reliably verified the anticipated deletion of Setd4 in the Rosa26-CreERT2 mediated inducible knockout model, we had difficulty to detect the endogenous Setd4 protein by western blot despite of attempts with several antibodies. In general, we also have experienced difficulty to detect endogenous SETD4 protein in human and mouse cells, although exogenous Setd4 protein can be detected. Several practical obstacles were noted during our study. Since there was

very limited number of publications on Setd4 gene, the authenticity of the commercial antibodies have not been fully validated. For example, the same commercial antibody used by Faria et al (81) did not work for western blot or immunofluorescence using the mouse tissues in our hands (data not shown). We have attempted to generate our own antibodies using recombinant Setd4 proteins. However, the expression and purification of recombinant of full length human SETD4 protein in *E.coli* was proven to be difficult, although it was reported to be available in the insect cell system (55). Without full length SETD4 protein, we could only generate antibodies against synthetic peptides, which often give rise to non-specific signals when blotting against endogenous proteins. Other possible obstacles are the low levels of endogenous Setd4 among the tested tissues, or existence of multiple isoforms, or heavy modifications of endogenous Setd4 protein.

To overcome the above challenge, we are now developing a new mouse model where the floxed allele of Setd4 is fused with a V5-Flag epitope tag using CRISPR approach (195). If this model is established successfully, we will be able to use the V5 or Flag tag to verify the effectiveness of protein depletion. This approach is being carried out in collaboration our mouse core facility.

7.3 Mechanisms by which Setd4 deletion enhances bone marrow recovery.

In this study, the *Setd4* deficient mice were found to be significantly more resistant to radiation-induced hematopoietic syndrome than the littermate wild type mice. Using

several long-term bone marrow transplantation assays, we found that an improved bone marrow niche might be responsible for the radiation resistance in the Setd4 deficient mice. However, the underlining molecular mechanism remains to be identified. We performed a preliminary cytokine array analysis. The initial results showed that 14 days post IR 8 Gy, *Setd4*$^{\Delta/\Delta}$ mouse exhibited increased BM plasma levels of G-CSF, SDF-1/CXCL12 and TIMP-1, and decreased level of CXCL9. Among these, SDF-1/CXCL12 is known as a chemokine critical for the maintenance and quiescence of HSCs (196). Absence of CXCL-12 and other adhesive interaction will result in egress of HSC into peripheral blood stream. Thus, increased level of this chemokine implied that a more restricted stage of HSCs in *Setd4*$^{\Delta/\Delta}$ BM than *Setd4*$^{flox/flox}$ BM. Currently, experiments are being designed to verify these findings.

In addition to bone marrow niche, we found that the Setd4 deficient HSC hierarchy have a growth advantage in un-irradiated mice but are more sensitive to radiation. It is obviously that these effects can have opposing effect on the animal sensitivity to irradiation. To investigate the molecular mechanism, we have isolated LK cells from the animals and performed a preliminary genome wide RNA sequencing analysis, which implicated a possible involvement of ER stress pathway in the Setd4 knockout mice. Many literatures demonstrate that several members in ER stress pathway in deed play important roles in lymphoma development (197,198). Currently, experiments using IHC, qRT-PCR, and immunoblot are being planned to verify these initial findings. It is worth mentioning that

the RNAseq analysis failed to correlate p53 pathway with Setd4 deletion, which is consistent with our animal experiments with Sedt4/p53 double knockout mice.

Our previous data uncovered that Setd4 is a critical cell fate determinate in DNA damage response by affecting HR and NHEJ (Jinjiang Fan, Shen lab unpublished). Our current findings further indicate that Setd4 knockout protects mice from radiation-induced death at 8 Gy dose. Supporting our results, depletion of the methyltransferase Set1p leads to enhanced cell death during chronological aging and increased sensitivity to apoptosis induction while loss of *DOT1* only slightly affects yeast survival (199). However, the co-disruption of the methyltransferase Set1p and Dot1p impedes early death in *S. cerevisiae* (199), indicating that SET domain methyltransferase family is an important trigger for cell death in *S. cerevisiae*.

7.4 Mechanism of T-lymphoma development in Setd4 deficient mice.

Our preliminary results (**Figures 35**) indicated that there is a difference of tumor subtypes developed from wild type and Setd4 deficient mice. However, it remains to be addressed whether there are distinct signaling networks between these tumors. Although mTOR and Wnt/Beta-catenin have been shown to play the critical role in the lymphoma (200,201), our IHC data do not support this possibility in Setd4-deficient mice model (data not shown). Additional studies on the genomic signature and gene expression profile of these tumors would allow us to fully distinguish the subtypes of tumor and gain additional insight on the

function of the Setd4 gene.

Although our data indicated that SETD4 knockout protects mice from radiation-induced thymic lymphoma, further experiments are needed to confirm the role of SETD4 in lymphoma. One potential analysis is the clonality determination of the TRBV locus (TCRVβ) of thymus or spleen cells from one WT mouse and *Setd4*$^{-/-}$ mice by using genomic DNA sequencing and PCR (157,202). Assessment of the T-cell antigen receptor β (TCRβ) locus showed that most radiation-induced lymphomas contained only one or two dominant rearrangements, and that lymphomas developed from the expansion of one or a small number of cells in the irradiated thymus (157).

The previous studies demonstrated that many factors (such as oncogene Ras, ERK1/2, STAT3, and SHP-2 and tumor suppressor gene p53) were involved in radiation-induced mouse thymic lymphomas (203-205). However, when compared the *Setd4*$^{-/-}$*; p53*$^{-/-}$ mice and *Setd4*$^{-/-}$ mice, a significant difference in phenotype (mainly based on their survive curves) was not observed following a 2 Gy γ-ray exposures, suggesting that p53 signal pathway is not a direct upstream or downstream of Setd4. Given that genetic alterations in *Fbxw7*, or p16INK4a, or Pten are also commonly found in human T-ALL (T-cell Acute Lymphoblastic Leukaemia) and murine thymic lymphomas, and *Fbxw7*, or p16INK4a, or Pten deletion in mice promotes IR-induced thymic lymphomas (206-208), to further confirm the role of Setd4 and uncover the potential mechanisms by which radiation induces thymic lymphomas, the combined knockout of Setd4 with Fbxw7 or p16INK4a or Pten

deletion might provide more information. Additional studies using this strategy may also help to establish a relationship between Setd4 and some known genetic mutations that contribute to thymic lymphoma development. Among three genes, Pten is very important because PTEN loss is at the center of a complex oncogenic network that sustains to drive tumorigenesis via activating multiple signaling pathways (209). Importantly, different Pten knockout models exactly recapitulated the development of T-cell lymphoma (210). Possibly, other targets for Fbxw7 or p16INK4a, such as Myc, c-Jun, E2F1, or mTorc1 (211,212), may also be important in this context and will require further investigation.

Although little is known about the molecular mechanisms and prognostic impact of *Setd4* alteration in T-cell lymphoma, our results offered some valuable clues. For example, our findings indicates that Setd4 knockout promotes CXCL12 and G-CSF (Granulocyte-colony stimulating factor) expression upon radiation. Numerous studies have already shown that G-CSF may be of therapeutic benefit to patients with T-cell acute lymphoblastic leukemia and other leukemia by disrupting the lymphoid niche (213). And G-CSF slowed disease in the majority of ALL xenografts (214). Also, G-CSF induces enhanced long-term hematopoietic recovery in radiated mice and prevented the mice from irradiation-induced death (215,216). The chemokine receptor CXCR4 and its ligand stromal cell-derived factor-1 (SDF-1/CXCL12) are important players in the cross-talk among lymphoma, myeloma and leukemia cells and their microenvironments (217). The overexpression of CXCR4 on the cell surface has been shown to be responsible for disease progression,

increasing tumor cell survival and chemoresistance and metastasis to organs with high CXCL12 levels (217). For example, CXCL12 inhibition with anti-CXCL12 L-ribonucleotide NOX-A12 significantly reduced the tumor burden and acted synergistically with bortezomib, probably by making the BM niche less permissive to leukemia (218). Furthermore, in a clinical phase IIa study, treatment with NOX-A12 induced myeloma cell mobilization and enhanced the clinical activity of bortezomib/dexamethasone in relapsed leukemia patients (218).

Together, our novel data suggests that Setd4 promotes T-cell lymphoma possibly by acting on tumor microenvironment. These assays might provide novel insights into the role of *Setd4* in tumor development and have identified a number of potential targets for therapeutic intervention. Similar to Setd4, the previous study reported that TLR4 knockout protects mice from radiation-induced thymic lymphoma by acting on tumor microenvironment: downregulation of IL6 and miR-21 (161). This study also explored the potential upstream factors of TLR4 that participate in ionizing radiation-induced thymic lymphoma. The high-mobility group box 1 protein (HMGB1) which could be rapidly induced by irradiation is also an important ligand of TLR4 (161). Since Setd4 knockout protects mice from radiation-induced thymic lymphoma possibly by acting on tumor microenvironment, it might be interesting to explore whether HMGB1 or other factor induced by radiation affects the Setd4 activation.

Although SETD4 was believed to be a non-histone methyltransferases (81) and it was

reported that Ar-SETD4 has enzymatic activity on H4K20me3 (55), no direct evidence is available to establish that SETD4 can methylate histone or non-histone proteins in human or mice. In the future, it would be important to identify the physiological substrates in order to address the mechanism by which SETD4 modulates lymphoma risk after DNA damage caused by radiation.

In summary, this study has suggested a critical role of Setd4 in the regulation of bone marrow recovery and radiation induced tumorigenesis. Future studies will need to be focused on the biochemical activities, the identification of authentic substrates, and the elucidation of the regulatory mechanisms of Setd4.

References

1. Bracken AP, Pasini D, Capra M, Prosperini E, Colli E, Helin K. EZH2 is downstream of the pRB‐E2F pathway, essential for proliferation and amplified in cancer. The EMBO journal **2003**;22:5323-35
2. Milne TA, Briggs SD, Brock HW, Martin ME, Gibbs D, Allis CD*, et al.* MLL targets SET domain methyltransferase activity to Hox gene promoters. Molecular cell **2002**;10:1107-17
3. Wang GG, Cai L, Pasillas MP, Kamps MP. NUP98–NSD1 links H3K36 methylation to Hox-A gene activation and leukaemogenesis. Nature cell biology **2007**;9:804
4. Rea S, Eisenhaber F, O'carroll D, Strahl BD, Sun Z-W, Schmid M*, et al.* Regulation of chromatin structure by site-specific histone H3 methyltransferases. Nature **2000**;406:593
5. Peters AH, O'Carroll D, Scherthan H, Mechtler K, Sauer S, Schöfer C*, et al.* Loss of the Suv39h histone methyltransferases impairs mammalian heterochromatin and genome stability. Cell **2001**;107:323-37
6. Lehnertz B, Ueda Y, Derijck AA, Braunschweig U, Perez-Burgos L, Kubicek S*, et al.* Suv39h-mediated histone H3 lysine 9 methylation directs DNA methylation to major satellite repeats at pericentric heterochromatin. Current Biology **2003**;13:1192-200
7. Shen X, Liu Y, Hsu Y-J, Fujiwara Y, Kim J, Mao X*, et al.* EZH1 mediates methylation on histone H3 lysine 27 and complements EZH2 in maintaining stem cell identity and executing pluripotency. Molecular cell **2008**;32:491-502
8. Wakeman TP, Wang Q, Feng J, Wang XF. Bat3 facilitates H3K79 dimethylation by DOT1L and promotes DNA damage‐induced 53BP1 foci at G1/G2 cell‐cycle phases. The EMBO journal **2012**;31:2169-81
9. FitzGerald J, Moureau S, Drogaris P, O'Connell E, Abshiru N, Verreault A*, et al.* Regulation of the DNA damage response and gene expression by the Dot1L histone methyltransferase and the 53Bp1 tumour suppressor. PLoS One **2011**;6:e14714
10. Chang Y, Sun L, Kokura K, Horton JR, Fukuda M, Espejo A*, et al.* MPP8 mediates the interactions between DNA methyltransferase Dnmt3a and H3K9 methyltransferase GLP/G9a. Nature communications **2011**;2:533
11. Petrossian TC, Clarke SG. Uncovering the human methyltransferasome. Molecular & Cellular Proteomics **2011**;10:M110. 000976
12. Arrowsmith CH, Bountra C, Fish PV, Lee K, Schapira M. Epigenetic protein families: a new frontier for drug discovery. Nature reviews Drug discovery **2012**;11:384
13. Spannhoff A, Hauser AT, Heinke R, Sippl W, Jung M. The emerging therapeutic potential of histone methyltransferase and demethylase inhibitors. ChemMedChem **2009**;4:1568-82
14. Dong C, Wu Y, Wang Y, Wang C, Kang T, Rychahou PG*, et al.* Interaction with Suv39H1 is critical for Snail-mediated E-cadherin repression in breast cancer. Oncogene **2013**;32:1351
15. Wang Y, Zhang H, Chen Y, Sun Y, Yang F, Yu W*, et al.* LSD1 is a subunit of the NuRD complex and targets the metastasis programs in breast cancer. Cell **2009**;138:660-72
16. Tahiliani M, Mei P, Fang R, Leonor T, Rutenberg M, Shimizu F*, et al.* The histone H3K4 demethylase SMCX links REST target genes to X-linked mental retardation. Nature **2007**;447:601

17. Melcher M, Schmid M, Aagaard L, Selenko P, Laible G, Jenuwein T. Structure-function analysis of SUV39H1 reveals a dominant role in heterochromatin organization, chromosome segregation, and mitotic progression. Molecular and Cellular Biology **2000**;20:3728-41
18. Okada Y, Feng Q, Lin Y, Jiang Q, Li Y, Coffield VM*, et al.* hDOT1L links histone methylation to leukemogenesis. Cell **2005**;121:167-78
19. Ng HH, Xu R-M, Zhang Y, Struhl K. Ubiquitination of histone H2B by Rad6 is required for efficient Dot1-mediated methylation of histone H3 lysine 79. Journal of Biological Chemistry **2002**;277:34655-7
20. Schultz J, Milpetz F, Bork P, Ponting CP. SMART, a simple modular architecture research tool: identification of signaling domains. Proceedings of the National Academy of Sciences **1998**;95:5857-64
21. Trievel RC, Beach BM, Dirk LM, Houtz RL, Hurley JH. Structure and catalytic mechanism of a SET domain protein methyltransferase. Cell **2002**;111:91-103
22. Marmorstein R. Structure of SET domain proteins: a new twist on histone methylation. Trends in biochemical sciences **2003**;28:59-62
23. Song J-J, Kingston RE. WDR5 interacts with mixed lineage leukemia (MLL) protein via the histone H3-binding pocket. Journal of Biological Chemistry **2008**;283:35258-64
24. Mersman DP, Du H-N, Fingerman IM, South PF, Briggs SD. Charge-based interaction conserved within histone H3 lysine 4 (H3K4) methyltransferase complexes is needed for protein stability, histone methylation, and gene expression. Journal of Biological Chemistry **2012**;287:2652-65
25. Kuzmichev A, Jenuwein T, Tempst P, Reinberg D. Different EZH2-containing complexes target methylation of histone H1 or nucleosomal histone H3. Molecular cell **2004**;14:183-93
26. Chen Y, Chen J, Yu J, Yang G, Temple E, Harbinski F*, et al.* Identification of mixed lineage leukemia 1 (MLL1) protein as a coactivator of heat shock factor 1 (HSF1) protein in response to heat shock protein 90 (HSP90) inhibition. Journal of Biological Chemistry **2014**;289:18914-27
27. Van Duyne R, Easley R, Wu W, Berro R, Pedati C, Klase Z*, et al.* Lysine methylation of HIV-1 Tat regulates transcriptional activity of the viral LTR. Retrovirology **2008**;5:40
28. Huang J, Dorsey J, Chuikov S, Zhang X, Jenuwein T, Reinberg D*, et al.* G9a and Glp methylate lysine 373 in the tumor suppressor p53. Journal of Biological Chemistry **2010**;285:9636-41
29. Lee JS, Kim Y, Kim IS, Kim B, Choi HJ, Lee JM*, et al.* Negative regulation of hypoxic responses via induced Reptin methylation. Molecular cell **2010**;39:71-85
30. Rathert P, Dhayalan A, Murakami M, Zhang X, Tamas R, Jurkowska R*, et al.* Protein lysine methyltransferase G9a acts on non-histone targets. Nature chemical biology **2008**;4:344
31. Sampath SC, Marazzi I, Yap KL, Sampath SC, Krutchinsky AN, Mecklenbräuker I*, et al.* Methylation of a histone mimic within the histone methyltransferase G9a regulates protein complex assembly. Molecular cell **2007**;27:596-608
32. Fei Q, Shang K, Zhang J, Chuai S, Kong D, Zhou T*, et al.* Histone methyltransferase SETDB1 regulates liver cancer cell growth through methylation of p53. Nature communications **2015**;6:8651
33. Kim E, Kim M, Woo D-H, Shin Y, Shin J, Chang N*, et al.* Phosphorylation of EZH2 activates STAT3 signaling via STAT3 methylation and promotes tumorigenicity of glioblastoma stem-like cells. Cancer cell **2013**;23:839-52

34. He A, Shen X, Ma Q, Cao J, von Gise A, Zhou P*, et al.* PRC2 directly methylates GATA4 and represses its transcriptional activity. Genes & development **2012**;26:37-42
35. Lu T, Jackson MW, Wang B, Yang M, Chance MR, Miyagi M*, et al.* Regulation of NF-κB by NSD1/FBXL11-dependent reversible lysine methylation of p65. Proceedings of the National Academy of Sciences **2010**;107:46-51
36. Saloura V, Vougiouklakis T, Zewde M, Deng X, Kiyotani K, Park J-H*, et al.* WHSC1L1-mediated EGFR mono-methylation enhances the cytoplasmic and nuclear oncogenic activity of EGFR in head and neck cancer. Scientific reports **2017**;7:40664
37. Yang L, Lin C, Liu W, Zhang J, Ohgi KA, Grinstein JD*, et al.* ncRNA-and Pc2 methylation-dependent gene relocation between nuclear structures mediates gene activation programs. Cell **2011**;147:773-88
38. Huang J, Perez-Burgos L, Placek BJ, Sengupta R, Richter M, Dorsey JA*, et al.* Repression of p53 activity by Smyd2-mediated methylation. Nature **2006**;444:629
39. Cho H-S, Hayami S, Toyokawa G, Maejima K, Yamane Y, Suzuki T*, et al.* RB1 methylation by SMYD2 enhances cell cycle progression through an increase of RB1 phosphorylation. Neoplasia **2012**;14:476-IN8
40. Donlin LT, Andresen C, Just S, Rudensky E, Pappas CT, Kruger M*, et al.* Smyd2 controls cytoplasmic lysine methylation of Hsp90 and myofilament organization. Genes & development **2012**;26:114-9
41. Kunizaki M, Hamamoto R, Silva FP, Yamaguchi K, Nagayasu T, Shibuya M*, et al.* The lysine 831 of vascular endothelial growth factor receptor 1 is a novel target of methylation by SMYD3. Cancer research **2007**;67:10759-65
42. Mazur PK, Reynoird N, Khatri P, Jansen PW, Wilkinson AW, Liu S*, et al.* SMYD3 links lysine methylation of MAP3K2 to Ras-driven cancer. Nature **2014**;510:283
43. Kurash JK, Lei H, Shen Q, Marston WL, Granda BW, Fan H*, et al.* Methylation of p53 by Set7/9 mediates p53 acetylation and activity in vivo. Molecular cell **2008**;29:392-400
44. Liu X, Wang D, Zhao Y, Tu B, Zheng Z, Wang L*, et al.* Methyltransferase Set7/9 regulates p53 activity by interacting with Sirtuin 1 (SIRT1). Proceedings of the National Academy of Sciences **2011**;108:1925-30
45. Munro S, Khaire N, Inche A, Carr S, La Thangue N. Lysine methylation regulates the pRb tumour suppressor protein. Oncogene **2010**;29:2357
46. Kontaki H, Talianidis I. Lysine methylation regulates E2F1-induced cell death. Molecular cell **2010**;39:152-60
47. Yang XD, Huang B, Li M, Lamb A, Kelleher NL, Chen LF. Negative regulation of NF‐κB action by Set9‐mediated lysine methylation of the RelA subunit. The EMBO journal **2009**;28:1055-66
48. Yang J, Huang J, Dasgupta M, Sears N, Miyagi M, Wang B*, et al.* Reversible methylation of promoter-bound STAT3 by histone-modifying enzymes. Proceedings of the National Academy of Sciences **2010**;107:21499-504
49. Oudhoff MJ, Freeman SA, Couzens AL, Antignano F, Kuznetsova E, Min PH*, et al.* Control of the hippo pathway by Set7-dependent methylation of Yap. Developmental cell **2013**;26:188-94
50. Calnan DR, Webb AE, White JL, Stowe TR, Goswami T, Shi X*, et al.* Methylation by Set9 modulates FoxO3 stability and transcriptional activity. Aging (Albany NY) **2012**;4:462

51. Kim D-W, Kim K-B, Kim J-Y, Seo S-B. Characterization of a novel histone H3K36 methyltransferase setd3 in zebrafish. Bioscience, biotechnology, and biochemistry **2011**;75:289-94
52. Eom GH, Kim K-B, Kim JH, Kim J-Y, Kim J-R, Kee HJ*, et al.* Histone methyltransferase SETD3 regulates muscle differentiation. Journal of Biological Chemistry **2011**;286:34733-42
53. Levy D, Kuo AJ, Chang Y, Schaefer U, Kitson C, Cheung P*, et al.* Lysine methylation of the NF-κB subunit RelA by SETD6 couples activity of the histone methyltransferase GLP at chromatin to tonic repression of NF-κB signaling. Nature immunology **2011**;12:29
54. Chang Y, Levy D, Horton JR, Peng J, Zhang X, Gozani O*, et al.* Structural basis of SETD6-mediated regulation of the NF-kB network via methyl-lysine signaling. Nucleic acids research **2011**;39:6380-9
55. Dai L, Ye S, Li H-W, Chen D-F, Wang H-L, Jia S-N*, et al.* SETD4 regulates cell quiescence and catalyzes the trimethylation of H4K20 during diapause formation in Artemia. Molecular and cellular biology **2017**;37:e00453-16
56. Wang P, Lin C, Smith ER, Guo H, Sanderson BW, Wu M*, et al.* Global analysis of H3K4 methylation defines MLL family member targets and points to a role for MLL1-mediated H3K4 methylation in the regulation of transcriptional initiation by RNA polymerase II. Molecular and cellular biology **2009**;29:6074-85
57. Dou Y, Milne TA, Ruthenburg AJ, Lee S, Lee JW, Verdine GL*, et al.* Regulation of MLL1 H3K4 methyltransferase activity by its core components. Nature Structural and Molecular Biology **2006**;13:713
58. Li Y, Han J, Zhang Y, Cao F, Liu Z, Li S*, et al.* Structural basis for activity regulation of MLL family methyltransferases. Nature **2016**;530:447
59. Herz H-M, Mohan M, Garruss AS, Liang K, Takahashi Y-h, Mickey K*, et al.* Enhancer-associated H3K4 monomethylation by Trithorax-related, the Drosophila homolog of mammalian Mll3/Mll4. Genes & development **2012**;26:2604-20
60. Denissov S, Hofemeister H, Marks H, Kranz A, Ciotta G, Singh S*, et al.* Mll2 is required for H3K4 trimethylation on bivalent promoters in embryonic stem cells, whereas Mll1 is redundant. Development **2014**;141:526-37
61. Wu M, Wang PF, Lee JS, Martin-Brown S, Florens L, Washburn M*, et al.* Molecular regulation of H3K4 trimethylation by Wdr82, a component of human Set1/COMPASS. Molecular and cellular biology **2008**;28:7337-44
62. Daser A, Rabbitts TH. Extending the repertoire of the mixed-lineage leukemia gene MLL in leukemogenesis. Genes & development **2004**;18:965-74
63. Brown MA, Sims RJ, Gottlieb PD, Tucker PW. Identification and characterization of Smyd2: a split SET/MYND domain-containing histone H3 lysine 36-specific methyltransferase that interacts with the Sin3 histone deacetylase complex. Molecular cancer **2006**;5:26
64. Sirinupong N, Brunzelle J, Ye J, Pirzada A, Nico L, Yang Z. Crystal structure of cardiac-specific histone methyltransferase SmyD1 reveals unusual active site architecture. Journal of Biological Chemistry **2010**;285:40635-44
65. Hamamoto R, Furukawa Y, Morita M, Iimura Y, Silva FP, Li M*, et al.* SMYD3 encodes a histone methyltransferase involved in the proliferation of cancer cells. Nature cell biology **2004**;6:731

66. Hu L, Zhu YT, Qi C, Zhu Y-J. Identification of Smyd4 as a potential tumor suppressor gene involved in breast cancer development. Cancer research **2009**;69:4067-72
67. Spellmon N, Holcomb J, Trescott L, Sirinupong N, Yang Z. Structure and function of SET and MYND domain-containing proteins. International journal of molecular sciences **2015**;16:1406-28
68. Nagandla H, Lopez S, Yu W, Rasmussen TL, Tucker HO, Schwartz RJ*, et al.* Defective myogenesis in the absence of the muscle-specific lysine methyltransferase SMYD1. Developmental biology **2016**;410:86-97
69. Rasmussen TL, Ma Y, Park CY, Harriss J, Pierce SA, Dekker JD*, et al.* Smyd1 facilitates heart development by antagonizing oxidative and ER stress responses. PloS one **2015**;10:e0121765
70. Komatsu S, Imoto I, Tsuda H, Kozaki K-i, Muramatsu T, Shimada Y*, et al.* Overexpression of SMYD2 relates to tumor cell proliferation and malignant outcome of esophageal squamous cell carcinoma. Carcinogenesis **2009**;30:1139-46
71. Voelkel T, Andresen C, Unger A, Just S, Rottbauer W, Linke WA. Lysine methyltransferase Smyd2 regulates Hsp90-mediated protection of the sarcomeric titin springs and cardiac function. Biochimica et Biophysica Acta (BBA)-Molecular Cell Research **2013**;1833:812-22
72. Nishioka K, Rice JC, Sarma K, Erdjument-Bromage H, Werner J, Wang Y*, et al.* PR-Set7 is a nucleosome-specific methyltransferase that modifies lysine 20 of histone H4 and is associated with silent chromatin. Molecular cell **2002**;9:1201-13
73. Estève P-O, Chin HG, Benner J, Feehery GR, Samaranayake M, Horwitz GA*, et al.* Regulation of DNMT1 stability through SET7-mediated lysine methylation in mammalian cells. Proceedings of the National Academy of Sciences **2009**;106:5076-81
74. Dhayalan A, Kudithipudi S, Rathert P, Jeltsch A. Specificity analysis-based identification of new methylation targets of the SET7/9 protein lysine methyltransferase. Chemistry & biology **2011**;18:111-20
75. Kassner I, Barandun M, Fey M, Rosenthal F, Hottiger MO. Crosstalk between SET7/9-dependent methylation and ARTD1-mediated ADP-ribosylation of histone H1. 4. Epigenetics & chromatin **2013**;6:1
76. Pradhan S, Chin HG, Estève P-O, Jacobsen SE. SET7/9 mediated methylation of non-histone proteins in mammalian cells. Epigenetics **2009**;4:383-7
77. Subramanian K, Jia D, Kapoor-Vazirani P, Powell DR, Collins RE, Sharma D*, et al.* Regulation of estrogen receptor α by the SET7 lysine methyltransferase. Molecular cell **2008**;30:336-47
78. Couture J-F, Collazo E, Hauk G, Trievel RC. Structural basis for the methylation site specificity of SET7/9. Nature Structural and Molecular Biology **2006**;13:140
79. Deering TG, Ogihara T, Trace AP, Maier B, Mirmira RG. Methyltransferase Set7/9 maintains transcription and euchromatin structure at islet-enriched genes. Diabetes **2009**;58:185-93
80. Tao Y, Neppl RL, Huang Z-P, Chen J, Tang R-H, Cao R*, et al.* The histone methyltransferase Set7/9 promotes myoblast differentiation and myofibril assembly. The Journal of cell biology **2011**;194:551-65
81. Faria JAQA, Corrêa NCR, de Andrade C, de Angelis Campos AC, de Almeida RdSS, Rodrigues TS*, et al.* SET domain-containing protein 4 (SETD4) is a newly identified cytosolic and nuclear lysine methyltransferase involved in breast cancer cell proliferation. Journal of cancer science & therapy

2013;5:58

82. Li G-M, Wang Y-G, Pan Q, Wang J, Fan J-G, Sun C. RNAi screening with shRNAs against histone methylation-related genes reveals determinants of sorafenib sensitivity in hepatocellular carcinoma cells. International journal of clinical and experimental pathology **2014**;7:1085
83. Zhu S, Xu Y, Song M, Chen G, Wang H, Zhao Y*, et al.* PRDM16 is associated with evasion of apoptosis by prostatic cancer cells according to RNA interference screening. Molecular medicine reports **2016**;14:3357-61
84. Jiang X, Liu C, Yu T, Zhang L, Meng K, Xing Z*, et al.* Genetic dissection of the Down syndrome critical region. Human molecular genetics **2015**;24:6540-51
85. Mettler Jr FA, Voelz GL. Major radiation exposure—what to expect and how to respond. New England Journal of Medicine **2002**;346:1554-61
86. Wang Y, Schulte BA, LaRue AC, Ogawa M, Zhou D. Total body irradiation selectively induces murine hematopoietic stem cell senescence. Blood **2006**;107:358-66
87. Shao L, Feng W, Li H, Gardner D, Luo Y, Wang Y*, et al.* Total body irradiation causes long-term mouse BM injury via induction of HSC premature senescence in an Ink4a-and Arf-independent manner. Blood **2014**;123:3105-15
88. Mendelson A, Frenette PS. Hematopoietic stem cell niche maintenance during homeostasis and regeneration. Nature medicine **2014**;20:833
89. Patchen M, MacVittie T, Williams J, Schwartz G, Souza L. Administration of interleukin-6 stimulates multilineage hematopoiesis and accelerates recovery from radiation-induced hematopoietic depression. Blood **1991**;77:472-80
90. Chen T, Burke KA, Zhan Y, Wang X, Shibata D, Zhao Y. IL-12 facilitates both the recovery of endogenous hematopoiesis and the engraftment of stem cells after ionizing radiation. Experimental Hematology **2007**;35:203-13
91. Mouthon M-A, Van der Meeren A, Gaugler M-H, Visser TP, Squiban C, Gourmelon P*, et al.* Thrombopoietin promotes hematopoietic recovery and survival after high-dose whole body irradiation. International Journal of Radiation Oncology• Biology• Physics **1999**;43:867-75
92. Jacobson L, Simmons E, Marks E, Robson M, Bethabd W, Gaston E. The role of the spleen in radiation injury and recovery. The Journal of laboratory and clinical medicine **1950**;35:746-70
93. Thomas ED, Lochte Jr HL, Lu WC, Ferrebee JW. Intravenous infusion of bone marrow in patients receiving radiation and chemotherapy. New England Journal of Medicine **1957**;257:491-6
94. Till JE, McCulloch EA. A direct measurement of the radiation sensitivity of normal mouse bone marrow cells. Radiation research **1961**;14:213-22
95. Verheij M, Bartelink H. Radiation-induced apoptosis. Cell and tissue research **2000**;301:133-42
96. Mauch P, Constine L, Greenberger J, Knospe W, Sullivan J, Liesveld JL*, et al.* Hematopoietic stem cell compartment: acute and late effects of radiation therapy and chemotherapy. International Journal of Radiation Oncology• Biology• Physics **1995**;31:1319-39
97. Dainiak N. Hematologic consequences of exposure to ionizing radiation. Experimental hematology **2002**;30:513-28
98. Lowe SW, Schmitt EM, Smith SW, Osborne BA, Jacks T. p53 is required for radiation-induced apoptosis in mouse thymocytes. Nature **1993**;362:847

99. Xia F, Wang X, Wang Y-H, Tsang N-M, Yandell DW, Kelsey KT*, et al.* Altered p53 status correlates with differences in sensitivity to radiation-induced mutation and apoptosis in two closely related human lymphoblast lines. Cancer research **1995**;55:12-5
100. Clarke A, Purdie C, Harrison D, Morris R, Bird C, Hooper M*, et al.* Thymocyte apoptosis induced by p53-dependent and independent pathways. Nature **1993**;362:849
101. Westphal CH, Rowan S, Schmaltz C, Elson A, Fisher DE, Leder P. atm and p53 cooperate in apoptosis and suppression of tumorigenesis, but not in resistance to acute radiation toxicity. Nature genetics **1997**;16:397
102. Dulić V, Kaufmann WK, Wilson SJ, Tisty TD, Lees E, Harper JW*, et al.* p53-dependent inhibition of cyclin-dependent kinase activities in human fibroblasts during radiation-induced G1 arrest. Cell **1994**;76:1013-23
103. Hall P, McKee P, Menage H, Dover R, Lane D. High levels of p53 protein in UV-irradiated normal human skin. Oncogene **1993**;8:203-7
104. Merritt AJ, Potten CS, Kemp CJ, Hickman JA, Balmain A, Lane DP*, et al.* The role of p53 in spontaneous and radiation-induced apoptosis in the gastrointestinal tract of normal and p53-deficient mice. Cancer research **1994**;54:614-7
105. Clarke AR, Gledhill S, Hooper ML, Bird CC, Wyllie AH. p53 dependence of early apoptotic and proliferative responses within the mouse intestinal epithelium following gamma-irradiation. Oncogene **1994**;9:1767-73
106. Midgley CA, Owens B, Briscoe CV, Thomas DB, Lane DP, Hall PA. Coupling between gamma irradiation, p53 induction and the apoptotic response depends upon cell type in vivo. Journal of Cell Science **1995**;108:1843-8
107. Komarova EA, Christov K, Faerman AI, Gudkov AV. Different impact of p53 and p21 on the radiation response of mouse tissues. Oncogene **2000**;19:3791
108. MacCallum DE, Hupp TR, Midgley CA, Stuart D, Campbell SJ, Harper A*, et al.* The p53 response to ionising radiation in adult and developing murine tissues. Oncogene **1996**;13:2575-87
109. Lowe SW, Bodis S, McClatchey A, Remington L, Ruley HE, Fisher DE*, et al.* p53 status and the efficacy of cancer therapy in vivo. Science **1994**;266:807-10
110. Falette N, Paperin M-P, Treilleux I, Gratadour A-C, Peloux N, Mignotte H*, et al.* Prognostic value of p53 gene mutations in a large series of node-negative breast cancer patients. Cancer research **1998**;58:1451-5
111. Gross A, McDonnell JM, Korsmeyer SJ. BCL-2 family members and the mitochondria in apoptosis. Genes & development **1999**;13:1899-911
112. Chipuk JE, Kuwana T, Bouchier-Hayes L, Droin NM, Newmeyer DD, Schuler M*, et al.* Direct activation of Bax by p53 mediates mitochondrial membrane permeabilization and apoptosis. Science **2004**;303:1010-4
113. Nakano K, Vousden KH. PUMA, a novel proapoptotic gene, is induced by p53. Molecular cell **2001**;7:683-94
114. Sakakura C, Sweeney EA, Shirahama T, Igarashi Y, Hakomori Si, Nakatani H*, et al.* Overexpression of bax sensitizes human breast cancer MCF‐7 cells to radiation‐induced apoptosis. International journal of cancer **1996**;67:101-5

115. Kitada S, Krajewski S, Miyashita T, Krajewska M, Reed JC. Gamma-radiation induces upregulation of Bax protein and apoptosis in radiosensitive cells in vivo. Oncogene **1996**;12:187-92
116. Chong MJ, Murray MR, Gosink EC, Russell HR, Srinivasan A, Kapsetaki M*, et al.* Atm and Bax cooperate in ionizing radiation-induced apoptosis in the central nervous system. Proceedings of the National Academy of Sciences **2000**;97:889-94
117. Yu H, Shen H, Yuan Y, XuFeng R, Hu X, Garrison SP*, et al.* Deletion of Puma protects hematopoietic stem cells and confers long-term survival in response to high-dose γ-irradiation. Blood **2010**;115:3472-80
118. Wu W-S, Heinrichs S, Xu D, Garrison SP, Zambetti GP, Adams JM*, et al.* Slug antagonizes p53-mediated apoptosis of hematopoietic progenitors by repressing puma. Cell **2005**;123:641-53
119. Erlacher M, Michalak EM, Kelly PN, Labi V, Niederegger H, Coultas L*, et al.* BH3-only proteins Puma and Bim are rate-limiting for γ-radiation–and glucocorticoid-induced apoptosis of lymphoid cells in vivo. Blood **2005**;106:4131-8
120. Lin Y, Ma W, Benchimol S. Pidd, a new death-domain–containing protein, is induced by p53 and promotes apoptosis. Nature genetics **2000**;26:122
121. Kolesnick RN, Haimovitz-Friedman A, Fuks Z. The sphingomyelin signal transduction pathway mediates apoptosis for tumor necrosis factor, Fas, and ionizing radiation. Biochemistry and Cell Biology **1994**;72:471-4
122. Reap EA, Roof K, Maynor K, Borrero M, Booker J, Cohen PL. Radiation and stress-induced apoptosis: a role for Fas/Fas ligand interactions. Proceedings of the National Academy of Sciences **1997**;94:5750-5
123. Finnberg N, Gruber JJ, Fei P, Rudolph D, Bric A, Kim S-H*, et al.* DR5 knockout mice are compromised in radiation-induced apoptosis. Molecular and cellular biology **2005**;25:2000-13
124. Wang S, El-Deiry WS. TRAIL and apoptosis induction by TNF-family death receptors. Oncogene **2003**;22:8628
125. Yamashita M, Nitta E, Suda T. Regulation of hematopoietic stem cell integrity through p53 and its related factors. Annals of the New York Academy of Sciences **2016**;1370:45-54
126. Domen J, Cheshier SH, Weissman IL. The role of apoptosis in the regulation of hematopoietic stem cells: Overexpression of Bcl-2 increases both their number and repopulation potential. Journal of Experimental Medicine **2000**;191:253-64
127. Li XH, Ha CT, Xiao M. MicroRNA-30 inhibits antiapoptotic factor Mcl-1 in mouse and human hematopoietic cells after radiation exposure. Apoptosis **2016**;21:708-20
128. Avila AI, Illing A, Becker F, Maerz LD, Morita Y, Philipp M*, et al.* Xpg limits the expansion of haematopoietic stem and progenitor cells after ionising radiation. Nucleic acids research **2016**;44:6252-61
129. Uyanik B, Grigorash B, Goloudina A, Demidov O. DNA damage-induced phosphatase Wip1 in regulation of hematopoiesis, immune system and inflammation. Cell death discovery **2017**;3:17018
130. Wang X, Dong F, Zhang S, Yang W, Yu W, Wang Z*, et al.* TGF-β1 Negatively Regulates the Number and Function of Hematopoietic Stem Cells. Stem Cell Reports **2018**
131. Castedo M, Perfettini J-L, Roumier T, Andreau K, Medema R, Kroemer G. Cell death by mitotic catastrophe: a molecular definition. Oncogene **2004**;23:2825

132. Wang J, Sun Q, Morita Y, Jiang H, Groß A, Lechel A*, et al.* A differentiation checkpoint limits hematopoietic stem cell self-renewal in response to DNA damage. Cell **2012**;148:1001-14
133. Campisi J, di Fagagna FdA. Cellular senescence: when bad things happen to good cells. Nature reviews Molecular cell biology **2007**;8:729
134. Roninson IB. Tumor cell senescence in cancer treatment. Cancer research **2003**;63:2705-15
135. Debacq-Chainiaux F, Erusalimsky JD, Campisi J, Toussaint O. Protocols to detect senescence-associated beta-galactosidase (SA-βgal) activity, a biomarker of senescent cells in culture and in vivo. Nature protocols **2009**;4:1798
136. di Fagagna FdA. Living on a break: cellular senescence as a DNA-damage response. Nature Reviews Cancer **2008**;8:512
137. Lessard J, Sauvageau G. Bmi-1 determines the proliferative capacity of normal and leukaemic stem cells. nature **2003**;423:255
138. Baker DJ, Wijshake T, Tchkonia T, LeBrasseur NK, Childs BG, Van De Sluis B*, et al.* Clearance of p16 Ink4a-positive senescent cells delays ageing-associated disorders. Nature **2011**;479:232
139. Alcorta DA, Xiong Y, Phelps D, Hannon G, Beach D, Barrett JC. Involvement of the cyclin-dependent kinase inhibitor p16 (INK4a) in replicative senescence of normal human fibroblasts. Proceedings of the National Academy of Sciences **1996**;93:13742-7
140. Lin AW, Barradas M, Stone JC, van Aelst L, Serrano M, Lowe SW. Premature senescence involving p53 and p16 is activated in response to constitutive MEK/MAPK mitogenic signaling. Genes & development **1998**;12:3008-19
141. Serrano M, Lin AW, McCurrach ME, Beach D, Lowe SW. Oncogenic ras provokes premature cell senescence associated with accumulation of p53 and p16INK4a. Cell **1997**;88:593-602
142. Meng A, Wang Y, Van Zant G, Zhou D. Ionizing radiation and busulfan induce premature senescence in murine bone marrow hematopoietic cells. Cancer research **2003**;63:5414-9
143. Méndez-Ferrer S, Michurina TV, Ferraro F, Mazloom AR, MacArthur BD, Lira SA*, et al.* Mesenchymal and haematopoietic stem cells form a unique bone marrow niche. nature **2010**;466:829
144. Wilson A, Trumpp A. Bone-marrow haematopoietic-stem-cell niches. Nature Reviews Immunology **2006**;6:93
145. Morrison SJ, Scadden DT. The bone marrow niche for haematopoietic stem cells. Nature **2014**;505:327
146. Carbonneau CL, Despars G, Rojas-Sutterlin S, Fortin A, Le O, Hoang T*, et al.* Ionizing radiation–induced expression of INK4a/ARF in murine bone marrow–derived stromal cell populations interferes with bone marrow homeostasis. Blood **2012**;119:717-26
147. Butler JM, Nolan DJ, Vertes EL, Varnum-Finney B, Kobayashi H, Hooper AT*, et al.* Endothelial cells are essential for the self-renewal and repopulation of Notch-dependent hematopoietic stem cells. Cell stem cell **2010**;6:251-64
148. Salter AB, Meadows SK, Muramoto GG, Himburg H, Doan P, Daher P*, et al.* Endothelial progenitor cell infusion induces hematopoietic stem cell reconstitution in vivo. Blood **2009**;113:2104-7
149. Dominici M, Rasini V, Bussolari R, Chen X, Hofmann TJ, Spano C*, et al.* Restoration and reversible expansion of the osteoblastic hematopoietic stem cell niche after marrow radioablation. Blood **2009**;114:2333-43

150. Little JB. Radiation carcinogenesis. Carcinogenesis **2000**;21:397-404
151. KAPLAN HS. The role of radiation in experimental leukemogenesis. Natl Cancer Inst Monogr **1964**;14:207-17
152. Kaplan HS, Brown MB, Paull J. Influence of bone-marrow injections on involution and neoplasia of mouse thymus after systemic irradiation. JNCI: Journal of the National Cancer Institute **1953**;14:303-16
153. Kaplan HS, Brown MB. Protection against radiation-induced lymphoma development by shielding and partial-body irradiation of mice. Cancer Research **1952**;12:441-4
154. Kemp CJ, Wheldon T, Balmain A. p53-deficient mice are extremely susceptible to radiation-induced tumorigenesis. Nature genetics **1994**;8:66
155. Hinkal G, Parikh N, Donehower LA. Timed somatic deletion of p53 in mice reveals age-associated differences in tumor progression. PloS one **2009**;4:e6654
156. Christophorou M, Ringshausen I, Finch A, Swigart LB, Evan G. The pathological response to DNA damage does not contribute to p53-mediated tumour suppression. Nature **2006**;443:214
157. Lee C-L, Castle KD, Moding EJ, Blum JM, Williams N, Luo L*, et al.* Acute DNA damage activates the tumour suppressor p53 to promote radiation-induced lymphoma. Nature communications **2015**;6:8477
158. Michalak EM, Vandenberg CJ, Delbridge AR, Wu L, Scott CL, Adams JM*, et al.* Apoptosis-promoted tumorigenesis: γ-irradiation-induced thymic lymphomagenesis requires Puma-driven leukocyte death. Genes & Development **2010**;24:1608-13
159. Ladi E, Yin X, Chtanova T, Robey EA. Thymic microenvironments for T cell differentiation and selection. Nature immunology **2006**;7:338
160. Robey EA, Bluestone JA. Notch signaling in lymphocyte development and function. Current opinion in immunology **2004**;16:360-6
161. Liu C, Gao F, Li B, Mitchel R, Liu X, Lin J*, et al.* TLR4 knockout protects mice from radiation-induced thymic lymphoma by downregulation of IL6 and miR-21. Leukemia **2011**;25:1516
162. Ventura A, Kirsch DG, McLaughlin ME, Tuveson DA, Grimm J, Lintault L*, et al.* Restoration of p53 function leads to tumour regression in vivo. Nature **2007**;445:661
163. Marino S, Vooijs M, van der Gulden H, Jonkers J, Berns A. Induction of medulloblastomas in p53-null mutant mice by somatic inactivation of Rb in the external granular layer cells of the cerebellum. Genes & development **2000**;14:994-1004
164. Miller RA, Chrisp C, Jackson AU, Galecki AT, Burke DT. Coordinated genetic control of neoplastic and nonneoplastic diseases in mice. The Journals of Gerontology Series A: Biological Sciences and Medical Sciences **2002**;57:B3-B8
165. Li J, He F, Zhang P, Chen S, Shi H, Sun Y*, et al.* Loss of Asxl2 leads to myeloid malignancies in mice. Nature Communications **2017**;8:15456
166. Lu H, Huang Y-Y, Mehrotra S, Droz-Rosario R, Liu J, Bhaumik M*, et al.* Essential roles of BCCIP in mouse embryonic development and structural stability of chromosomes. PLoS genetics **2011**;7:e1002291
167. Holzenberger M, Lenzner C, Leneuve P, Zaoui R, Hamard G, Vaulont S*, et al.* Cre-mediated germline mosaicism: a method allowing rapid generation of several alleles of a target gene. Nucleic acids

research **2000**;28:e92-e

168. Vooijs M, Jonkers J, Berns A. A highly efficient ligand‐regulated Cre recombinase mouse line shows that LoxP recombination is position dependent. EMBO reports **2001**;2:292-7
169. Hayashi S, McMahon AP. Efficient recombination in diverse tissues by a tamoxifen-inducible form of Cre: a tool for temporally regulated gene activation/inactivation in the mouse. Developmental biology **2002**;244:305-18
170. Mao X, Fujiwara Y, Orkin SH. Improved reporter strain for monitoring Cre recombinase-mediated DNA excisions in mice. Proceedings of the National Academy of Sciences **1999**;96:5037-42
171. Sandhu U, Cebula M, Behme S, Riemer P, Wodarczyk C, Metzger D*, et al.* Strict control of transgene expression in a mouse model for sensitive biological applications based on RMCE compatible ES cells. Nucleic acids research **2010**;39:e1-e
172. Potten CS. Radiation, the ideal cytotoxic agent for studying the cell biology of tissues such as the small intestine. Radiation research **2004**;161:123-36
173. Terry NH, Travis EL. The influence of bone marrow depletion on intestinal radiation damage. International Journal of Radiation Oncology• Biology• Physics **1989**;17:569-73
174. Schultheiss T, Kun L, Ang K, Stephens L. Radiation response of the central nervous system. International Journal of Radiation Oncology• Biology• Physics **1995**;31:1093-112
175. Challen GA, Boles N, Lin KYK, Goodell MA. Mouse hematopoietic stem cell identification and analysis. Cytometry Part A **2009**;75:14-24
176. Mayle A, Luo M, Jeong M, Goodell MA. Flow cytometry analysis of murine hematopoietic stem cells. Cytometry Part A **2013**;83:27-37
177. Amrani YM, Gill J, Matevossian A, Alonzo ES, Yang C, Shieh J-H*, et al.* The Paf oncogene is essential for hematopoietic stem cell function and development. Journal of Experimental Medicine **2011**:jem. 20102170
178. Ward JM, Rehg JE, Morse III HC. Differentiation of rodent immune and hematopoietic system reactive lesions from neoplasias. Toxicologic pathology **2012**;40:425-34
179. Koulnis M, Pop R, Porpiglia E, Shearstone JR, Hidalgo D, Socolovsky M. Identification and analysis of mouse erythroid progenitors using the CD71/TER119 flow-cytometric assay. Journal of visualized experiments: JoVE **2011**
180. Pop R, Shearstone JR, Shen Q, Liu Y, Hallstrom K, Koulnis M*, et al.* A key commitment step in erythropoiesis is synchronized with the cell cycle clock through mutual inhibition between PU. 1 and S-phase progression. PLoS biology **2010**;8:e1000484
181. Lotem J, Sachs L. Hematopoietic cells from mice deficient in wild-type p53 are more resistant to induction of apoptosis by some agents. Blood **1993**;82:1092-6
182. Cui Y, Hisha H, Yang G, Fan T, Jin T, Li Q*, et al.* Optimal protocol for total body irradiation for allogeneic bone marrow transplantation in mice. Bone marrow transplantation **2002**;30:843
183. Dykstra B, Kent D, Bowie M, McCaffrey L, Hamilton M, Lyons K*, et al.* Long-term propagation of distinct hematopoietic differentiation programs in vivo. Cell stem cell **2007**;1:218-29
184. Sudo K, Ema H, Morita Y, Nakauchi H. Age-associated characteristics of murine hematopoietic stem cells. Journal of Experimental Medicine **2000**;192:1273-80
185. Yang Q, Esplin B, Borghesi L. E47 regulates hematopoietic stem cell proliferation and energetics but

not myeloid lineage restriction. Blood **2011**;117:3529-38

186. Joyce JA, Fearon DT. T cell exclusion, immune privilege, and the tumor microenvironment. Science **2015**;348:74-80
187. Gabrilovich DI, Ostrand-Rosenberg S, Bronte V. Coordinated regulation of myeloid cells by tumours. Nature Reviews Immunology **2012**;12:253
188. Youn J-I, Nagaraj S, Collazo M, Gabrilovich DI. Subsets of myeloid-derived suppressor cells in tumor-bearing mice. The Journal of Immunology **2008**;181:5791-802
189. Kumar V, Patel S, Tcyganov E, Gabrilovich DI. The nature of myeloid-derived suppressor cells in the tumor microenvironment. Trends in immunology **2016**;37:208-20
190. Condamine T, Ramachandran I, Youn J-I, Gabrilovich DI. Regulation of tumor metastasis by myeloid-derived suppressor cells. Annual review of medicine **2015**;66:97-110
191. Donehower LA, Harvey M, Slagle BL, McArthur MJ, Montgomery Jr CA, Butel JS*, et al.* Mice deficient for p53 are developmentally normal but susceptible to spontaneous tumours. Nature **1992**;356:215
192. Jacks T, Remington L, Williams BO, Schmitt EM, Halachmi S, Bronson RT*, et al.* Tumor spectrum analysis in p53-mutant mice. Current biology **1994**;4:1-7
193. Lakso M, Pichel JG, Gorman JR, Sauer B, Okamoto Y, Lee E*, et al.* Efficient in vivo manipulation of mouse genomic sequences at the zygote stage. Proceedings of the National Academy of Sciences **1996**;93:5860-5
194. Gallardo TD, John GB, Shirley L, Contreras CM, Akbay EA, Haynie JM*, et al.* Genomewide discovery and classification of candidate ovarian fertility genes in the mouse. Genetics **2007**;177:179-94
195. Lackner DH, Carré A, Guzzardo PM, Banning C, Mangena R, Henley T*, et al.* A generic strategy for CRISPR-Cas9-mediated gene tagging. Nature communications **2015**;6:10237
196. Sugiyama T, Kohara H, Noda M, Nagasawa T. Maintenance of the hematopoietic stem cell pool by CXCL12-CXCR4 chemokine signaling in bone marrow stromal cell niches. Immunity **2006**;25:977-88
197. Xie H, Tang C-HA, Song JH, Mancuso A, Del Valle JR, Cao J*, et al.* IRE1α RNase–dependent lipid homeostasis promotes survival in Myc-transformed cancers. The Journal of clinical investigation **2018**;128
198. Muralidharan S, Bhadury J, Nilsson L, Green L, McLure K, Nilsson J. BET bromodomain inhibitors synergize with ATR inhibitors to induce DNA damage, apoptosis, senescence-associated secretory pathway and ER stress in Myc-induced lymphoma cells. Oncogene **2016**;35:4689
199. Walter D, Matter A, Fahrenkrog B. Loss of histone H3 methylation at lysine 4 triggers apoptosis in Saccharomyces cerevisiae. PLoS genetics **2014**;10:e1004095
200. Calimeri T, Ferreri AJ. m‐TOR inhibitors and their potential role in haematological malignancies. British journal of haematology **2017**;177:684-702
201. Xueling G, Wang X. Role of Wnt canonical pathway in hematological malignancies. Journal of hematology & oncology **2010**;3:33
202. Bachy E, Urb M, Chandra S, Robinot R, Bricard G, De Bernard S*, et al.* CD1d-restricted peripheral T cell lymphoma in mice and humans. Journal of Experimental Medicine **2016**:jem. 20150794
203. Yamamoto T, Isomura M, Xu Y, Liang J, Yagasaki H, Kamachi Y*, et al.* PTPN11, RAS and FLT3 mutations in childhood acute lymphoblastic leukemia. Leukemia research **2006**;30:1085-9

204. Feist M, Schwarzfischer P, Heinrich P, Sun X, Kemper J, von Bonin F*, et al.* Cooperative STAT/NF-κB signaling regulates lymphoma metabolic reprogramming and aberrant GOT2 expression. Nature communications **2018**;9:1514

205. Chang G, Xiao W, Xu Z, Yu D, Li B, Zhang Y*, et al.* Pterostilbene induces cell apoptosis and cell cycle arrest in T-cell leukemia/lymphoma by suppressing the ERK1/2 pathway. BioMed research international **2017**;2017

206. Snijders AM, Mao J-H. Co-Expression Network Analysis of Fbxw7-Associated LncRNAs Reveals Their Functions in Radiation-Induced Thymic Lymphoma. Insights in cancer research **2016**;1:1

207. Schoppmeyer K, Norris PS, Haas M. Inhibition of T-cell acute lymphoblastic leukemia proliferation in vivo by re-expression of the p16INK4a tumor suppressor gene. Neoplasia **1999**;1:128-37

208. Sunaoshi M, Amasaki Y, Hirano-Sakairi S, Blyth BJ, Morioka T, Kaminishi M*, et al.* The effect of age at exposure on the inactivating mechanisms and relative contributions of key tumor suppressor genes in radiation-induced mouse T-cell lymphomas. Mutation Research/Fundamental and Molecular Mechanisms of Mutagenesis **2015**;779:58-67

209. Yamaguchi Y, Takabatake T, Kakinuma S, Amasaki Y, Nishimura M, Imaoka T*, et al.* Complicated biallelic inactivation of Pten in radiation-induced mouse thymic lymphomas. Mutation Research/Fundamental and Molecular Mechanisms of Mutagenesis **2010**;686:30-8

210. Tesio M, Trinquand A, Macintyre E, Asnafi V. Oncogenic PTEN functions and models in T-cell malignancies. Oncogene **2016**;35:3887

211. Lin Y, Diccianni M, Kim Y, Lin H, Lee C, Lin R*, et al.* Human p16γ, a novel transcriptional variant of p16 INK4A, coexpresses with p16 INK4A in cancer cells and inhibits cell-cycle progression. Oncogene **2007**;26:7017

212. Mihashi Y, Mizoguchi M, Takamatsu Y, Ishitsuka K, Iwasaki H, Koga M*, et al.* C-MYC and its main ubiquitin ligase, FBXW7, influence cell proliferation and prognosis in adult T-cell leukemia/lymphoma. The American journal of surgical pathology **2017**;41:1139-49

213. Basnett J, Xie V, Cisterne A, Bradstock K, Bendall L. Regulation of the bone marrow microenvironment by G-CSF: Effects of G-CSF on acute lymphoblastic leukaemia. PloS one **2017**;12:e0188042

214. Basnett J, Cisterne A, Bradstock KF, Bendall LJ. Effects of G-CSF On Acute Lymphoblastic Leukemia. Am Soc Hematology; 2012.

215. Rodrigues-Moreira S, Moreno SG, Ghinatti G, Lewandowski D, Hoffschir F, Ferri F*, et al.* Low-dose irradiation promotes persistent oxidative stress and decreases self-renewal in hematopoietic stem cells. Cell reports **2017**;20:3199-211

216. Bernitz JM, Daniel M, Fstkchyan YS, Moore K. Granulocyte-colony stimulating factor mobilizes dormant hematopoietic stem cells without proliferation in mice. Blood **2017**:blood-2016-11-752923

217. Peled A, Klein S, Beider K, Burger JA, Abraham M. Role of CXCL12 and CXCR4 in the pathogenesis of hematological malignancies. Cytokine **2018**;109:11-6

218. Ludwig H, Weisel K, Petrucci M, Leleu X, Cafro A, Garderet L*, et al.* Olaptesed pegol, an anti-CXCL12/SDF-1 Spiegelmer, alone and with bortezomib–dexamethasone in relapsed/refractory multiple myeloma: A Phase IIa Study. Leukemia **2017**;31:997